TEHNICAL REPORT **Report No.: ESSO/INCOIS/CSG/TR/01(2018)**

A Report on implementation of operational Global and Indian Ocean HYCOM at INCOIS

by

Sudheer Joseph, Srinivasu U.,Vijay P. , Aswanth Srinivasan & Siva Reddy S.

Indian National Centre for Ocean Information Services (INCOIS)
Earth System Science Organization (ESSO)
Ministry of Earth Sciences (MoES)
HYDERABAD, INDIA
www.incois.gov.in

30 MARCH, 2018

DOCUMENT CONTROL SHEET

Earth System Science Organization (ESSO)
Ministry of Earth Sciences (MoES)
Indian National Centre for Ocean Information Services (INCOIS)

ESSO Document Number: ESSO/INCOIS/CSG/TR/01(2018)
Title of the report: A Report on implementation of operational Global and Indian Ocean HYCOM at INCOIS

Author(s) [Last name, First name]:
Joseph Sudheer, Srinivasu U.,Vijay P., Srinivasan Aswanth & Siva Reddy S.
Ocean Atmosphere Coupled System Group (CSG), INCOIS
Type of Document:
Technical Report (TR)
Number of pages : 100
Number of Figures : 52
Number of references:22
Keywords: Ocean model, Ocean forecast, HYCOM, Validation, Indian Ocean
Security classification: Open
Distribution: Open
Date of publication: 30 March, 2018

Abstract (100 words)

A state of the art operational forecasting system with data assimilation (DA) is established at INCOIS, which is the first of it's kind in the country. The Indian Ocean model is the highest resolution operational system with DA available for the basin compared to any operational agency in the world. The core of the system is a $1/16^{th}$ eddy resolving Indian ocean Hybrid Coordinate Model (HYCOM), nested to a $1/4^{th}$ Global HYCOM which provides lateral boundary conditions to the high-resolution model. The system uses data assimilation scheme based on Tentral Statistical Interpolation (T-SIS) scheme. A five-year hindcast for the period 2012 to 2016 has been carried out using both setups. This report presents a detailed evaluation of both global and Indian ocean models in comparison with observations and two other established systems, NRL HYCOM and GODAS from INCOIS. The five-year hindcast results show that both Indian Ocean and global model simulated SST, SSS, SLA, currents and vertical structure of the ocean favourably when compared with observations and other models. Bias, RMSD, correlation and skill score compared to observations from each of the four models for selected parameters are evaluated as part of this exercise. Sea-level and currents, show a notable better performance for the new setups at INCOIS over NRL-HYCOM and INCOIS-GODAS.

A Report on implementation of operational Global and Indian Ocean HYCOM at INCOIS

Sudheer Joseph, Srinivasu U.,Vijay P., Aswanth Srinivasan & Siva Reddy,
Indian National Centre for Ocean Information Services
Hyderabad - 55

Contents

List of Figures

List of Tables

Abstract

A state of the art operational forecasting system with data assimilation (DA) is established at INCOIS, which is the first of it's kind in the country. The Indian Ocean model is the highest resolution operational system with DA available for the basin compared to any operational agency in the world. The core of the system is a $\frac{1}{16}^{\circ}$ eddy resolving Indian ocean Hybrid Coordinate Model (HYCOM), nested to a $\frac{1}{4}^{\circ}$ Global HYCOM which provides lateral boundary conditions to the high-resolution model. The system uses data assimilation scheme based on Tentral Statistical Interpolation (T-SIS) scheme. A five-year hindcast for the period 2012 to 2016 has been carried out using both setups. This report presents a detailed evaluation of both global and Indian ocean models in comparison with observations and two other established systems, NRL HYCOM and GODAS from INCOIS. The five-year hindcast results show that both Indian Ocean and global model simulated SST, SSS, SLA, currents and vertical structure of the ocean favourably when compared with observations and other models. Bias, RMSD, correlation and skill score compared to observations from each of the four models for selected parameters are evaluated as part of this exercise. Sea-level and currents, show a notable better performance for the new setups at INCOIS over NRL-HYCOM and INCOIS-GODAS.

1 Introduction

Lives of a large percentage of India's population is closely associated with the ocean surrounding the Indian sub-continent regarding their food, marine resources, transportation, search and rescue operations etc. Accurate and timely forecasts of the oceanic parameters for the ocean surrounding the subcontinent are vital for the optimal use of the resources and the socio-economic wellbeing of the country.

The INCOIS Tendral Ocean Prediction System (INCOIS-TOPS) consists of a global 25 km resolution model (ITOPSG) and a nested 6 km resolution Indian Ocean model(ITOPSI). The fine resolution Indian Ocean model shares the same vertical layer structure as the global model. Both these models are constrained by assimilation of ocean observations and produce daily analyses and forecasts, for 5 to 7 days ahead. INCOIS-TOPS has been developed in close collaboration between INCOIS and Tendral LLC to support diverse operational requirements at INCOIS. The goal is to provide information about the current and future state of the ocean derived from a model running at resolutions better than or equal to systems running at leading forecasting centres in the world. While forecasting centres such as the US Navy and the EU-French Mercator systems model the entire world ocean at 8-10 km resolution, we have chosen a multi-resolution approach. A fundamental feature of the multi-resolution approach is the ability to deploy an optimised model for the region of interest, in this case, the Indian Ocean. It has been realised for several years now that no one ocean model type or configuration can be optimal for all regions of the world ocean. By downscaling and deploying model configuration optimised for the local conditions the hope is to obtain better representation and predictions of the phenomena of interest at specific regions. Further, the multi-resolution system also offers a built-in ability for producing probability forecasts which could be very useful in the context of decision making.

Forecasting systems are typically composed of three independent components, the numerical ocean circulation model, observations and the data assimilation (DA) technique. Such systems incorporate information from observations in synergy with high-resolution ocean models to produce estimates of the ocean state better than what can be obtained by using either measurements or models in isolation. All three components are equally important to be able to accurately predict the ocean conditions. In general, the ocean circulation is dominated by the presence of ubiquitous non-linear localized eddies and quasi-linear non-localized waves. Non-linear interaction among the existing waves trigger barotropic and baroclinic instabilities leading to further generation, interaction and decay of eddies - a process by which energy is spread over a wide spectrum of scales. In designing a forecasting system, a well-tuned ocean model resolving eddies generated by instabilities and one that can reproduce the ocean circulation in a statistical sense is a first requirement. However, such a model will still contain errors, approximations and will be run with imprecisely known inputs. In such a scenario observations are necessary to constrain the model state and compensate for errors in the forcing and missing model physics.

In data assimilative systems the data-model differences are used in a feedback loop to keep the evolving model trajectory close to the observations. The assimilative algorithms are designed to interpolate sparse observations in time and space while extrapolating the observations to provide corrections to unobserved variables.

In developing TOPS our goals were to first obtain a finely tuned ocean model capable of representing the phenomena in the Indian Ocean accurately. Over the last year we have been testing various model configurations and assimilation parameters including the choice of vertical layers, advection schemes, error correlation length scales, background variances, type of observations, update frequency and many other parameters. These tests have yielded a robust configuration for the system and have been deployed in a operational setup. Herein we describe the details of the model, observations and the DA scheme.

1.1 The Model

At the heart of any modern data assimilative modeling system is a numerical ocean model skillful in simulating features of interest. IOFS uses the latest version of the HYbrid Coordinate Ocean Model (HYCOM, http://hycom.org), a model that is widely used by the oceanographic community. The centerpiece of HYCOM is a generalized vertical coordinate designed to quasi-optimally resolve vertical structure throughout the ocean [Bleck, 2002]. Typically, it is isopycnic in the interior stratified to minimize spurious diapycnal mixing, level or pressure coordinates near the surface to provide resolution in the surface mixed layer, and terrain-following in coastal regions to accurately represents flow-topography interactions . The nature of the model's vertical layers vary both in space and time with the background state at any given instant and is defined by a vertical grid generator. The coordinate system adopted in HYCOM allows for the use of advanced subgrid scale parameterizations in the ocean mixed layer while retaining the advantages of an isopycnal model in the ocean interior [Bleck, 2002, Chassignet et al., 2003, 2006b].

The HYCOM code employs a structured finite volume discretization to solve five prognostic equations on the Arakawa C-grid: one for each horizontal velocity component, a layer thickness tendency or mass conservation equation, and two conservations equations for the thermodynamic variables (salinity and temperature). These equations are complemented by an equation of state. The prognostic equations are leap-frog time integrated with a split-explicit treatment of the external and internal modes [Bleck and Smith, 1990]. Momentum advection is calculated using a second order enstrophy conserving scheme [Sadourny, 1975, Bleck and Boudra, 1986, Bleck and Smith, 1990]. The tracer and continuity equations are solved with second order flux corrected transport [Zalesak, 1979, Iskandarani et al., 2005].

INCOIS-TOPS configuration of HYCOM is similar to configurations used in other HYCOM based operation centers such as NRL and NCEP. The model is configured with 32 hybrid layers with potential densities referenced to 2000 db. The target densities are set to: 27.10, 28.10,28.90, 29.70, 30.50, 30.95, 31.50, 32.05, 32.60, 33.15, 33.70, 34.25, 34.75, 35.15, 35.50, 35.80, 36.04,36.20, 36.38, 36.52, 36.62, 36.70, 36.77, 36.83,36.89, 36.97,37.02, 37.06, 37.10, 37.17, 37.30,37.42 in sigma2 units.

The model bathymetry is a combination of ETOPO1 and GEBCO products with local corrections in the Indian Ocean, Gulf of Mexico and Brazil current regions. The atmospheric forcing is derived from NOAA's Global Forecast System. Three hourly fields of air temperature and vapor mixture at 2 m, surface downward and upward long and short-wave radiation, precipitation and 10 m wind speeds are used to derive the forcing fields. Wind stress is derived from 10 m winds using a formula devised by Kara et al. [2005]. The surface fluxes are forced with a bulk parameterization as detailed in Kara et al. [2000]. The fine resolution Indian Ocean model is one way nested within the global model. The slow variables are relaxed in 10-grid point buffer zone while a method of characteristics based scheme is used for the fast variables. Monthly climatological river discharge from NRL is used to specify a virtual salinity flux to include the effects of river inflow. The model tracer and continuity equations are solved using the second order flux corrected transport scheme [Iskandarani et al., 2005]. The KPP schme is used for vertical mixing [Large et al., 1994]. The vertical remapping between various layer types is done by a Weighted Essentially Non-Oscillatory (WENO) piecewise parabolic scheme. The water column heating by penetrating shortwave radiation is based on satellite derived climatological turbidity levels.

1.2 Observations

INCOIS-TOPS has potential to ingest data from several sources of observations, including remotly sensed satellite Sea Surface Temperature (SST) and Sea Level Anomalies (SLA), in-situ temperature and salinity profiles obtained from ship surveys, moorings, profiling

floats, and gliders. However, characteristics of the presently used data and their availability are listed in Table 1 below. Remotely sensed sea level anomalies (SLA) and SST as well as in-situ temperature/salinity (T/S) profiles are considered to be backbone of the system and thus are systematically assimilated in both models. Other observations–drifters, acoustic Doppler current profilers (ADCPs) and high frequency radar are appropriate for the fine resolution Indian Ocean model and can be assimilated with suitable modificatons to the assimilation code. Although all observations are obtained from quality controlled datasets, additional checks and careful preprocessing of the data is undertaken to ensure that there are no obvious erroneous values in the data stream since such values can lead to the persistence and propagation of these errors in a data sparse environment.

Table 1: Details of Observations Assimilated in ITOPSI & ITOPSG

Observation	Source	Type	Latency
Sea Level Anomalies (SLA)	ftp.sltac.cls.fr	along track	near real time
Foundation Temperature	podaac-ftp.jpl.nasa.gov	gridded	2 days
ARGO T/S	ftp://usgodae.org	point	1 day

1.3 Data Assimilation

We use a Tendral-Statistical Interpolation (T-SIS) DA scheme which is based on multivariate linear statistical estimation wherein, the Best Linear Unbiased Estimate (BLUE) of the model state or the analysis, $\mathbf{x}^a$, is obtained by updating the the model-forecast $\mathbf{x}^f$ using

$$\mathbf{x}^a = \mathbf{x}^f + \mathbf{K}(\mathbf{y} - \mathbf{H}\mathbf{x}^f) \tag{1}$$

where $\mathbf{y}$ is the data to be assimilated, $\mathbf{H}$ is the observation operator, $\mathbf{K}$ is the gain matrix. The Gauss-Markov formula provide the gain matrix that is optimal in a least-square sense (Bennet 92, Wunsch 96) as

$$\mathbf{K} = \mathbf{P}^f\mathbf{H}^T(\mathbf{H}\mathbf{P}^f\mathbf{H}^T + \mathbf{R})^{-1} \tag{2}$$

where $\mathbf{P}^f$ and $\mathbf{R}$ are the forecast and the observation error covariances. Formally, $\mathbf{P}^f$ is the covariance matrix of the forecast error $\mathbf{e^f} = \mathbf{x}^f - \mathbf{x}^{\text{true}}$ assuming statistically unbiased forecast $\text{E}(\mathbf{e^f}) = \mathbf{0}$ where E is an ensemble average and $\mathbf{x}^{\text{true}}$ is the true state of the ocean.

T-SIS offers the flexibility to be fully multivariate or use sub vectors for corrections. In general, the model state vector used in estimation procedures contains all of the prognostic variables. However, the state vector used for T-SIS is a subset of the HYCOM prognostic variables, specifically layer thickness, layer temperature, layer salinity, layer density, and the diagnosed SSH anomaly. In addition, the state vector is further subdivided into three sub-vectors, one consisting of SSH anomaly, another of layer thickness, and another consisting of layer temperature, salinity, and density. Each sub-vector is assumed to be uncorrelated with the others, making the error covariance block diagonal.

The SSH anomaly field is not directly assimilated because in HYCOM, it is diagnosed from the prognostic bottom pressure and internal density fields. Instead, a layerized version of the Cooper and Haines [1996] procedure is used to adjust model layer thicknesses in the isopycnic-coordinate interior in response to SSH anomaly innovations. Prior to calculating SSH innovations, the mean dynamic topography (MDT) is added back into the altimetry observations.

To optimize system performance for the HYCOM Lagrangian vertical coordinate system (essentially a stack of shallow water layers), subsurface profile observations are first layerized (re-mapped onto the model hybrid isopycnic-sigma-z vertical coordinate system)

prior to assimilation. The analysis procedure then updates each layer separately in a vertically decoupled manner. For temperature profiles that do not have corresponding salinity profiles, synthetic salinity profiles are generated from climatological T-S relationships [Thacker et al., 2004] to permit layerization. In the absence of robust cross correlations, the full state vector is split into sub vectors. In the models pressure layers, T&S are corrected. In isopycnal layers, thickness and one of either T/S is corrected. Profile data is first assimilated to obtain an intermediate state is then corrected with altimeter data. Velocity is not directly updated instead geostrophic velocity corrections are estimated from corrected state. The analysis process is designed to ensure that the mean model state is constrained mainly by T/S profiles while the variability around the mean is then constrained by the altimeter data. The analysis is performed in the model grid space using a simple, non-adaptive, distance-based localization using observations within the localization window around a particular grid point. A quasi-Gaussian, isotropic, distance-dependent localization function [Gaspari and Cohn, 1999] is used to impose a smooth localization of the error covariance and the innovations to yield a spatially continuous analysis.

1.4 Models used for Intercomparison

Quantitative assessments of selected model simulated parameters are carried out with independent observations which are not used in DA in whichever cases such observations are available. Apart from this, we have also compared five-year hindcast results with NRL-HYCOM (NHYCOM) run by US-Navy [Chassignet et al., 2009, 2006a, 2007a,b] and GODAS analysis system run at INCOIS (IGODAS) [Ravichandran et al., 2013, Sivareddy et al., 2015]. These models were chosen on account of their track record for several years and data availability. NHYCOM uses the Navy Coupled Ocean Data Assimilation (NCODA), and IGODAS uses 3D var based data assimilation.

Table 2: Details of Observations Assimilated in NHYCOM & IGODAS

System	Model	DA-Scheme	Data sets used for DA
NHYCOM	HYCOM $\frac{1}{12}^\circ$ Mercator grid	NCODA	AVHRR GAC SST(8 km),AVHRR LAC SST (2 km),GOES SST (12 km), Insitu-ship,drifting buoys, Profiles-xbts,CTDs,ARGO floats,fixed buoys, SSHA-Aviso, Sea ice SSM/I
IGODAS	MOM $\frac{1}{2}^\circ X \frac{1}{2}^\circ$ to $\frac{1}{2}^\circ X \frac{1}{4}^\circ$	3D-VAR	T&S profiles for the top 700m, from: Argo, Moored buoys (RAMA, PIRATA/TRITON, TAO, NIOT buoys), and ship-based (XBT, CTD, XCTD,). Using Newtonian relaxation scheme model SST is nudged towards satellite blended gridded fields of SST.

2 Evaluation of SST simulations

In this section, the simulated SST from INCOIS-TOPS-Indian Ocean(ITOPSI), INCOIS-TOPS-Global Ocean(ITOPSG), INCOIS-GODAS (IGODAS) and NRL-HYCOM (NHYCOM) for the Indian Ocean domain are evaluated using foundation SST from JPL NAVO analysis as the reference data. ITOPSI and ITOPSG simulations are with Data Assimilation (DA) at the 4-day interval. Such interval in DA allows us to assess the model's skill for four days period for which there is no DA along with the ability of the assimilation scheme.

2.1 Comparison of model SST using GHRSST

For the comparison with GHRSST which is at higher resolution (10KM), it is interpolated bi-linearly to model grid except for ITOPSI where the model is at higher resolution, and therefore the model data is interpolated to the observational grid.

Basin-scale spatial maps of bias (model-observation), root mean square difference (RMSD) and Correlation are prepared using each model in comparison with observed SST. Further to this, quantitative assessment is made for each parameter for the basin by counting the number of grid points falling in a range of valid bins for each statistical parameter. Spatial maps of each model is presented below for each of the years from 2012 to 2016.

Maps of basin-scale SST bias shows that there is a general pattern of colder model SST compared to observed SST indicated by negative values approximately between 5°N and 5°S of the equator for both ITOPSI and ITOPSG. On the other hand, model SST is observed to be warmer compared to GHRSST away from the equator for above two models. While IGODAS do not have regions of strong negative biases, it has large patches of positive bias in northern AS, BoB and small areas of the same in the southern Indian Ocean. Such a pattern indicates IGODAS is warmer compared to GHRSST in the regions mentioned above. NHYCOM is colder compared to observation in the eastern Indian ocean extending to BoB and south China Sea. Although there are certain changes associated with the inter-annual variability, the above described warmer and colder biases persists across years in respective models. Among the four models, NHYCOM has maximum % of SST with minimum bias consistently for all five years followed by IGODAS, ITOPSI and ITOPSG which shows slight changes interannually.

The basin-scale RMSD is maximum near to the western boundaries in all four models. Similarly, there are higher RMSD along the south-east coast of Australia and south China Sea. NHYCOM has relatively lower errors compared to other three model even in highly dynamic regions like Great Whirl (GW) region and southeastern corner of the basin where Agulhas rings get generated and propagate to Atlantic ocean. However, NHYCOM has higher RMSD in BoB compared to other models. The interannual variability of RMSD is relatively less for all models compared to the same of bias. Five year average performance of four models show that they have 40 to 65% of SST grids with RMSD less than 0.5°C and among them NHYCOM has highest % of data points with minimum RMSD and ITOPSI with minimum % of data for the same range.

For all four models, for 80% of the Indian Ocean basin, they correlate above 0.8 with GHRSST. For all of them, the correlation for eastern equatorial Indian Ocean is weak and is severe in case of NHYCOM. It is interesting to note that the eastern tropical Indian Ocean has the minimum bias and moderate RMSD compared to other parts of the basin with the lowest correlation. This pattern indicates that this region has the lowest variability of SST in the basin. About 10% of the SST in the model grids shows the correlation between 0.6 to 0.8. Among the four models, ITOPSI has the highest correlation above 0.8 for the highest percentage of area in the Indian Ocean consistently for all three years except for the year 2012 during which ITOPSG got a slightly better correlation.

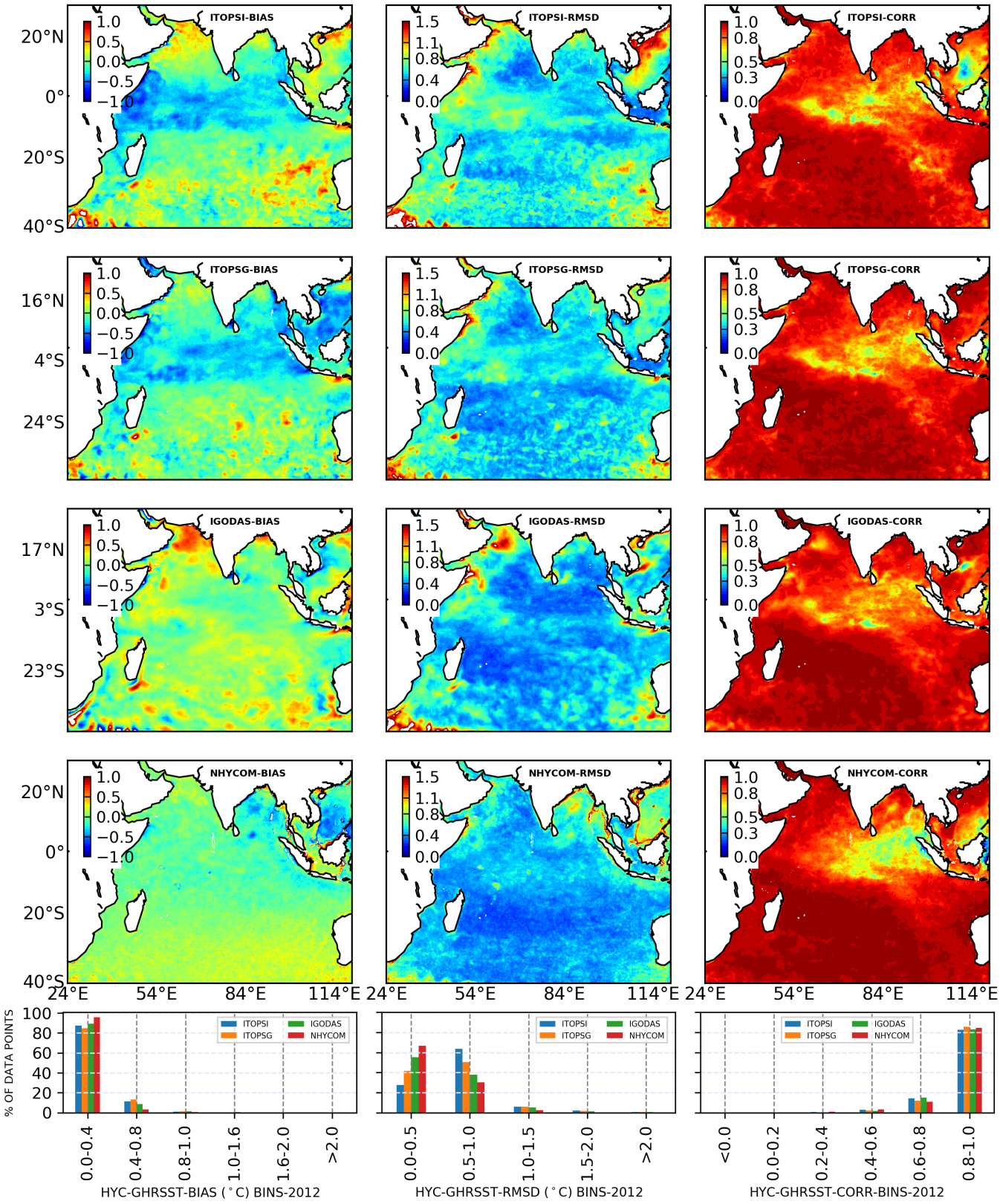

Figure 1: Comparison of SST simulations from ITOPSI, ITPOSG, IGODAS and NHYCOM with GHRSST for year 2012.

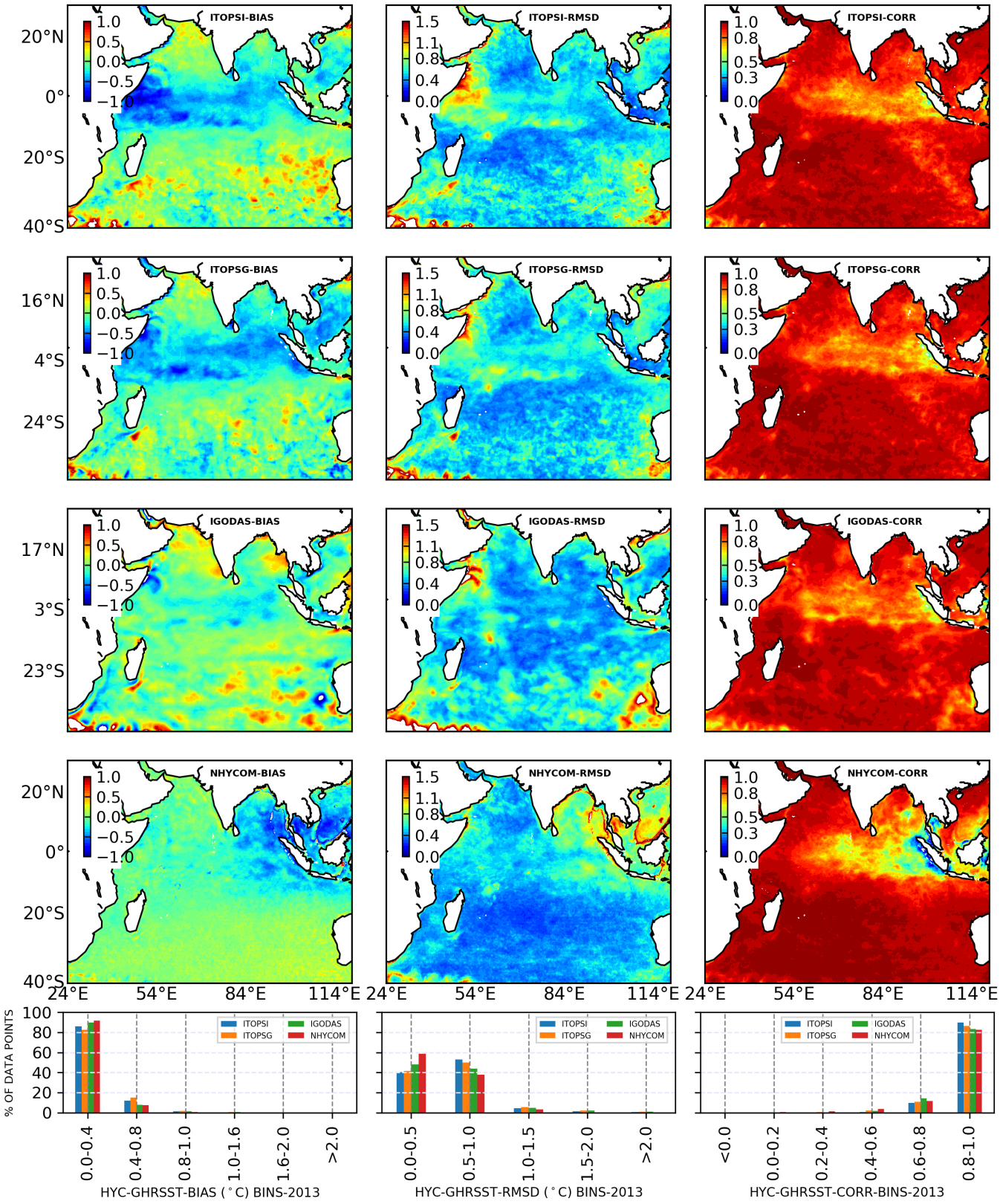

Figure 2: Comparison of SST simulations from ITOPSI, ITPOSG, IGODAS and NHYCOM with GHRSST for year 2013.

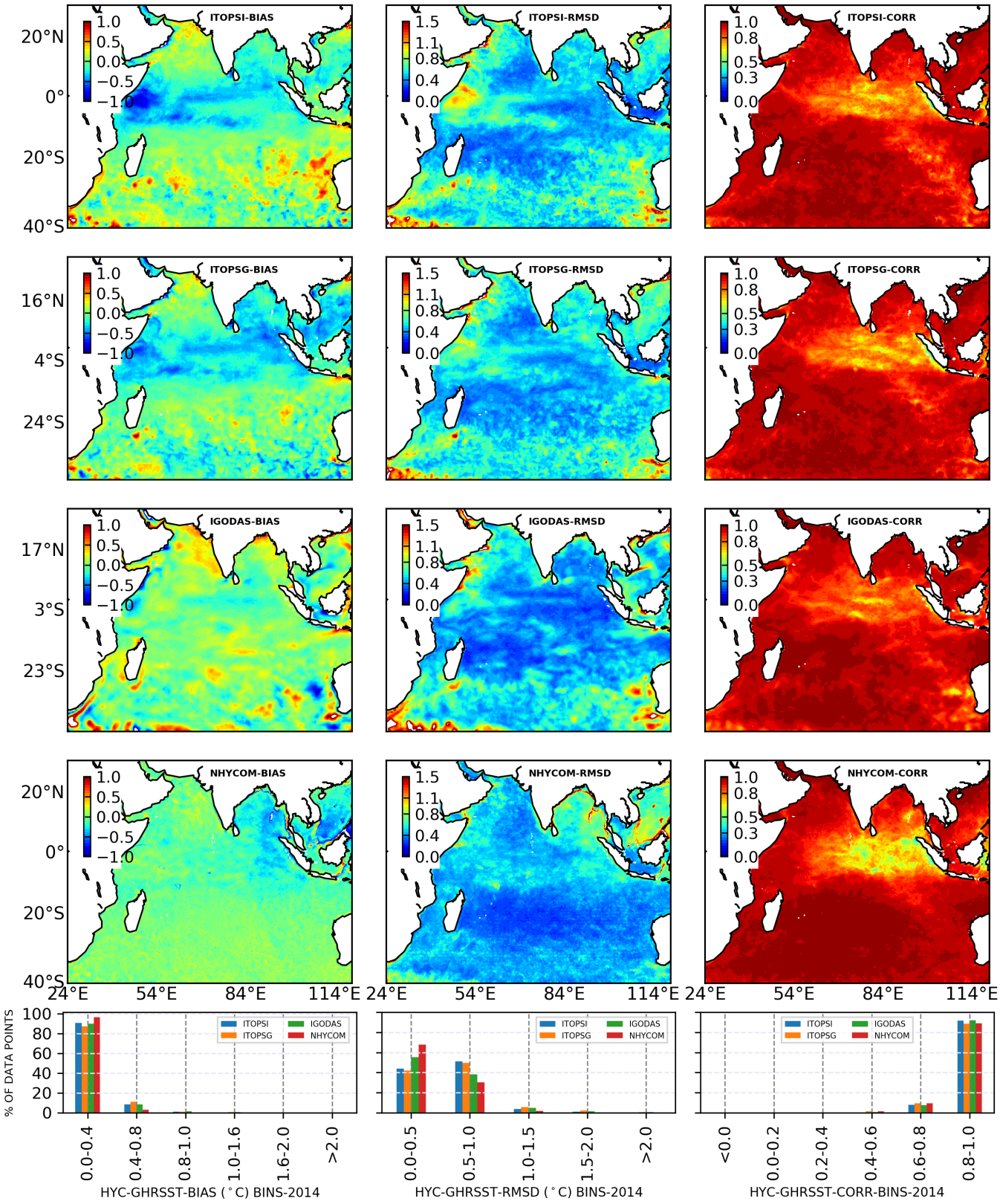

Figure 3: Comparison of SST simulations from ITOPSI, ITPOSG, IGODAS and NHYCOM with GHRSST

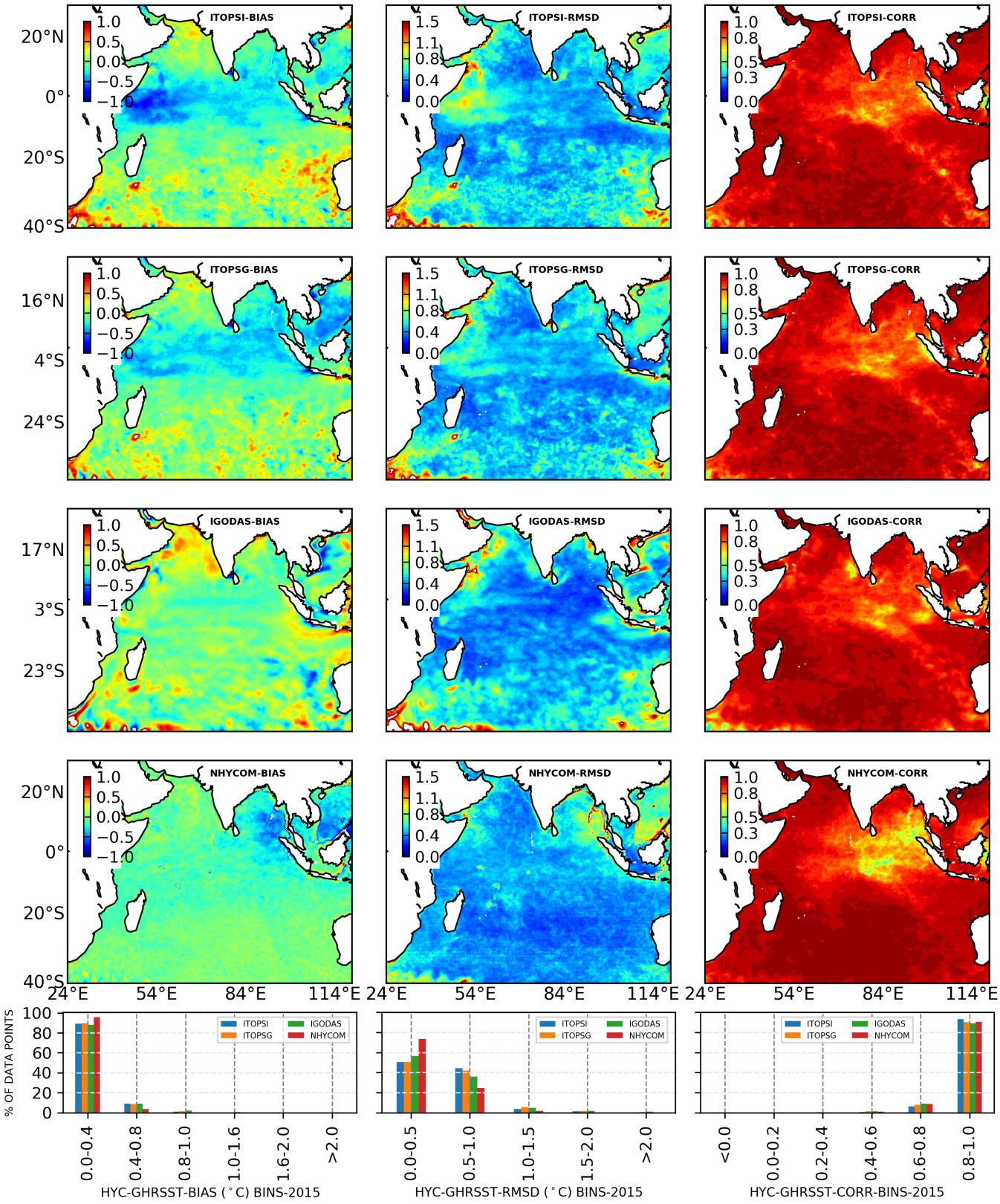

Figure 4: Comparison of SST simulations from ITOPSI, ITPOSG, IGODAS and NHYCOM with GHRSST

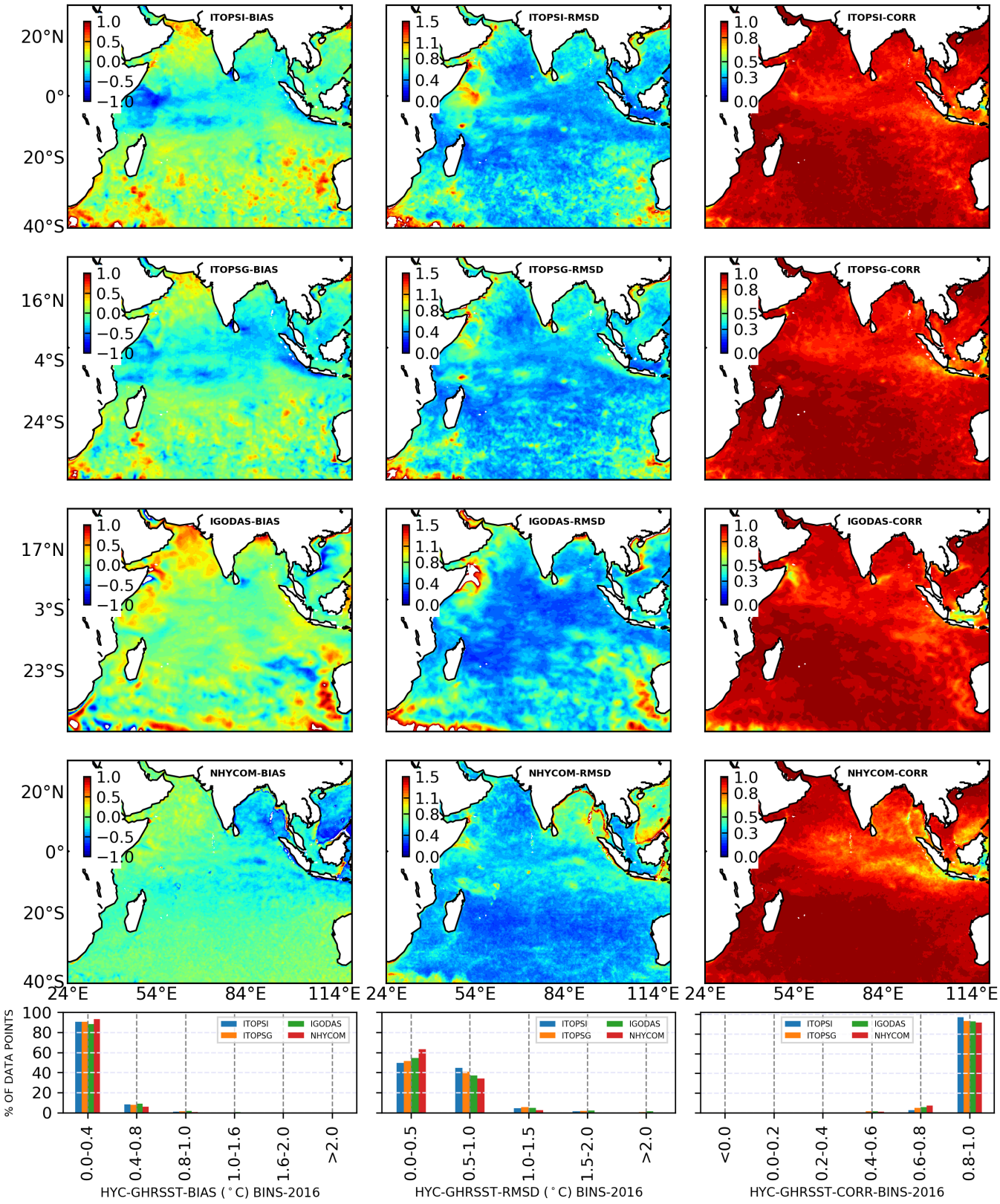

Figure 5: Comparison of SST simulations from ITOPSI, ITPOSG, IGODAS and NHYCOM with GHRSST

Ranking of models based on SST simulation

The quality of each model simulation is assessed with the help of target bins for each statistical parameter, such that the model with a maximum number of grid points falling under highest target bin, is the best performing one. For bias and RMSD target bins are with ranges of 0.0 to 0.4°C and 0.0 to 0.5°C respectively compared to the reference data. In case of correlation, the target is highest % of data falling in correlation bin of 0.8 to 1.0. Percentage of data points falling in an optimal bin of each parameter is shown in Table- 3. Following the above convention, ranks of each model against each statistical parameter considered are presented in Table - 4.

Table 3: Ranks of models based on % of grid points falling in target bins of statistical parameters. Each column contains % of data in highest target bin for years 2012 to 2016 separated by a forward slash. Bold numbers in bracket indicate mean for five years.

Model	BIAS	RMSD	CORR
ITOPSI	87/86/90/89/90 **(88.4)**	55/66/68/72/71 **(66.4)**	82/89/91/93/97 **(90.4)**
ITOPSG	84/82/87/89/90 **(86.4)**	66/66/67/71/72 **(68.4)**	85/86/88/90/93 **(88.4)**
IGODAS	89/89/89/88/88 **(88.6)**	72/68/73/72/71 **(71.2)**	83/83/92/89/92 **(87.8)**
NHYCOM	95/91/96/95/93 **(94.0)**	81/74/88/85/79 **(81.4)**	84/82/89/90/91 **(87.2)**

Table 4: Ranking of Models against statistical parameters considered

MODEL	BIAS	RMSD	CORR
ITOPSI	3	4	1
ITOPSG	3	3	2
IGODAS	2	2	3
NHYCOM	1	1	4

2.2 Comparison of model SST using RAMA buoys

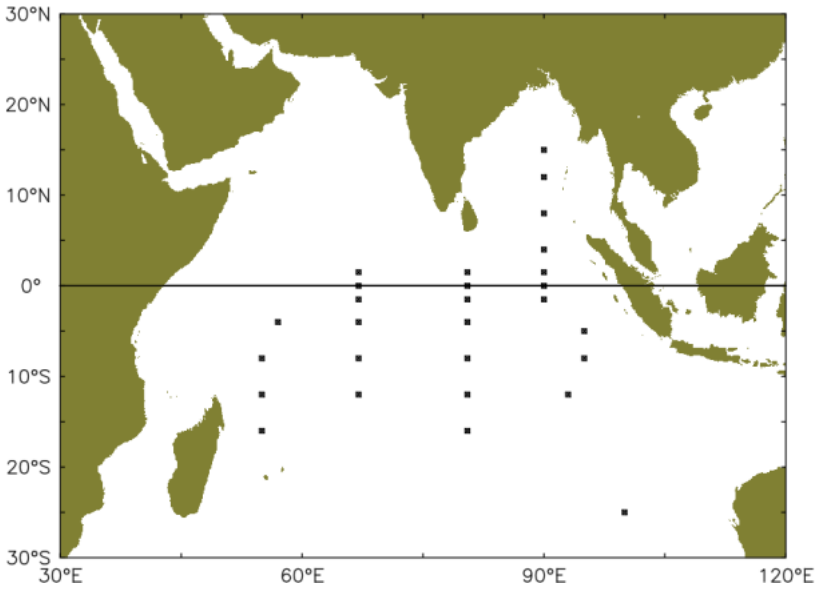

Figure 6: Location map of RAMA buoys used for validation of SST from models

RAMA buoys provide a unique opertunity to validate OGCMs at many open ocean locations in the Indian Ocean. We have chosen 24 RAMA buoys which had long timeseries of SST data for the period 2012–2016 to vaidate selected OGCMS. Mean, standard deviation, bias, RMSD, correlation and Skill score for each model is calculated and presented in Figure- 7 and in tabular form from Tables - 4 to 9. Statistical tables demonstrate that all four models captured the mean and variability in SST well and with in a range of +/-0.02 °C SST in case of mean and +/- 0.04 in case of standard deviation. IGODAS shows minimum bias followed by NHYCOM, ITOPSI and ITOPSG respectively. Nevertheless, maximum SST biases shown by all four models are within +/-0.3 °C with the exception of one or two locations. There is an anomalouly high RMSD close to 2°C for NHYCOM and close to 1°C for other models in case of location 25S100E (Figure- 7, 4^{th} panel from top). This may be due to the sensor error in RAMA. All four models show very good correlation values above 0.8 and 0.9 in most of the sites with exeption of one or two. Ranks from one to four of each model is calculated at each location of RAMA, such that a given model with minimum RMSD, maximum correlation and maximum skill score ranks one and presented in Figure- 8. Root mean square differences of IGODAS are lowest for 17 locations followed by NHYCOM in 4 locations and 2 locations for ITOPSI and 1 location for itospg (Figure- 8, top panel). However, it may be noted that all four models show RMSD of SST less than 0.5 °C wnich is close to the accuracy of satellite SST assimilated. Among the four models, IGODAS ranks 1 with higest correlation for 16 locations, followed by ITOPSG and NHYCOM ranking 1 for 6 locations and ITOPSI ranking 1 for 3 locations. Skill score is calculated following the method of Kara et al. [2008]. Skill score of 1 means model is able to perform as good as observations. In case of SST skill score for most of the locations are above 0.6 and in many cases it is above 0.8 for all four models. Among the four, IGODAS ranks 1 for 17 locations folowed by NHYCOM for 4 locations and ITOPSG and ITOPSI being raked 1 at 2 locations each. Apart from the bar charts and tabular forms, time series and taylor diagrams of SST from all four models in comparison with RAMA SST is presented in Figures- 9 to 11.

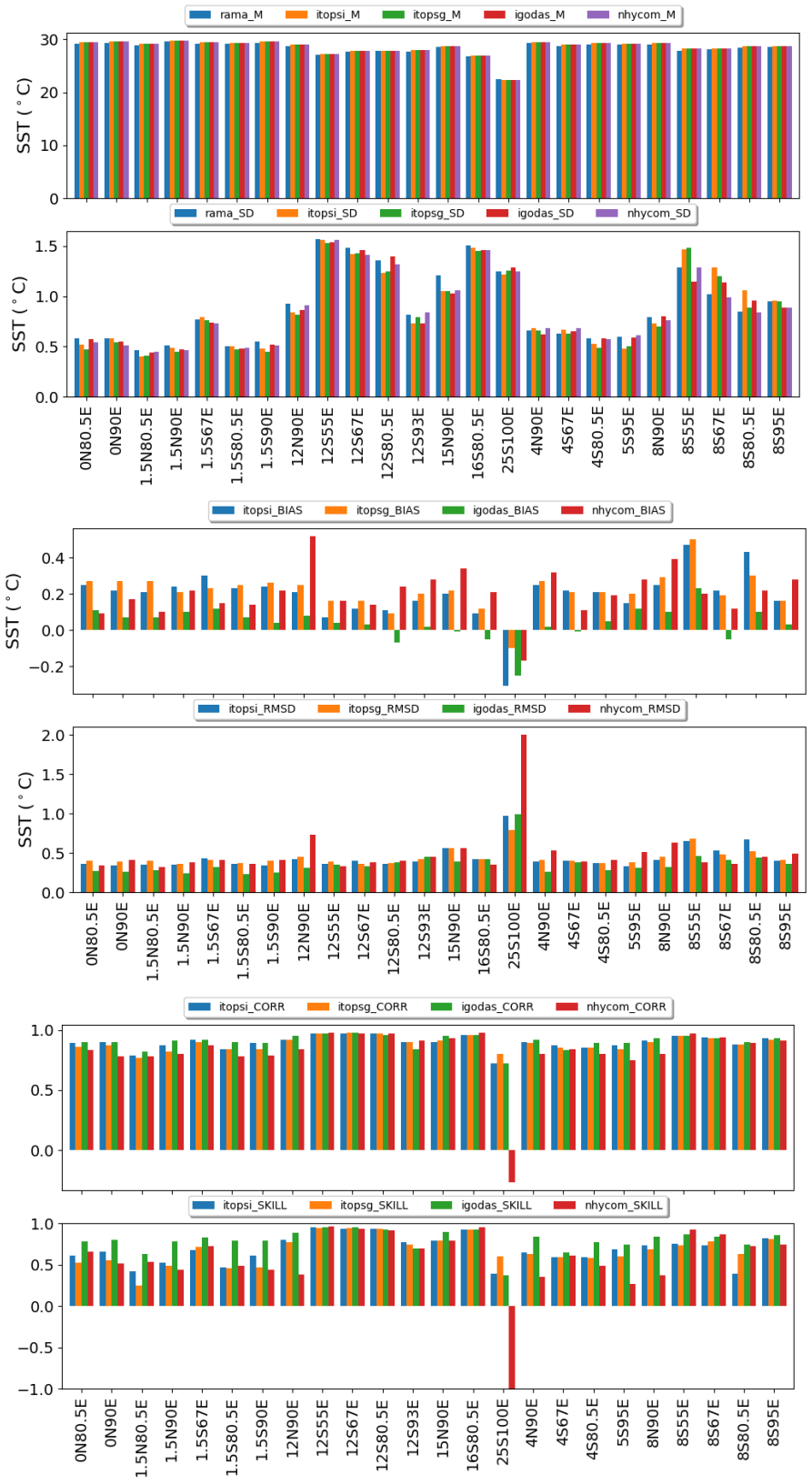

Figure 7: Comparison of SST from 4 models in terms of mean,standard deviation, bias, rmsd, correlation and skill score with respect to RAMA buoys for the period 2012-2016.

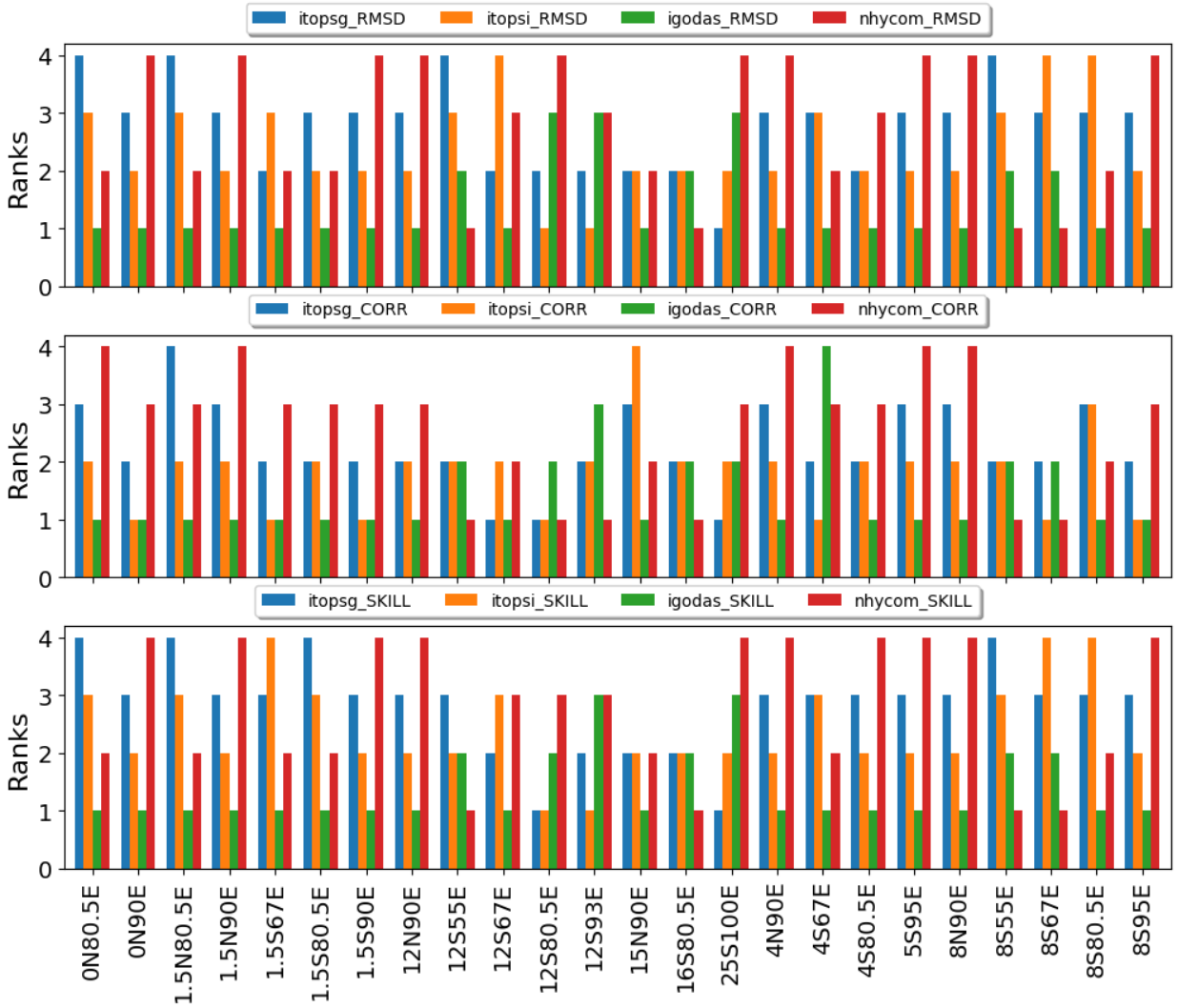

Figure 8: Ranks of four models in terms of their RMSD, correlation and skill score for SST from 24 RAMA buoy locations. Model with minimum rmsd, maximum correlation & skill score are given a rank of 1 indicating best performance and the one with maximum RMSD, minimum correlation and minimum skill score is given a rank of 4. Intermediae ones are given ranks of 2 and 3.

Table 5: Mean values of SST from 24 RAMA buoys for the period 2012–2016 compared with same of selected four ocean models.

Location	Nobs	rama_M	itopsg_M	itopsi_M	igodas_M	nhycom_M
0N80.5E	1179.0	29.12	29.39	29.39	29.39	29.39
0N90E	1163.0	29.33	29.60	29.60	29.60	29.60
1.5N80.5E	648.0	28.86	29.12	29.12	29.12	29.12
1.5N90E	255.0	29.53	29.74	29.74	29.74	29.74
1.5S67E	943.0	29.17	29.40	29.40	29.40	29.40
1.5S80.5E	1443.0	29.09	29.34	29.34	29.33	29.33
1.5S90E	627.0	29.32	29.58	29.58	29.58	29.60
12N90E	1801.0	28.76	29.00	29.01	29.00	29.00
12S55E	930.0	27.08	27.24	27.23	27.24	27.24
12S67E	810.0	27.64	27.81	27.81	27.81	27.81
12S80.5E	1647.0	27.77	27.86	27.86	27.86	27.86
12S93E	962.0	27.73	27.92	27.92	27.92	27.92
15N90E	1820.0	28.54	28.76	28.76	28.76	28.76
16S80.5E	1313.0	26.84	26.96	26.96	26.96	26.96
25S100E	808.0	22.42	22.32	22.33	22.33	22.33
4N90E	935.0	29.23	29.50	29.50	29.50	29.50
4S67E	1144.0	28.75	28.96	28.97	28.96	28.96
4S80.5E	1615.0	29.06	29.28	29.28	29.27	29.27
5S95E	1276.0	28.98	29.18	29.18	29.18	29.18
8N90E	1022.0	29.01	29.30	29.30	29.29	29.29
8S55E	645.0	27.80	28.30	28.30	28.29	28.29
8S67E	916.0	28.13	28.32	28.32	28.33	28.33
8S80.5E	1587.0	28.34	28.64	28.65	28.64	28.64
8S95E	1456.0	28.50	28.66	28.65	28.66	28.66

Table 6: Standard deviations of SST from 24 RAMA buoys for the period 2012–2016 compared with same of selected four ocean models.

Location	Nobs	rama_SD	itopsg_SD	itopsi_SD	igodas_SD	nhycom_SD
0N80.5E	1179.0	0.58	0.47	0.52	0.57	0.54
0N90E	1163.0	0.58	0.54	0.58	0.55	0.51
1.5N80.5E	648.0	0.46	0.41	0.40	0.44	0.45
1.5N90E	255.0	0.51	0.45	0.49	0.47	0.46
1.5S67E	943.0	0.77	0.76	0.79	0.74	0.73
1.5S80.5E	1443.0	0.50	0.47	0.50	0.48	0.49
1.5S90E	627.0	0.55	0.45	0.48	0.52	0.51
12N90E	1801.0	0.93	0.82	0.84	0.86	0.91
12S55E	930.0	1.57	1.53	1.56	1.54	1.56
12S67E	810.0	1.48	1.43	1.42	1.46	1.41
12S80.5E	1647.0	1.36	1.25	1.23	1.40	1.32
12S93E	962.0	0.82	0.79	0.73	0.73	0.84
15N90E	1820.0	1.21	1.05	1.05	1.03	1.06
16S80.5E	1313.0	1.51	1.45	1.48	1.46	1.46
25S100E	808.0	1.25	1.26	1.22	1.29	1.25
4N90E	935.0	0.66	0.66	0.68	0.62	0.68
4S67E	1144.0	0.63	0.63	0.67	0.65	0.68
4S80.5E	1615.0	0.58	0.49	0.53	0.58	0.57
5S95E	1276.0	0.60	0.50	0.48	0.59	0.61
8N90E	1022.0	0.79	0.70	0.73	0.80	0.76
8S55E	645.0	1.29	1.48	1.47	1.15	1.29
8S67E	916.0	1.02	1.20	1.29	1.14	0.99
8S80.5E	1587.0	0.85	0.89	1.06	0.96	0.84
8S95E	1456.0	0.95	0.95	0.96	0.89	0.89

Table 7: Bias of simulated SST from selected four ocean models with respect to 24 RAMA buoys for the period 2012–2016.

Location	Nobs	itopsg_BIAS	itopsi_BIAS	igodas_BIAS	nhycom_BIAS
0N80.5E	1179.0	0.27	0.25	0.11	0.09
0N90E	1163.0	0.27	0.22	0.07	0.17
1.5N80.5E	648.0	0.27	0.21	0.07	0.10
1.5N90E	255.0	0.21	0.24	0.10	0.22
1.5S67E	943.0	0.23	0.30	0.12	0.15
1.5S80.5E	1443.0	0.25	0.23	0.07	0.14
1.5S90E	627.0	0.26	0.24	0.04	0.22
12N90E	1801.0	0.25	0.21	0.08	0.52
12S55E	930.0	0.16	0.07	0.04	0.16
12S67E	810.0	0.16	0.12	0.03	0.14
12S80.5E	1647.0	0.09	0.11	-0.07	0.24
12S93E	962.0	0.20	0.16	0.02	0.28
15N90E	1820.0	0.22	0.20	-0.01	0.34
16S80.5E	1313.0	0.12	0.09	-0.05	0.21
25S100E	808.0	-0.10	-0.31	-0.25	-0.17
4N90E	935.0	0.27	0.25	0.02	0.32
4S67E	1144.0	0.21	0.22	-0.01	0.11
4S80.5E	1615.0	0.21	0.21	0.05	0.19
5S95E	1276.0	0.20	0.15	0.12	0.28
8N90E	1022.0	0.29	0.25	0.10	0.39
8S55E	645.0	0.50	0.47	0.23	0.20
8S67E	916.0	0.19	0.22	-0.05	0.12
8S80.5E	1587.0	0.30	0.43	0.10	0.22
8S95E	1456.0	0.16	0.16	0.03	0.28

Table 8: Root Mean Square Difference (RMSD) of simulated SST from selected four ocean models with respect to 24 RAMA buoys for the period 2012–2016.

Location	Nobs	itopsg_RMSD	itopsi_RMSD	igodas_RMSD	nhycom_RMSD
0N80.5E	1179.0	0.40	0.36	0.27	0.34
0N90E	1163.0	0.39	0.34	0.26	0.41
1.5N80.5E	648.0	0.40	0.35	0.28	0.32
1.5N90E	255.0	0.36	0.35	0.24	0.38
1.5S67E	943.0	0.41	0.43	0.32	0.41
1.5S80.5E	1443.0	0.37	0.36	0.23	0.36
1.5S90E	627.0	0.40	0.34	0.25	0.41
12N90E	1801.0	0.45	0.42	0.31	0.73
12S55E	930.0	0.39	0.36	0.35	0.33
12S67E	810.0	0.36	0.40	0.33	0.38
12S80.5E	1647.0	0.37	0.36	0.38	0.40
12S93E	962.0	0.42	0.39	0.45	0.45
15N90E	1820.0	0.56	0.56	0.39	0.56
16S80.5E	1313.0	0.42	0.42	0.42	0.35
25S100E	808.0	0.79	0.97	0.99	2.00
4N90E	935.0	0.41	0.39	0.26	0.53
4S67E	1144.0	0.40	0.40	0.38	0.39
4S80.5E	1615.0	0.37	0.37	0.28	0.41
5S95E	1276.0	0.38	0.33	0.31	0.51
8N90E	1022.0	0.45	0.41	0.32	0.63
8S55E	645.0	0.68	0.65	0.46	0.38
8S67E	916.0	0.48	0.53	0.41	0.36
8S80.5E	1587.0	0.52	0.67	0.44	0.45
8S95E	1456.0	0.41	0.40	0.36	0.49

Table 9: Correlation of SST from selected four ocean models with respect to 24 RAMA buoys for the period 2012–2016.

Location	Nobs	itopsg_CORR	itopsi_CORR	igodas_CORR	nhycom_CORR
0N80.5E	1179.0	0.86	0.89	0.90	0.83
0N90E	1163.0	0.87	0.90	0.90	0.78
1.5N80.5E	648.0	0.77	0.79	0.82	0.78
1.5N90E	255.0	0.82	0.87	0.91	0.80
1.5S67E	943.0	0.90	0.92	0.92	0.87
1.5S80.5E	1443.0	0.84	0.84	0.90	0.78
1.5S90E	627.0	0.84	0.89	0.89	0.79
12N90E	1801.0	0.92	0.92	0.95	0.84
12S55E	930.0	0.97	0.97	0.97	0.98
12S67E	810.0	0.98	0.97	0.98	0.97
12S80.5E	1647.0	0.97	0.97	0.96	0.97
12S93E	962.0	0.90	0.90	0.84	0.91
15N90E	1820.0	0.91	0.90	0.95	0.93
16S80.5E	1313.0	0.96	0.96	0.96	0.98
25S100E	808.0	0.80	0.72	0.72	-0.27
4N90E	935.0	0.89	0.90	0.92	0.80
4S67E	1144.0	0.85	0.87	0.83	0.84
4S80.5E	1615.0	0.85	0.85	0.89	0.80
5S95E	1276.0	0.84	0.87	0.89	0.75
8N90E	1022.0	0.90	0.91	0.93	0.80
8S55E	645.0	0.95	0.95	0.95	0.97
8S67E	916.0	0.93	0.94	0.93	0.94
8S80.5E	1587.0	0.88	0.88	0.90	0.89
8S95E	1456.0	0.92	0.93	0.93	0.91

Table 10: Skill score of SST from selected four ocean models with respect to 24 RAMA buoys for the period 2012–2016.

Location	Nobs	itopsg_SKILL	itopsi_SKILL	igodas_SKILL	nhycom_SKILL
0N80.5E	1179.0	0.52	0.61	0.78	0.66
0N90E	1163.0	0.55	0.66	0.80	0.51
1.5N80.5E	648.0	0.25	0.42	0.63	0.53
1.5N90E	255.0	0.49	0.52	0.78	0.44
1.5S67E	943.0	0.71	0.68	0.83	0.72
1.5S80.5E	1443.0	0.46	0.47	0.79	0.49
1.5S90E	627.0	0.47	0.61	0.79	0.44
12N90E	1801.0	0.77	0.80	0.89	0.38
12S55E	930.0	0.94	0.95	0.95	0.96
12S67E	810.0	0.94	0.93	0.95	0.93
12S80.5E	1647.0	0.93	0.93	0.92	0.91
12S93E	962.0	0.74	0.77	0.70	0.70
15N90E	1820.0	0.79	0.79	0.90	0.79
16S80.5E	1313.0	0.92	0.92	0.92	0.95
25S100E	808.0	0.60	0.39	0.37	-1.58
4N90E	935.0	0.63	0.65	0.84	0.35
4S67E	1144.0	0.59	0.59	0.65	0.61
4S80.5E	1615.0	0.58	0.59	0.77	0.49
5S95E	1276.0	0.60	0.69	0.74	0.27
8N90E	1022.0	0.69	0.73	0.84	0.37
8S55E	645.0	0.73	0.75	0.87	0.92
8S67E	916.0	0.78	0.73	0.84	0.87
8S80.5E	1587.0	0.63	0.39	0.74	0.72
8S95E	1456.0	0.81	0.82	0.86	0.74

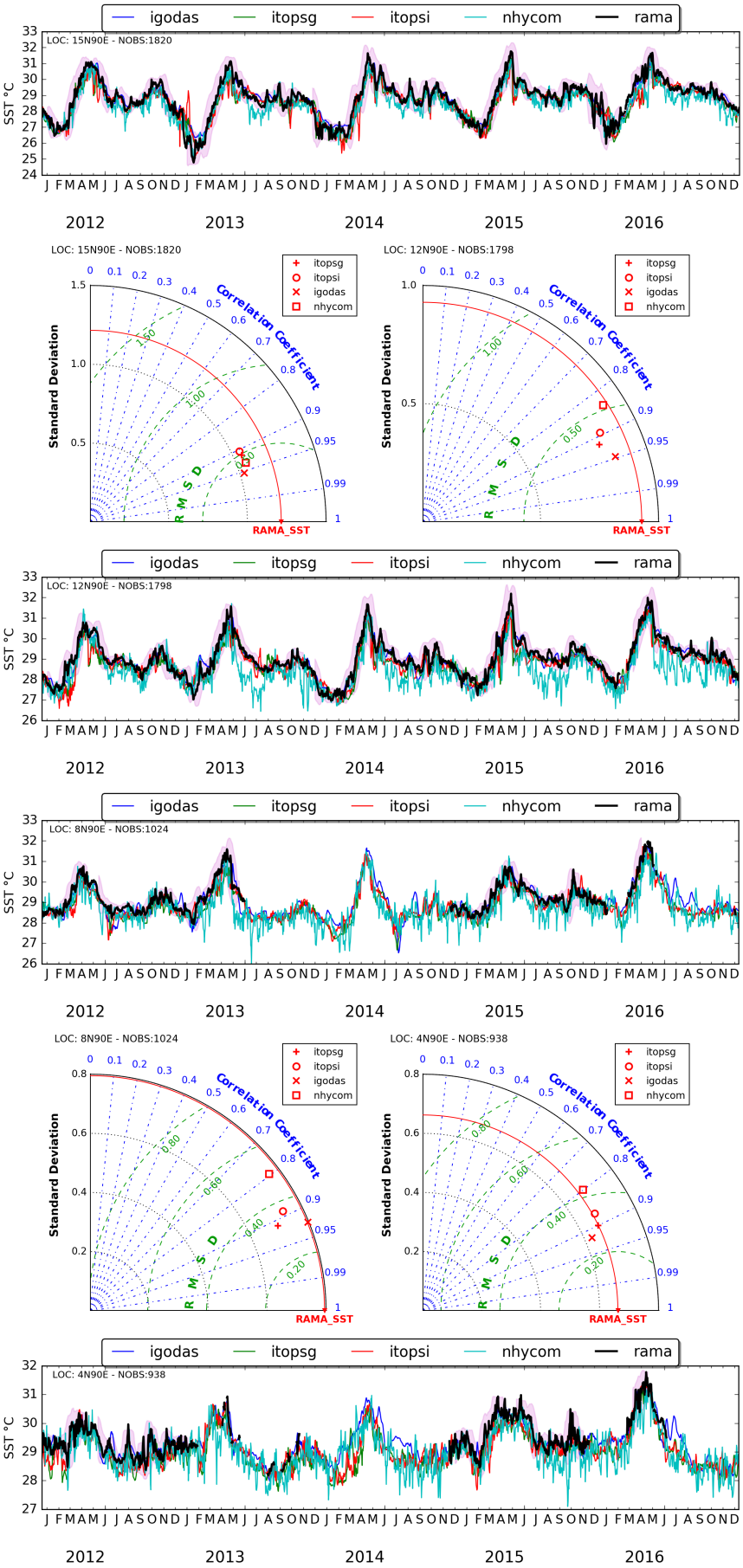

Figure 9: Comparison of SST from RAMA buoys in BoB with models. Pink envelope around RAMA data shows (+/-) 2-std of RAMA SST.

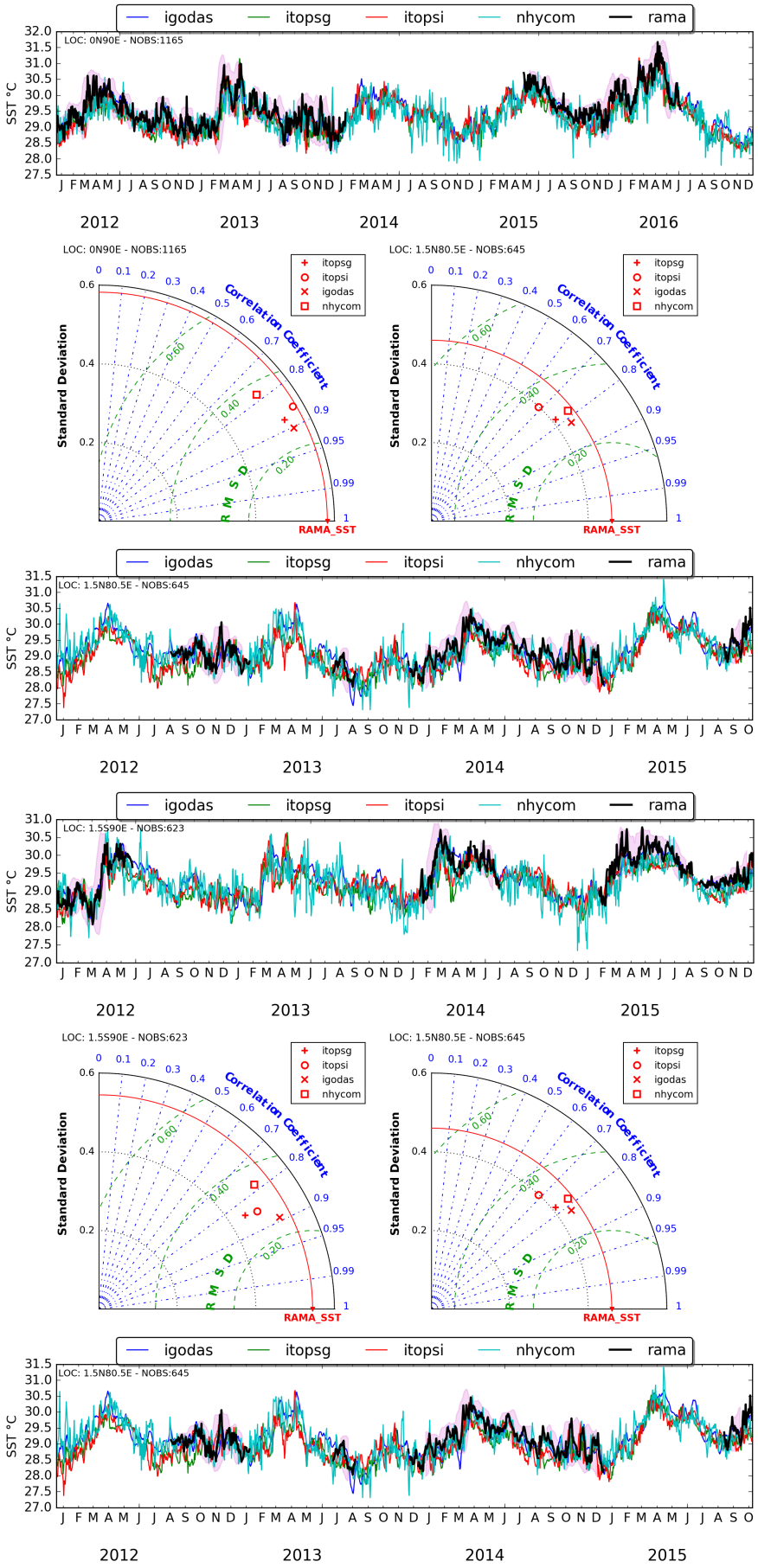

Figure 10: Comparison of SST from RAMA buoys in EEIO with models. Pink envelope around RAMA data shows (+/-) 2-std of RAMA SST.

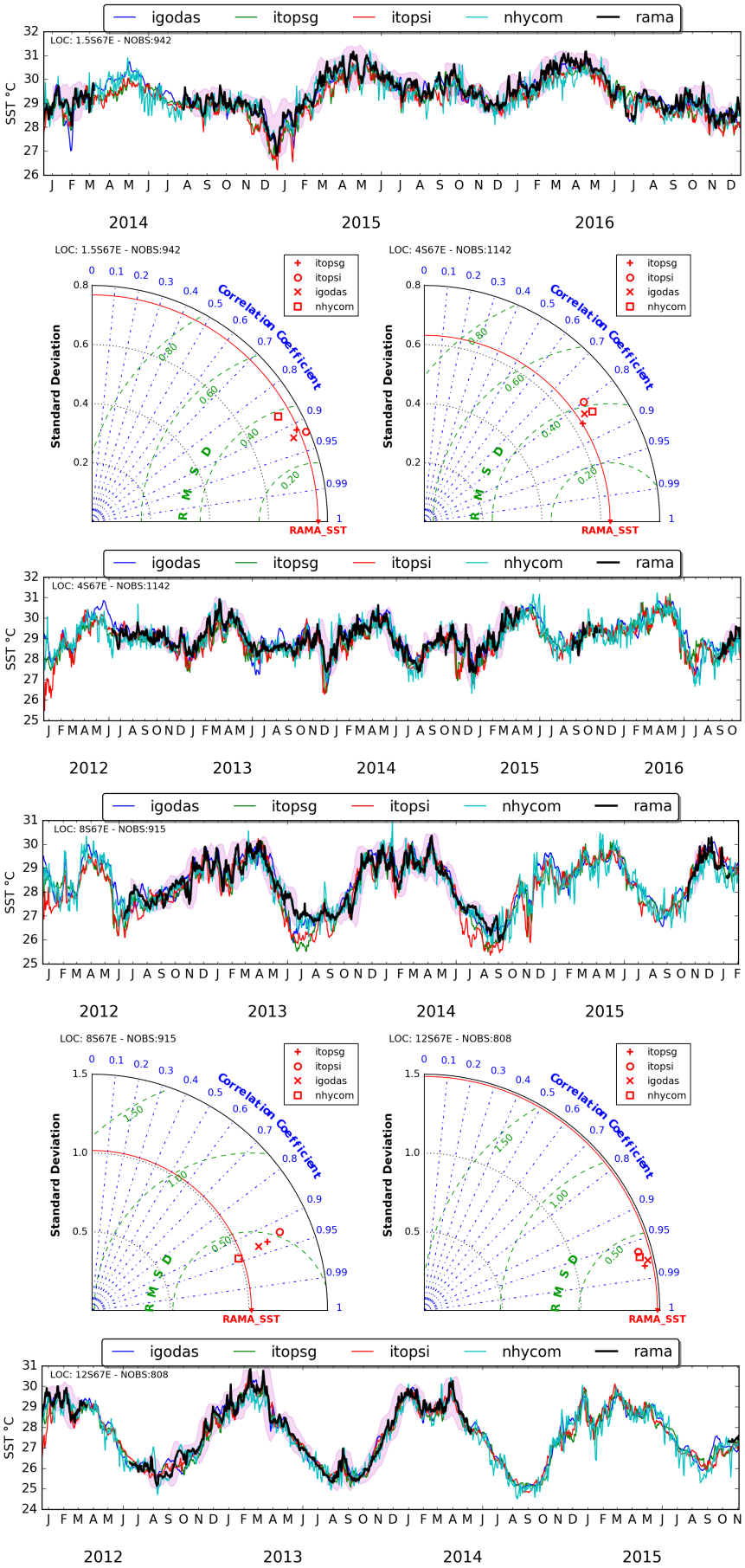

Figure 11: Comparison of SST from RAMA buoys along 67E with models. Pink envelope around RAMA data shows (+/-) 2 std of RAMA SST.

3 Evaluation of Sea Surface Salinity simulations using RAMA buoys

Figure 12: Comparison of SSS from 4 models in terms of mean,standard deviation, bias, rmsd, correlation and skill score with respect to RAMA buoys for the period 2012-2016.

Sea Surface Salinity (SSS) simulated by selected OGCMs, are validated using 24 RAMA buoys which had long timeseries of SSS data for the period 2012–2016. Mean, standard deviation, bias, RMSD, correlation and Skill score for each model is calculated and presented in Figure- 12 and in tabular form Tables - 10 to 15. Figure- 12 and corresponding tables shows that all four models captured the mean of SSS reasonably well. But all the models under estimated the variability of SSS by 0.1 to 0.3 psu of Salinity at many locations. Among the four models, NHYCOM and IGODAS captured the surface salinity variability closest to the observations in most of the cases. IGODAS shows minimum bias followed by ITOPSG,ITOPSI and NHYCOM respectively. Maximum SSS biases shown by all four models are with in +/-0.2 PSU except for locations, where highest bias is arund 0.7 psu for location 8S100E. For all four models, RMSD of SSS is less than 0.3 psu at most of the locations. There are three locations (15N90E, 4S57E and 8S100E) marked by anomalouly high RMSD above 0.5psu for all models. All four models show relatively lower correlation values compared to SST. The values of correlation ranges from 0.3 to 0.6 in most of the sites with few exeptions of higher and lower correlation values.

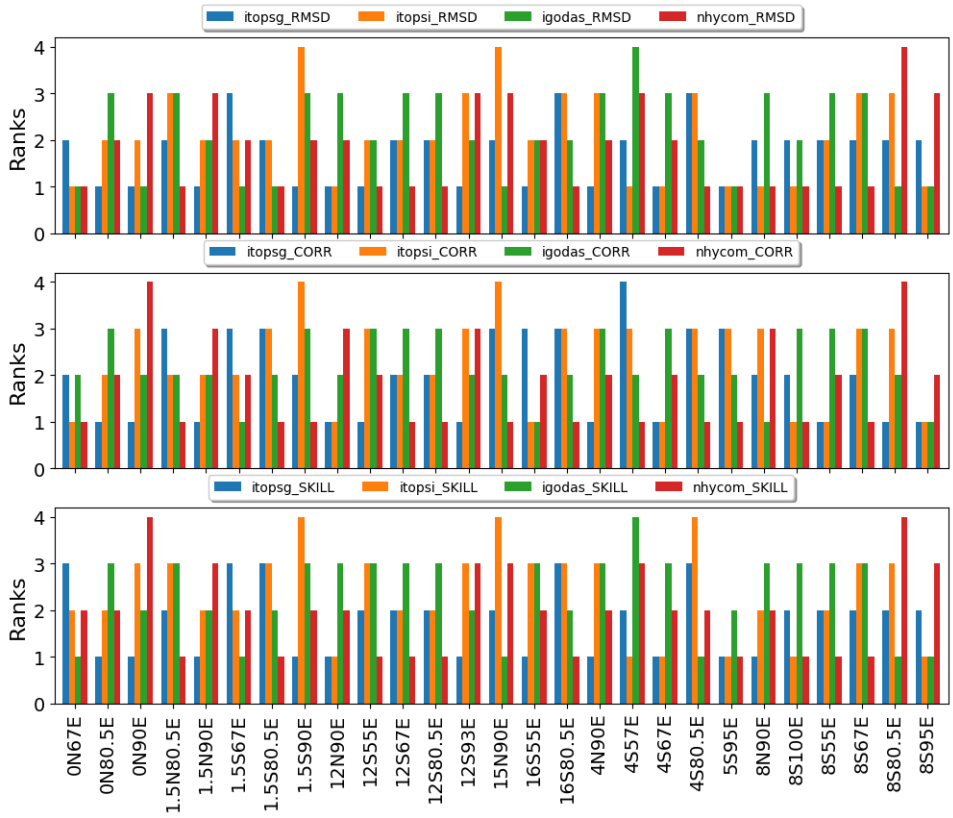

Figure 13: Ranks of four models in terms of their RMSD, correlation and skill score for SSS from 24 RAMA buoy locations. Model with minimum RMSD, maximum correlation & skill score are given a rank of 1 and the one with maximum RMSD, minimum correlation and minimum skill score is given a rank of 4. Intermediae ones are given ranks of 2 and 3

As in the case of SST, ranks of each model is determined for SSS considering minimum RMSD, maximum correlation and skill score from each model and presented as bar charts in Figure- 13. Regarding RMSD of SSS, NHYCOM performed well among the four models with minimum RMSD at 12 locations, followed by ITOPSG at 10 locations and IGODAS and ITOPSI showing minimum RMSD at 7 and 4 sites respectively. Highest correlations were demonstrated by NHYCOM at 13 locations followed by ITOPSG at 10 sites. ITOPSI and IGODAS had highest correlations only at 3 locations each. Though the ranks are stated as above, it may be noted that the differences between the correlations

are not very high among the models. Comparison of skill scores among the four shows that, ITOPSG and NHYCOM have best skills at 9 locations with slightly better skill scores compared to other two models which showed best skills at 3 positions each. Apart from the bar charts and tabular forms, time series and Taylor diagrams of SSS from all four models in comparison with RAMA SSS are presented in Figures- 14 to 16.

Table 11: Mean values of SSS from 24 RAMA buoys for the period 2012–2016 compared with same of selected four ocean models.

Location	Nobs	rama_M	itopsg_M	itopsi_M	igodas_M	nhycom_M
0N67E	857.0	35.14	35.11	35.11	35.11	35.11
0N80.5E	1014.0	34.80	34.73	34.73	34.73	34.73
0N90E	982.0	34.25	34.16	34.16	34.16	34.16
1.5N80.5E	390.0	34.79	34.73	34.73	34.73	34.73
1.5N90E	133.0	34.20	34.06	34.06	34.06	34.06
1.5S67E	928.0	35.08	35.05	35.05	35.05	35.05
1.5S80.5E	1036.0	34.80	34.67	34.67	34.67	34.67
1.5S90E	487.0	34.28	34.24	34.24	34.24	34.24
12N90E	1168.0	33.10	33.09	33.09	33.09	33.09
12S55E	923.0	34.87	34.95	34.95	34.95	34.95
12S67E	668.0	34.63	34.69	34.69	34.69	34.69
12S80.5E	1644.0	34.37	34.40	34.40	34.40	34.40
12S93E	790.0	34.24	34.13	34.13	34.13	34.13
15N90E	1009.0	32.68	32.34	32.34	32.34	32.34
16S55E	459.0	34.91	34.96	34.96	34.96	34.96
16S80.5E	787.0	34.51	34.55	34.55	34.55	34.55
4N90E	644.0	33.91	33.89	33.89	33.89	33.89
4S57E	228.0	35.15	34.57	34.57	34.57	34.57
4S67E	555.0	35.04	35.00	35.00	35.00	35.00
4S80.5E	1088.0	34.67	34.62	34.62	34.62	34.61
5S95E	1266.0	34.13	34.11	34.11	34.11	34.10
8N90E	888.0	33.56	33.62	33.62	33.62	33.69
8S100E	202.0	33.90	32.97	32.97	32.97	32.97
8S55E	644.0	34.94	35.07	35.07	35.07	35.10
8S67E	913.0	34.75	34.80	34.80	34.80	34.80
8S80.5E	1259.0	34.42	34.43	34.43	34.43	34.38
8S95E	1451.0	34.13	34.02	34.02	34.02	34.00

Table 12: Standard deviations of SSS from 24 RAMA buoys for the period 2012–2016 compared with same of selected four ocean models.

Location	Nobs	rama_SD	itopsg_SD	itopsi_SD	igodas_SD	nhycom_SD
0N67E	857.0	0.36	0.22	0.21	0.32	0.26
0N80.5E	1014.0	0.36	0.28	0.26	0.34	0.28
0N90E	982.0	0.34	0.22	0.21	0.30	0.27
1.5N80.5E	390.0	0.48	0.30	0.29	0.37	0.22
1.5N90E	133.0	0.31	0.19	0.19	0.32	0.16
1.5S67E	928.0	0.28	0.17	0.16	0.26	0.22
1.5S80.5E	1036.0	0.35	0.21	0.20	0.26	0.25
1.5S90E	487.0	0.25	0.20	0.18	0.25	0.21
12N90E	1168.0	0.57	0.30	0.28	0.57	0.35
12S55E	923.0	0.22	0.15	0.13	0.24	0.19
12S67E	668.0	0.34	0.16	0.16	0.26	0.23
12S80.5E	1644.0	0.33	0.20	0.19	0.34	0.25
12S93E	790.0	0.23	0.12	0.12	0.23	0.17
15N90E	1009.0	0.84	0.46	0.42	0.65	0.44
16S55E	459.0	0.19	0.10	0.10	0.21	0.16
16S80.5E	787.0	0.22	0.13	0.13	0.19	0.16
4N90E	644.0	0.56	0.41	0.34	0.63	0.41
4S57E	228.0	0.42	0.14	0.15	0.17	0.21
4S67E	555.0	0.22	0.13	0.12	0.19	0.16
4S80.5E	1088.0	0.39	0.22	0.22	0.36	0.29
5S95E	1266.0	0.27	0.19	0.20	0.20	0.22
8N90E	888.0	0.48	0.32	0.34	0.61	0.28
8S100E	202.0	1.11	0.11	0.09	0.21	0.22
8S55E	644.0	0.31	0.18	0.19	0.31	0.21
8S67E	913.0	0.54	0.31	0.29	0.55	0.33
8S80.5E	1259.0	0.52	0.34	0.29	0.48	0.35
8S95E	1451.0	0.30	0.18	0.16	0.27	0.24

Table 13: Bias of simulated SSS from selected four ocean models with respect to 24 RAMA buoys for the period 2012–2016.

Location	Nobs	itopsg_BIAS	itopsi_BIAS	igodas_BIAS	nhycom_BIAS
0N67E	857.0	-0.03	-0.06	0.04	-0.05
0N80.5E	1014.0	-0.07	-0.10	0.04	-0.06
0N90E	982.0	-0.10	-0.12	-0.07	-0.13
1.5N80.5E	390.0	-0.05	-0.10	0.09	-0.08
1.5N90E	133.0	-0.14	-0.14	0.00	-0.26
1.5S67E	928.0	-0.03	-0.05	0.02	-0.04
1.5S80.5E	1036.0	-0.13	-0.15	-0.03	-0.12
1.5S90E	487.0	-0.04	-0.09	-0.03	-0.09
12N90E	1168.0	-0.01	0.04	0.13	-0.07
12S55E	923.0	0.08	0.10	0.00	0.04
12S67E	668.0	0.06	0.07	-0.06	-0.03
12S80.5E	1644.0	0.03	0.04	-0.01	-0.07
12S93E	790.0	-0.11	-0.13	-0.00	-0.14
15N90E	1009.0	-0.34	-0.39	-0.15	-0.48
16S55E	459.0	0.05	0.05	-0.09	0.05
16S80.5E	787.0	0.04	0.05	-0.02	-0.06
4N90E	644.0	-0.02	-0.09	0.15	-0.19
4S57E	228.0	-0.58	-0.56	-0.68	-0.68
4S67E	555.0	-0.04	-0.02	-0.10	-0.06
4S80.5E	1088.0	-0.05	-0.07	-0.06	-0.10
5S95E	1266.0	-0.02	-0.04	-0.08	-0.12
8N90E	888.0	0.06	0.06	0.02	-0.02
8S100E	202.0	-0.93	-0.95	-0.88	-0.92
8S55E	644.0	0.14	0.16	0.04	0.06
8S67E	913.0	0.05	0.07	0.00	-0.06
8S80.5E	1259.0	0.01	0.05	0.05	-0.16
8S95E	1451.0	-0.10	-0.10	-0.07	-0.15

Table 14: Root Mean Square Difference (RMSD) of simulated SSS from selected four ocean models with respect to 24 RAMA buoys for the period 2012–2016.

Location	Nobs	itopsg_RMSD	itopsi_RMSD	igodas_RMSD	nhycom_RMSD
0N67E	857.0	0.19	0.21	0.17	0.17
0N80.5E	1014.0	0.21	0.24	0.26	0.22
0N90E	982.0	0.25	0.28	0.25	0.29
1.5N80.5E	390.0	0.45	0.45	0.47	0.41
1.5N90E	133.0	0.28	0.30	0.36	0.40
1.5S67E	928.0	0.18	0.19	0.16	0.17
1.5S80.5E	1036.0	0.35	0.36	0.27	0.27
1.5S90E	487.0	0.19	0.23	0.22	0.20
12N90E	1168.0	0.48	0.51	0.62	0.53
12S55E	923.0	0.16	0.18	0.19	0.16
12S67E	668.0	0.26	0.28	0.30	0.24
12S80.5E	1644.0	0.20	0.22	0.22	0.18
12S93E	790.0	0.22	0.24	0.23	0.26
15N90E	1009.0	0.84	0.88	0.77	0.85
16S55E	459.0	0.18	0.18	0.19	0.19
16S80.5E	787.0	0.17	0.19	0.16	0.14
4N90E	644.0	0.33	0.40	0.49	0.42
4S57E	228.0	0.73	0.72	0.77	0.76
4S67E	555.0	0.16	0.17	0.23	0.18
4S80.5E	1088.0	0.26	0.26	0.23	0.22
5S95E	1266.0	0.26	0.24	0.26	0.26
8N90E	888.0	0.43	0.40	0.54	0.40
8S100E	202.0	1.45	1.47	1.45	1.39
8S55E	644.0	0.23	0.25	0.26	0.21
8S67E	913.0	0.34	0.35	0.36	0.33
8S80.5E	1259.0	0.26	0.31	0.25	0.32
8S95E	1451.0	0.24	0.24	0.23	0.27

Table 15: Correlation of SSS from selected four ocean models with respect to 24 RAMA buoys for the period 2012–2016.

Location	Nobs	itopsg_CORR	itopsi_CORR	igodas_CORR	nhycom_CORR
0N67E	857.0	0.89	0.88	0.89	0.91
0N80.5E	1014.0	0.84	0.81	0.74	0.82
0N90E	982.0	0.75	0.68	0.72	0.66
1.5N80.5E	390.0	0.41	0.46	0.45	0.56
1.5N90E	133.0	0.60	0.54	0.35	0.34
1.5S67E	928.0	0.80	0.79	0.83	0.82
1.5S80.5E	1036.0	0.43	0.38	0.65	0.73
1.5S90E	487.0	0.69	0.57	0.64	0.74
12N90E	1168.0	0.54	0.43	0.43	0.41
12S55E	923.0	0.77	0.78	0.66	0.74
12S67E	668.0	0.72	0.63	0.54	0.73
12S80.5E	1644.0	0.81	0.77	0.79	0.87
12S93E	790.0	0.61	0.53	0.51	0.42
15N90E	1009.0	0.43	0.37	0.52	0.55
16S55E	459.0	0.40	0.36	0.66	0.46
16S80.5E	787.0	0.64	0.56	0.69	0.82
4N90E	644.0	0.82	0.73	0.70	0.74
4S57E	228.0	-0.06	-0.03	0.52	0.56
4S67E	555.0	0.69	0.64	0.49	0.65
4S80.5E	1088.0	0.80	0.80	0.83	0.85
5S95E	1266.0	0.43	0.52	0.48	0.60
8N90E	888.0	0.50	0.59	0.53	0.38
8S100E	202.0	0.12	-0.07	-0.09	0.42
8S55E	644.0	0.83	0.78	0.66	0.76
8S67E	913.0	0.83	0.84	0.79	0.84
8S80.5E	1259.0	0.90	0.86	0.88	0.84
8S95E	1451.0	0.70	0.67	0.70	0.68

Table 16: Skill score of SSS from selected four ocean models with respect to 24 RAMA buoys for the period 2012–2016.

Location	Nobs	itopsg_SKILL	itopsi_SKILL	igodas_SKILL	nhycom_SKILL
0N67E	857.0	0.71	0.66	0.79	0.77
0N80.5E	1014.0	0.66	0.57	0.49	0.64
0N90E	982.0	0.48	0.35	0.46	0.29
1.5N80.5E	390.0	0.11	0.15	0.06	0.27
1.5N90E	133.0	0.17	0.09	-0.32	-0.60
1.5S67E	928.0	0.60	0.54	0.67	0.64
1.5S80.5E	1036.0	0.01	-0.09	0.40	0.41
1.5S90E	487.0	0.44	0.18	0.28	0.39
12N90E	1168.0	0.29	0.18	-0.20	0.11
12S55E	923.0	0.47	0.39	0.28	0.51
12S67E	668.0	0.42	0.33	0.22	0.52
12S80.5E	1644.0	0.61	0.54	0.56	0.71
12S93E	790.0	0.15	-0.02	0.03	-0.27
15N90E	1009.0	0.01	-0.09	0.17	-0.02
16S55E	459.0	0.07	0.03	-0.06	0.00
16S80.5E	787.0	0.37	0.26	0.44	0.60
4N90E	644.0	0.66	0.49	0.23	0.43
4S57E	228.0	-2.07	-1.98	-2.40	-2.33
4S67E	555.0	0.43	0.40	-0.11	0.34
4S80.5E	1088.0	0.57	0.56	0.66	0.64
5S95E	1266.0	0.11	0.20	0.09	0.11
8N90E	888.0	0.21	0.32	-0.27	0.05
8S100E	202.0	-0.68	-0.75	-0.69	-0.56
8S55E	644.0	0.43	0.32	0.30	0.53
8S67E	913.0	0.61	0.59	0.57	0.63
8S80.5E	1259.0	0.75	0.65	0.77	0.59
8S95E	1451.0	0.36	0.33	0.40	0.18

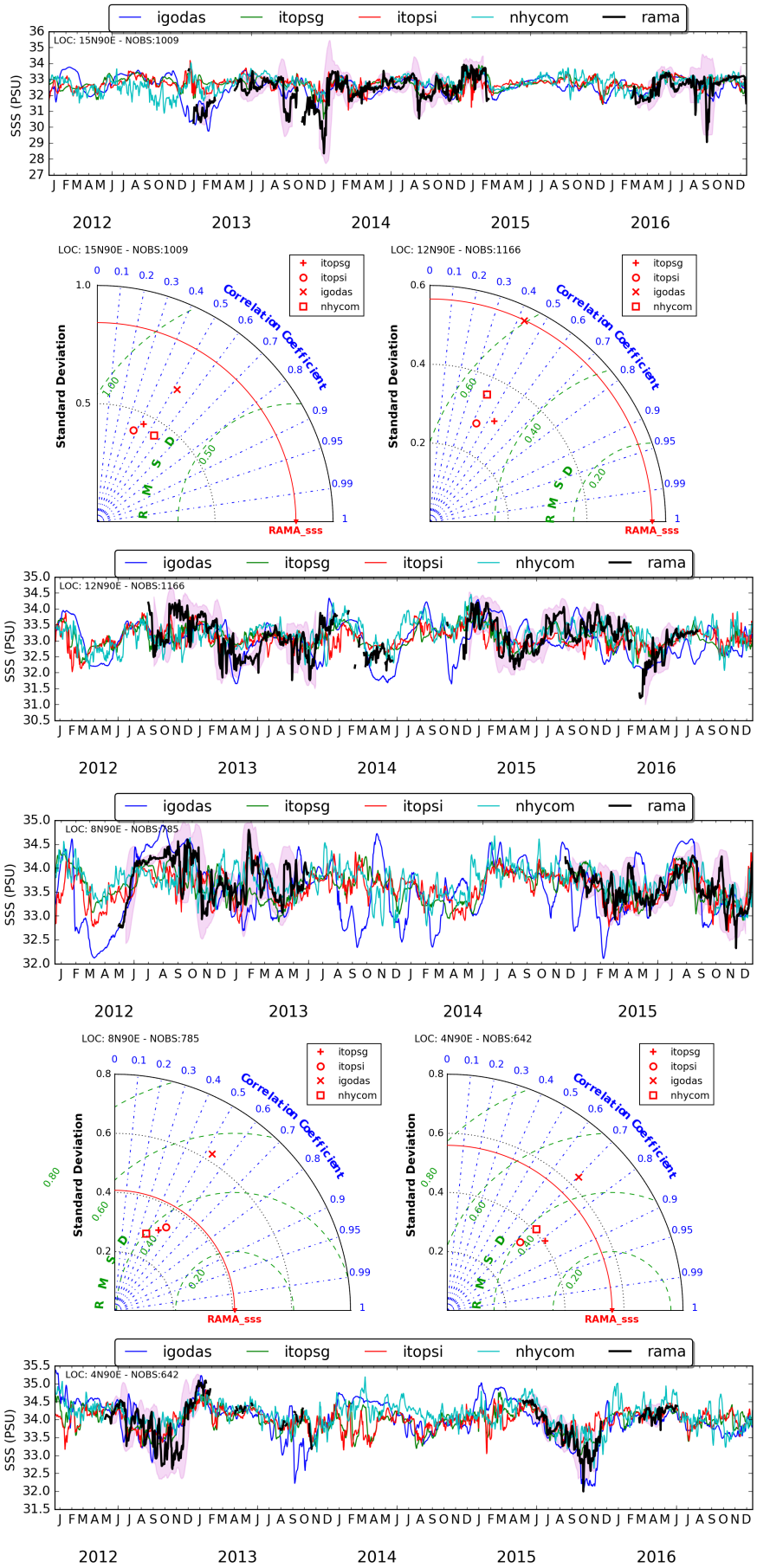

Figure 14: Comparison of SSS from RAMA buoys in BoB with models. Pink envelope around RAMA data shows (+/-) 2-std of RAMA SSS.

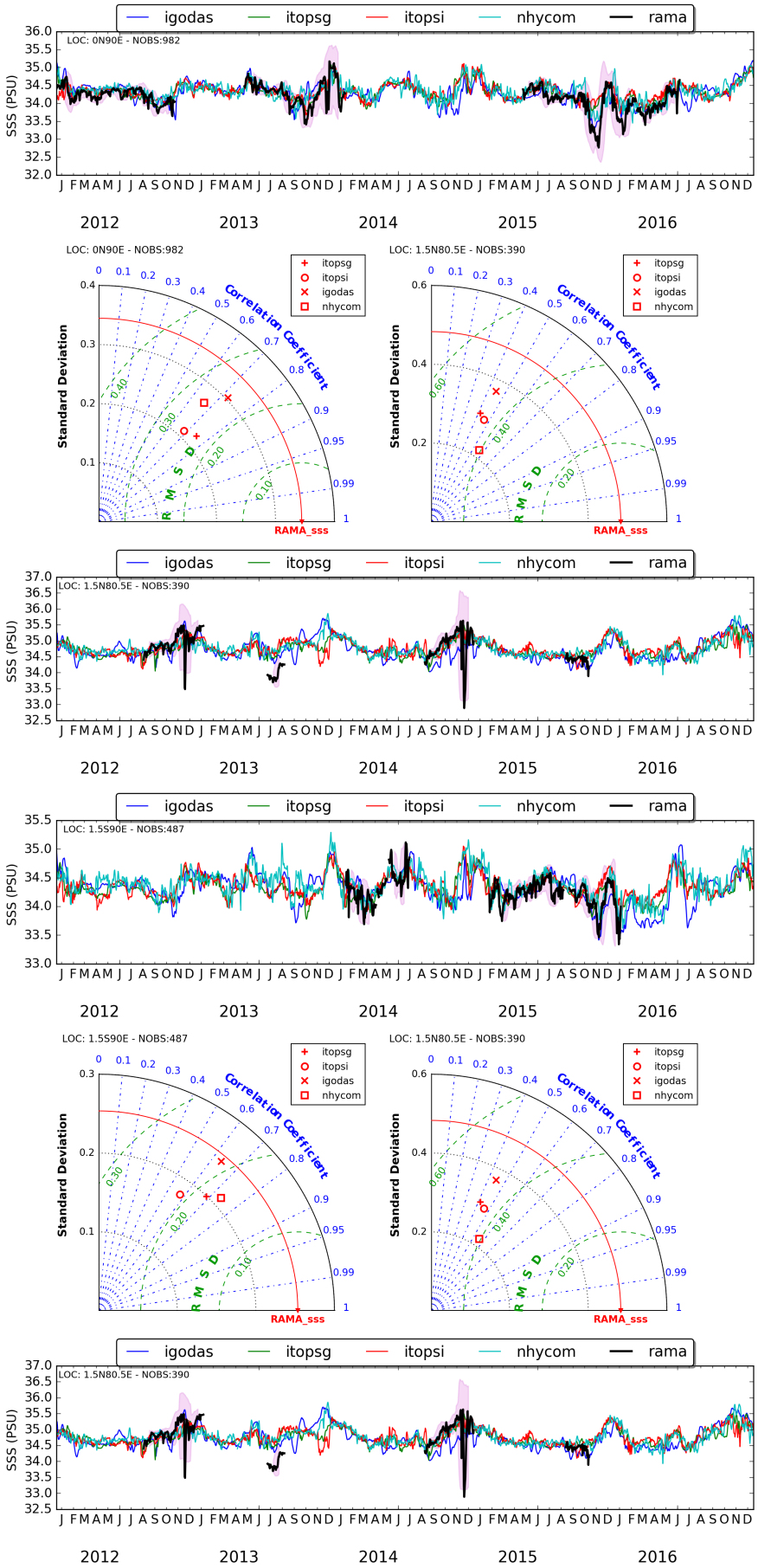

Figure 15: Comparison of SSS from RAMA buoys in EEIO with models. Pink envelope around RAMA data shows (+/-) 2-std of RAMA SSS.

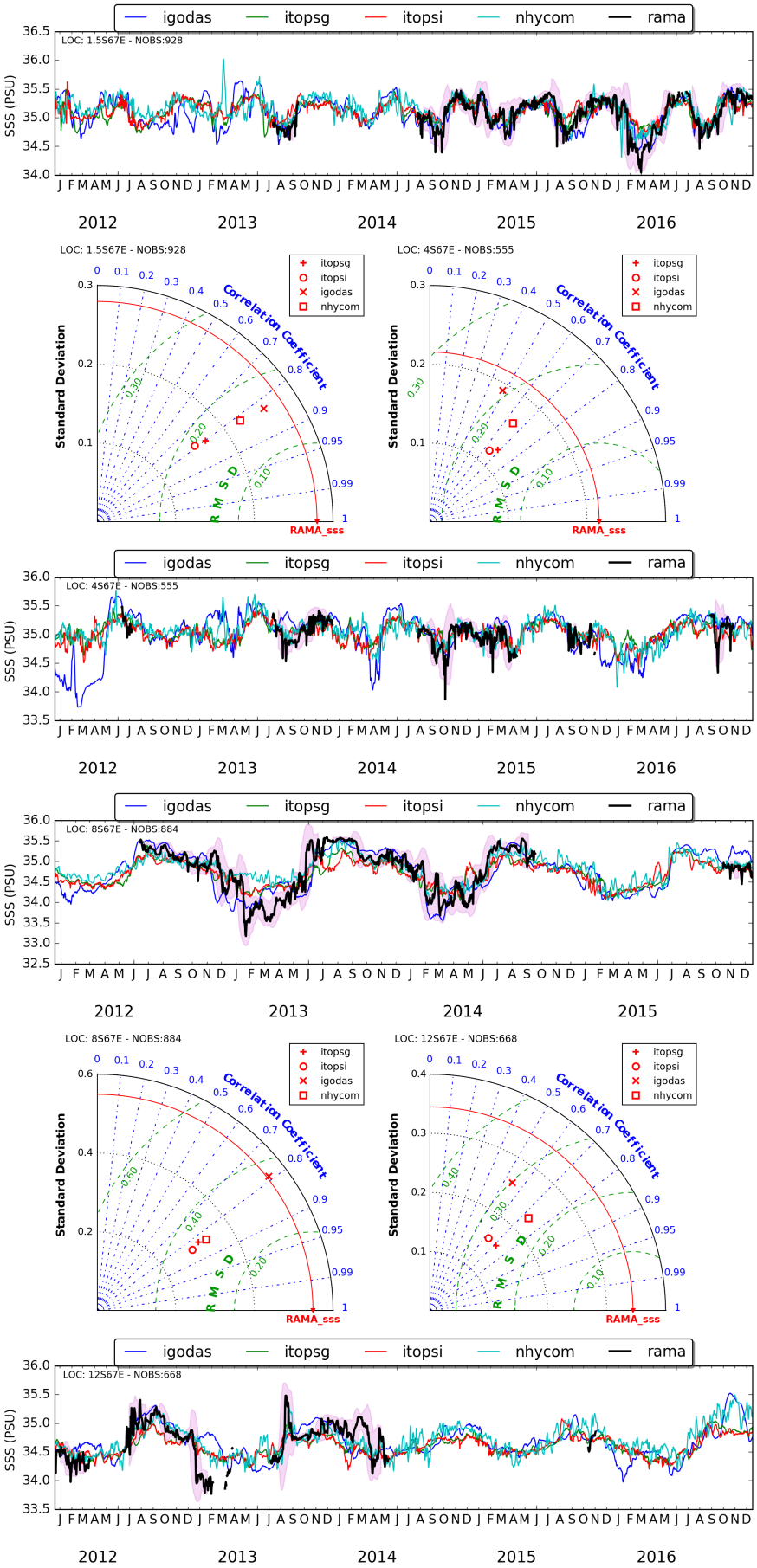

Figure 16: Comparison of SSS from RAMA buoys along 67E with models. Pink envelope around RAMA data shows (+/-) 2-std of RAMA SSS.

4 Evaluation of Sea Level Anomaly simulations

Sea level and projections of it in different time scales has serious implications to coastal zone management and administraton. Hence accurate forecast of the sea-level is one of the critical parameters of ocean simulations used by large groups of policymakers. Sea level anomalies (SLA) from four selected models is validated in this section by comparing them with the multi-satellite gridded maps from AVISO. As mean dynamic topography is not defined uniformly among the models and in case of Aviso, the time mean is removed from each grid point before subjecting the modelled and observed data to statistical analysis. Basin-scale maps of bias, RMSD and correlation of each model with observation is computed and presented as maps in Figures - 17 to 21. For quantitative comparison absolute biases, RMSD and correlation values from each grid points are partitioned into several bins and presented as bar charts at bottom raws of map panels.

Validation of SLA from the first year of hindcast is presented in Figure - 17. Maps of biases for the year 2012 (Figure - 17) shows that minimum values on basin scale bias are for NHYCOM with 49 % of grid points having a bias between 0-5 cm bin compared to the aviso SLA. IGODAS has 24% of grids in above bin followed by 16% in case of ITOPSI and 10% ITOPSG. For the year 2013, ITOPSI has the minimum bias with 24% of SLA values having a bias of 0-5 cm followed by IGODAS with 23% values, ITOPSG with 21% and NHYCOM with 18% of values. ITOPSG shows minimum bias for the year 2014 with 26% of data having less than 5cm biases followed by ITOPSI with 24%, IGODAS with 20% and NHYCOM 13% respectively. For the years 2015 and 2016, the biases are higher in all four models indicated by less number of grid points with biases less than 5 cm. RMSD of SLA shows good performance in case of all four models compared to AVISO SLA. Regarding correlation, ITOPSG shows the best performance having 67 to 72% of grid points having a correlation between 0.8 to 1 for the five year period. ITOPSI stands second with 50 to 62% grid points with highest bin correlations. NHYCOM and IGODAS stand 3^{rd} and 4^{th} position with 51 to 59% and 21 to 31% grid points respectively in the highest correlation bin.

High biases are seen in the south-western corner of the basin for all four models and is one of the most dynamic regions where Agulhas rings originates and spread to Atlantic ocean. In general southern Indian ocean has higher biases. Minimum biases are seen in the eastern equatorial Indian ocean for all four models. About 50% of the SLA from NHYCOM has less than 5 cm bias for the year 2012 which is exceptional compared other years of it and other models, where approximately 20% data is seen to be in this range in general. For all the models, more than 50% of the data is having biases in the range of 5 to 10cm.

RMSD is less than 2 cm for 80% of data from all the models for the five year period. RMSD is more than 7 cm in eddy rich south-western Indian Ocean for all four models with varying intensity. IGODAS has high RMSD in general for the southern Indian Ocean compared to other models, as its resolution is only about half degree there. Another common area with poor RMSD is western AS, north of great whirl which is a dynamic westeren boundary region.

Spatial maps of correlation show similar spatial distribution in case of ITOPSI, ITOPSG and NHYCOM. In case of IGODAS, the highest correlation is limited to the equatorial Indian Ocean and the southeastern Arabian Sea. All four models show a unique region with highest correlation in southeastern Indian ocean between 10S to 20S. In general, all models show a poor correlation in the southern Indian Ocean, which is particularly so in the case of IGODAS as it has a lower resolution for the region.

Evaluation of 2012 SLA simulations

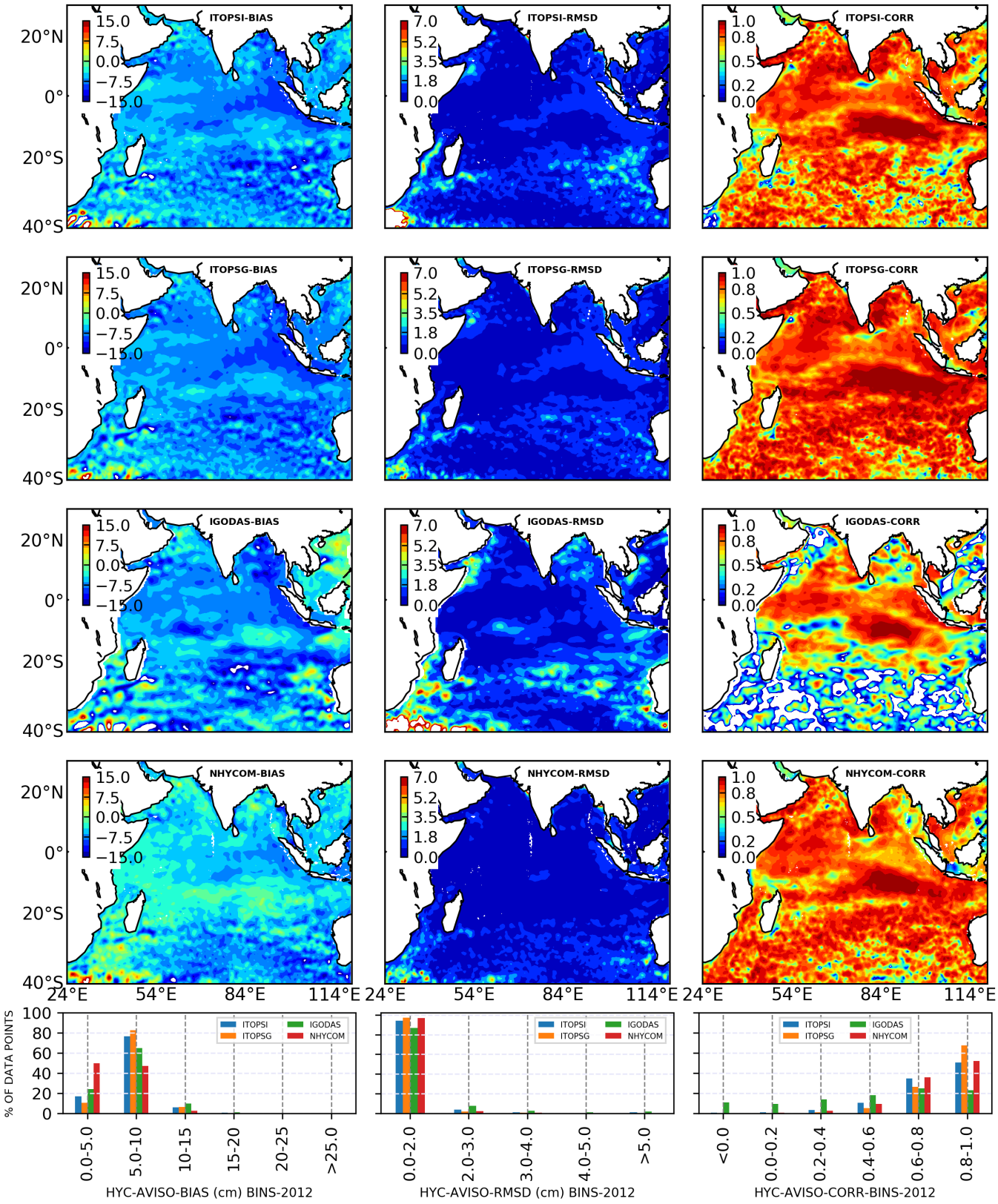

Figure 17: Comparison of 2012 SLA simulations from ITOPSI, ITPOSG, IGODAS and NHYCOM with AVISO gridded SLA.

Evaluation of 2013 SLA simulations

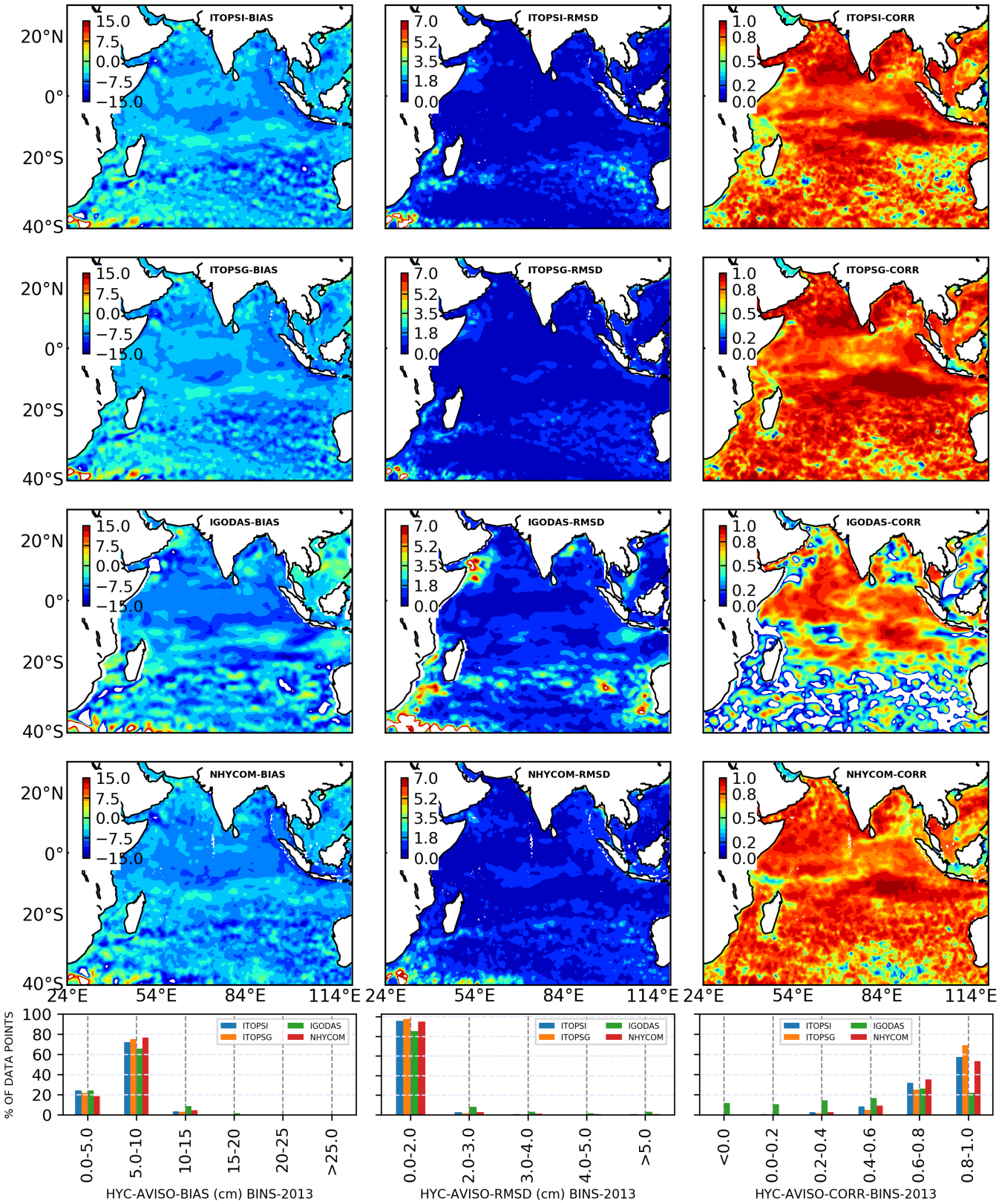

Figure 18: Comparison of 2013 SLA simulations from ITOPSI, ITPOSG, IGODAS and NHYCOM with AVISO gridded SLA.

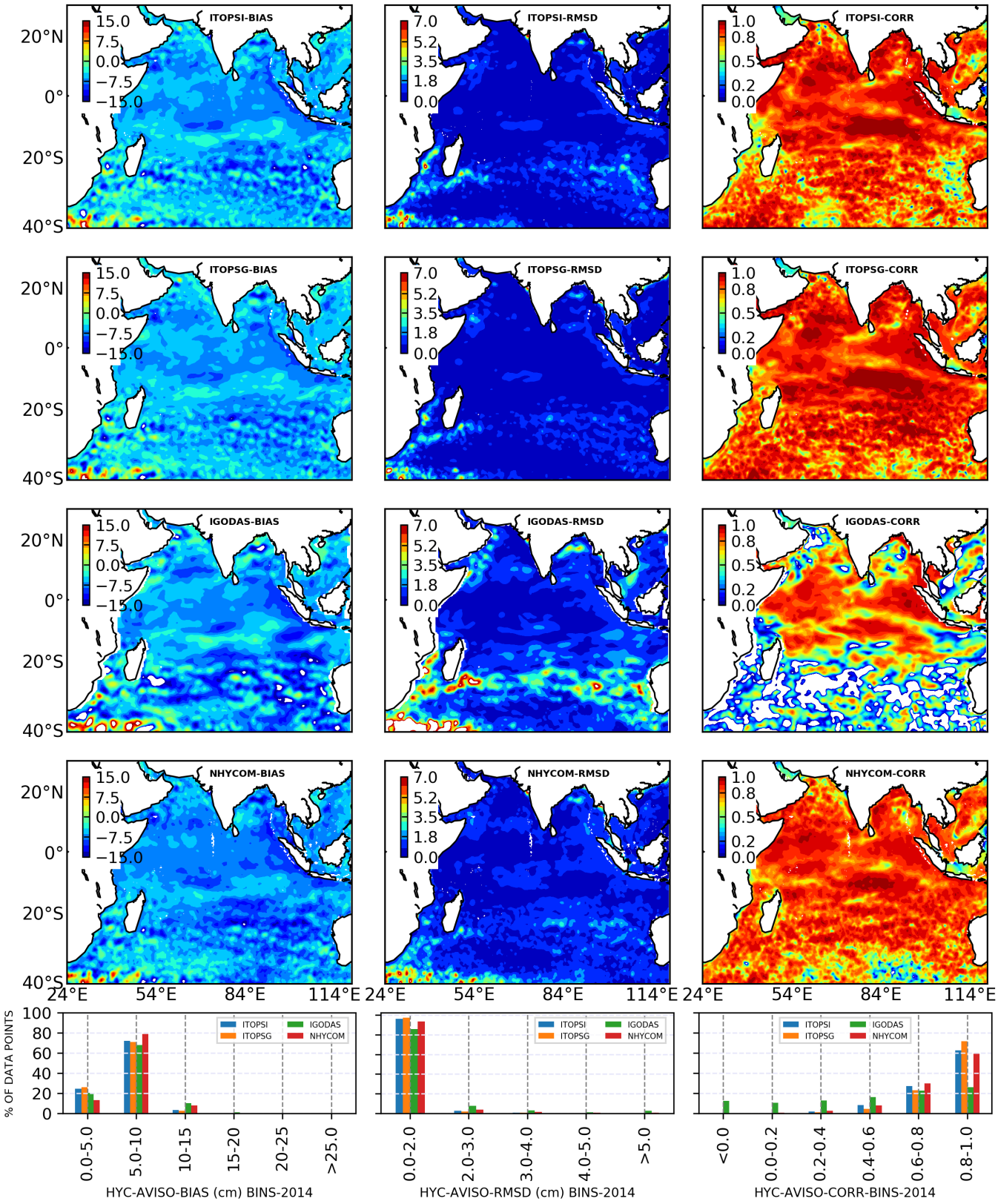

Figure 19: Comparison of 2014 SLA simulations from ITOPSI, ITPOSG, IGODAS and NHYCOM with AVISO gridded SLA.

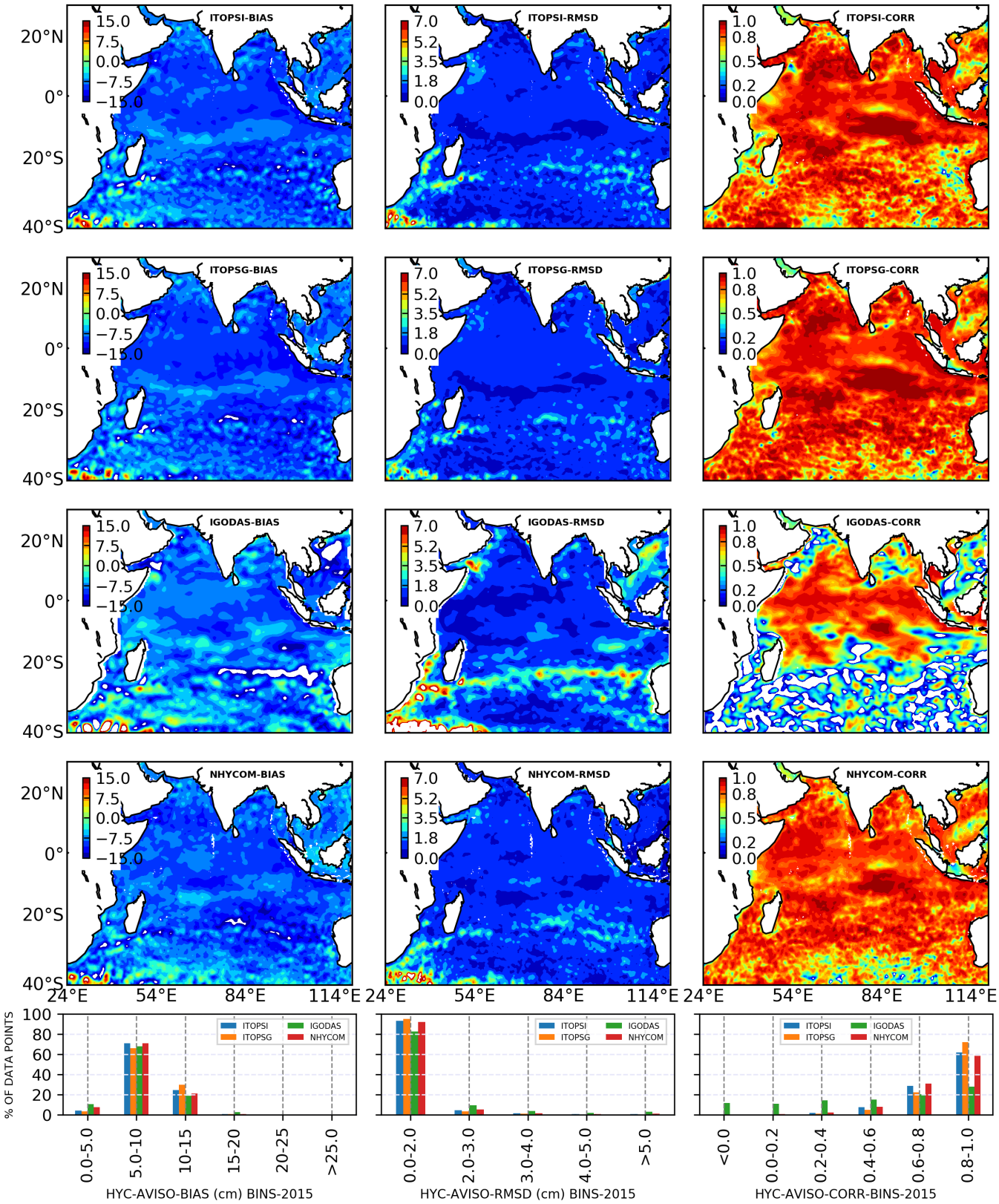

Figure 20: Comparison of 2015 SLA simulations from ITOPSI, ITPOSG, IGODAS and NHYCOM with AVISO gridded SLA.

Evaluation of 2016 SLA simulations

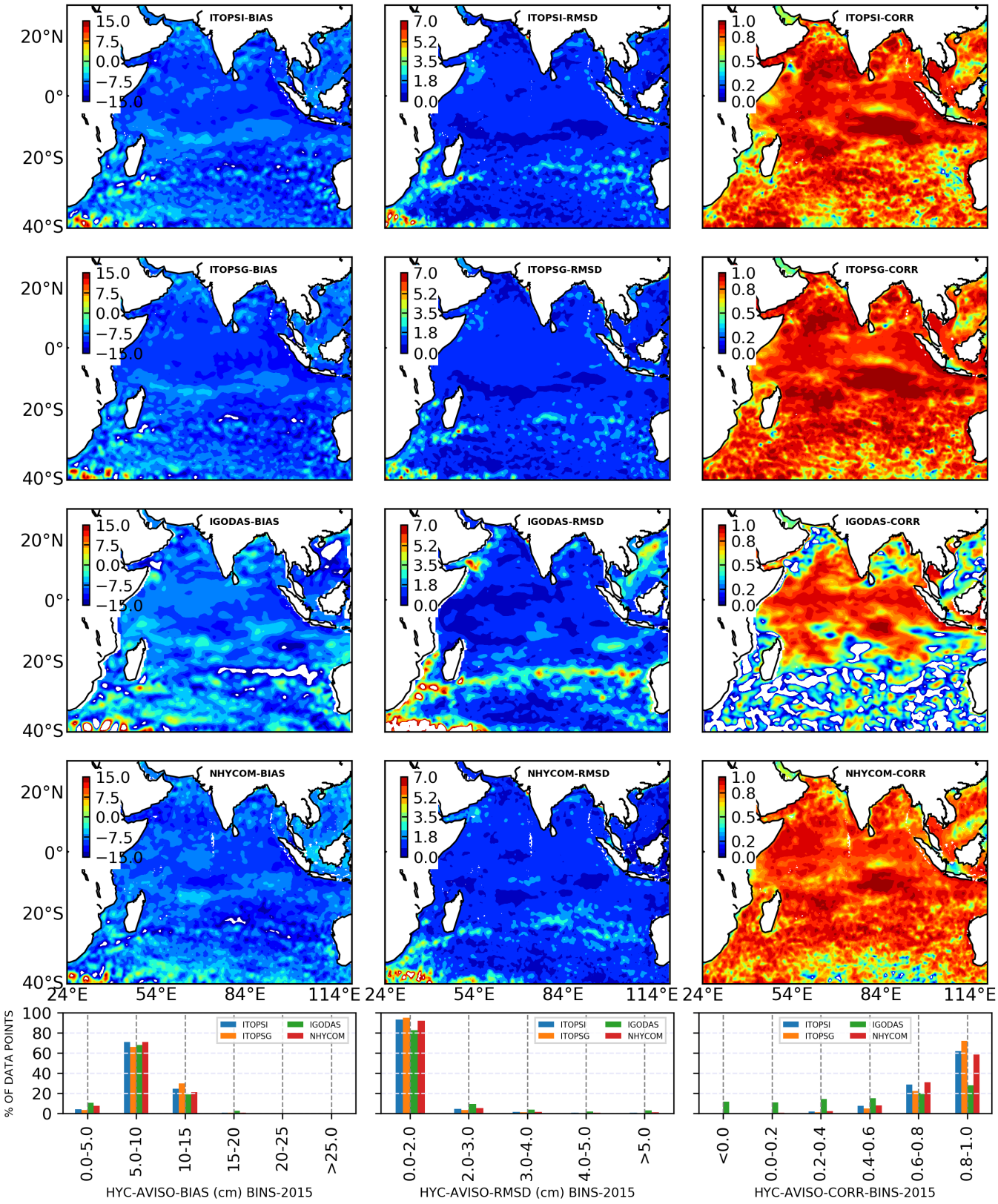

Figure 21: Comparison of 2016 SLA simulations from ITOPSI, ITPOSG, IGODAS and NHYCOM with AVISO gridded SLA.

5 Evaluation of Surface currents using OSCAR data

The accurate prediction of ocean currents is one of the essential parameters which is in high demand from the operational oceanography user community. However, precise simulation of ocean currents is a challenging task due to deficiencies in model physics as well as the same in atmospheric forcing. In this section, we have compared simulated currents from selected four models with OSCAR currents [Bonjean and Lagerloef, 2002] on a basin-scale. We have extracted the OSCAR data for the Indian Ocean available at $\frac{1}{3}^{\circ}$ resolution and with seven-day temporal resolution. The simulated currents from each model are interpolated to the OSCAR grid. Spatial maps of bias RMSD and correlation are computed from each model in comparison with OSCAR. For the quantitative examination of the above maps, the number of grid points falling under predefined target bins of each statistical parameter mentioned above was calculated and presented as bar-charts beside spatial maps of each statistical parameter considered. In case of bias, the absolute values are used for creating bins.

Maps of bias, RMSD and correlation calculated for each year from 2012 to 2016 are presented in Figures 22 to 31 (column-I) for both zonal and meridional components. A common defect shown in all four models is the negative bias observed in equatorial zonal currents Figures 22 to 31 for each year analysed with a certain percentage of interannual variability in intensity and east-west location of the negatively biased patch. Further, there is a positive bias for all models south of equator which extend almost across the basin. Among the four models, ITOPSG has the least bias for the negatively and positive belts described above followed by ITOPSI, IGODAS and NHYCOM in increasing order of biases. In case of meridional currents, no such location-specific bias is observed in any of the models considered.

The maps of RMSD shows maximum errors along the equator in case of both zonal and meridional components of currents Figures 22 to 31 (column-II). There is an amplification of RMSD at the western part of the equator near the highly dynamic Great Whirl (GW) region in all models. Apart from this, errors are amplified along the western boundary of the basin in general, which is also enhanced at the southwestern corner of the basin, where Agulhas rings develop and spreads to Atlantic ocean. Among the four models, RMSD is minimum for ITPOSG followed by ITOPSI,IGODAS and NHYCOM respectively in the increasing order of RMSD for both zonal and meridional components of currents.

Figures 22 to 31 (column-III) shows correlation maps for both zonal and meridional components of simulated currents from selected four models. Unlike the bias and RMSD values, correlation shows large spatial variability within the basin. There are several pockets of higher and lover correlation areas within the basin. In general, all the hycom models shows the highest correlation in the south of the equator at the eastern side of the basin. Western parts of both Arabian Sea and Bay of Bengal also shows relatively better correlations. Notable regions of poor correlation are eastern side of BoB, the eastern boundary of the equator and southern Indian ocean. In case of meridional currents, poor correlations are observed along the equator as a pattern for ITOPSI, ITOPSG and NHYCOM. In general correlations of IGODAS with OSCAR currents are poor compared to other three models away from equator. Among the four models, ITOPSG consistently showed the best correlation with 34 to 38% grid points of correlation values between 0.6 to 0.8 followed by ITOPSI with 31 to 35% grid points falling same range of correlation. NHYCOM has 30 to 35% grid points falling in above range of correlation. IGODAS has less than 20% grid points within above range of correlation.

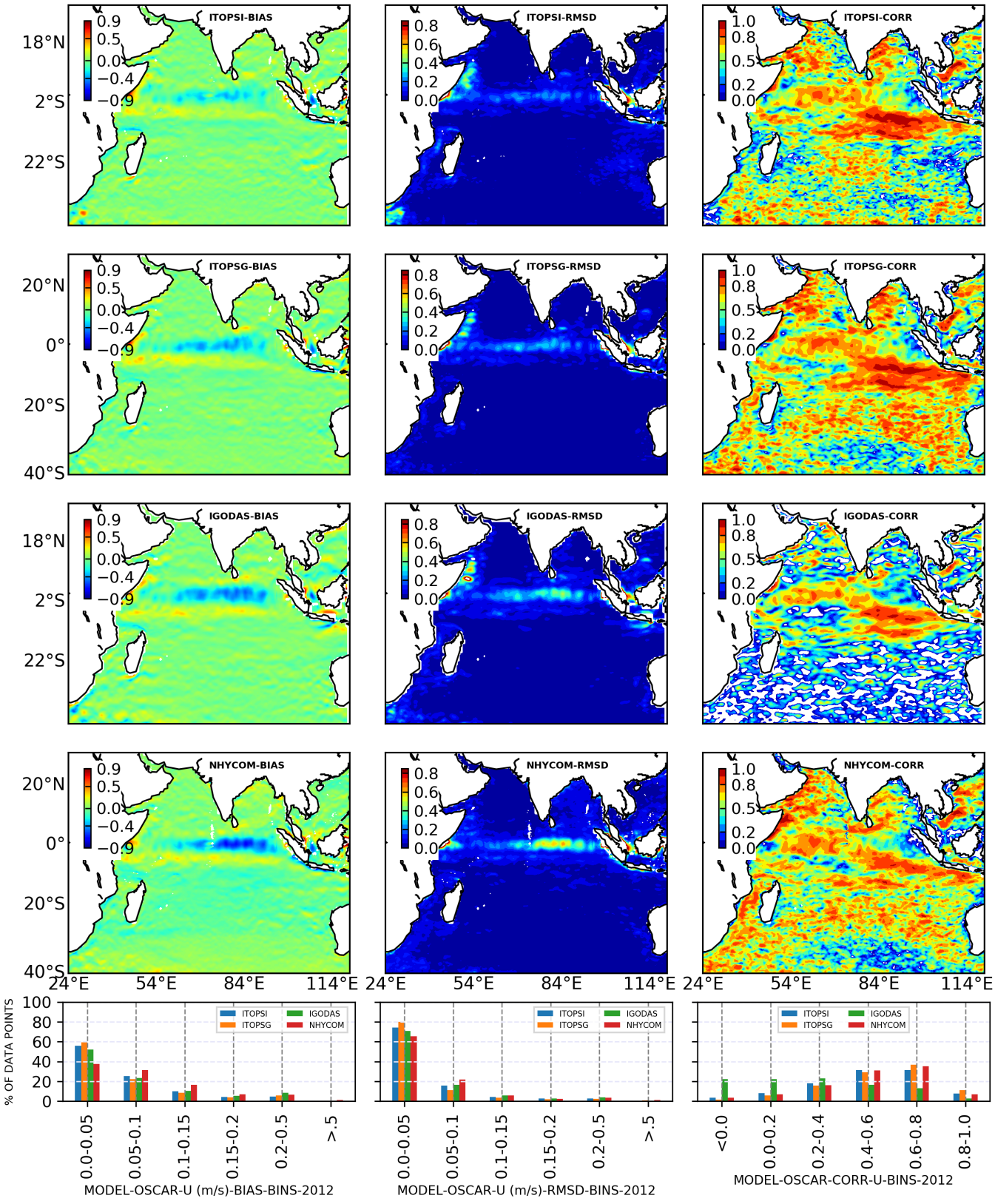

Figure 22: Comparison of 2012 Zonal current (u) simulations from ITOPSI, ITPOSG, IGODAS and NHYCOM with OSCAR Zonal Currents

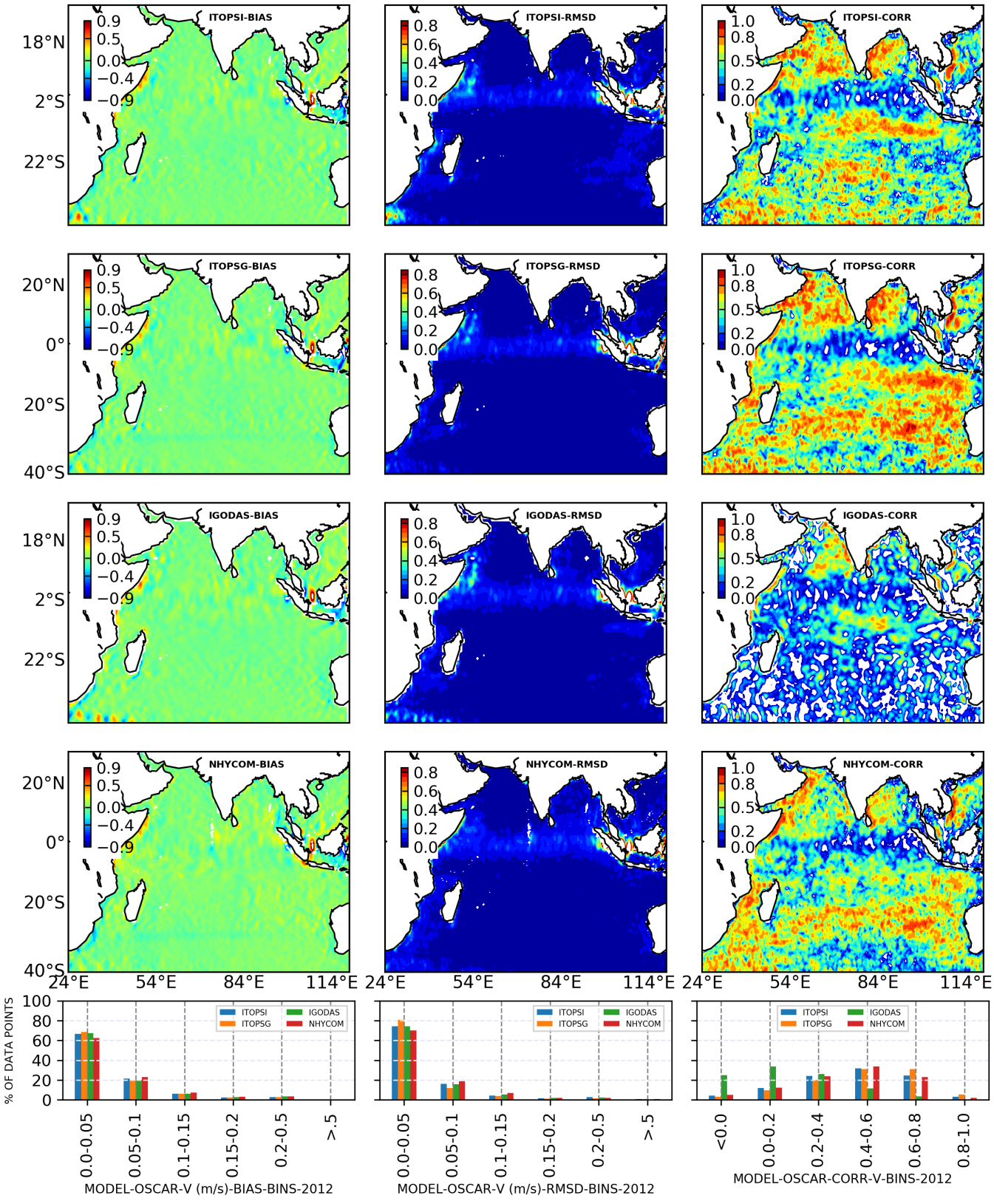

Figure 23: Comparison of 2012 meridional current (v) simulations from ITOPSI, ITPOSG, IGODAS and NHYCOM with OSCAR meridional Currents

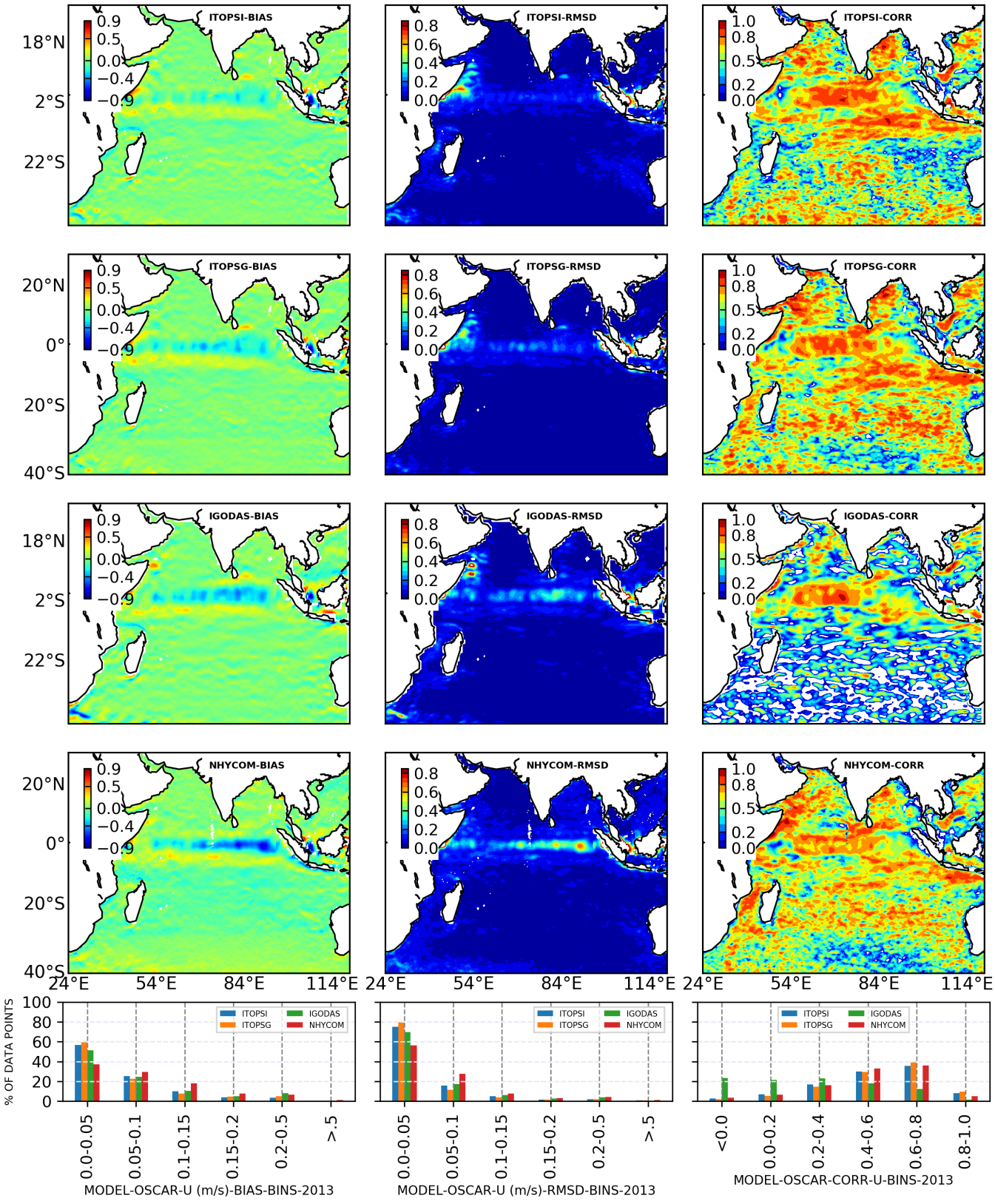

Figure 24: Comparison of 2013 Zonal current (u) simulations from ITOPSI, ITPOSG, IGODAS and NHYCOM with OSCAR Zonal Currents

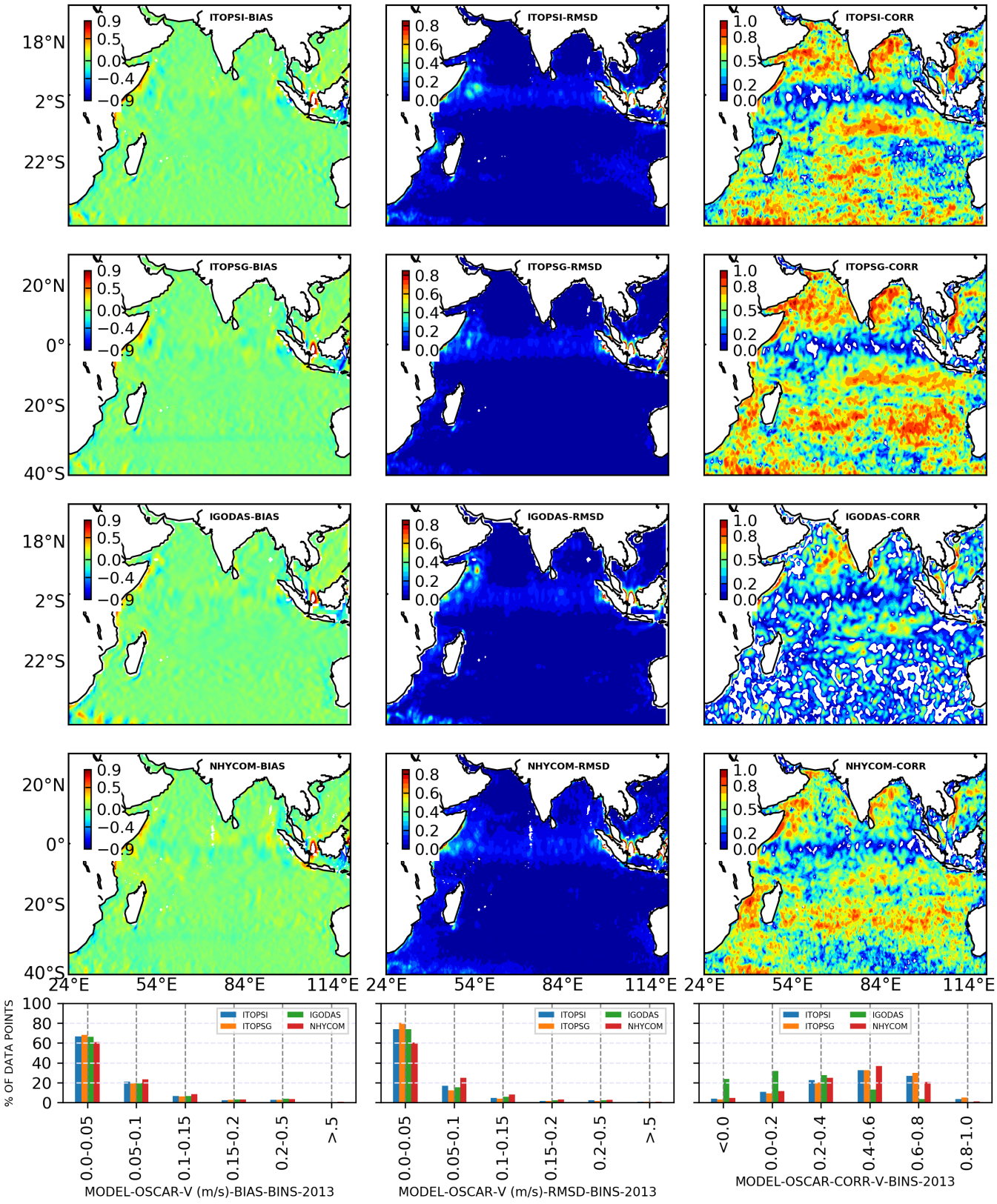

Figure 25: Comparison of 2013 meridional current (v) simulations from ITOPSI, ITPOSG, IGODAS and NHYCOM with OSCAR meridional Currents

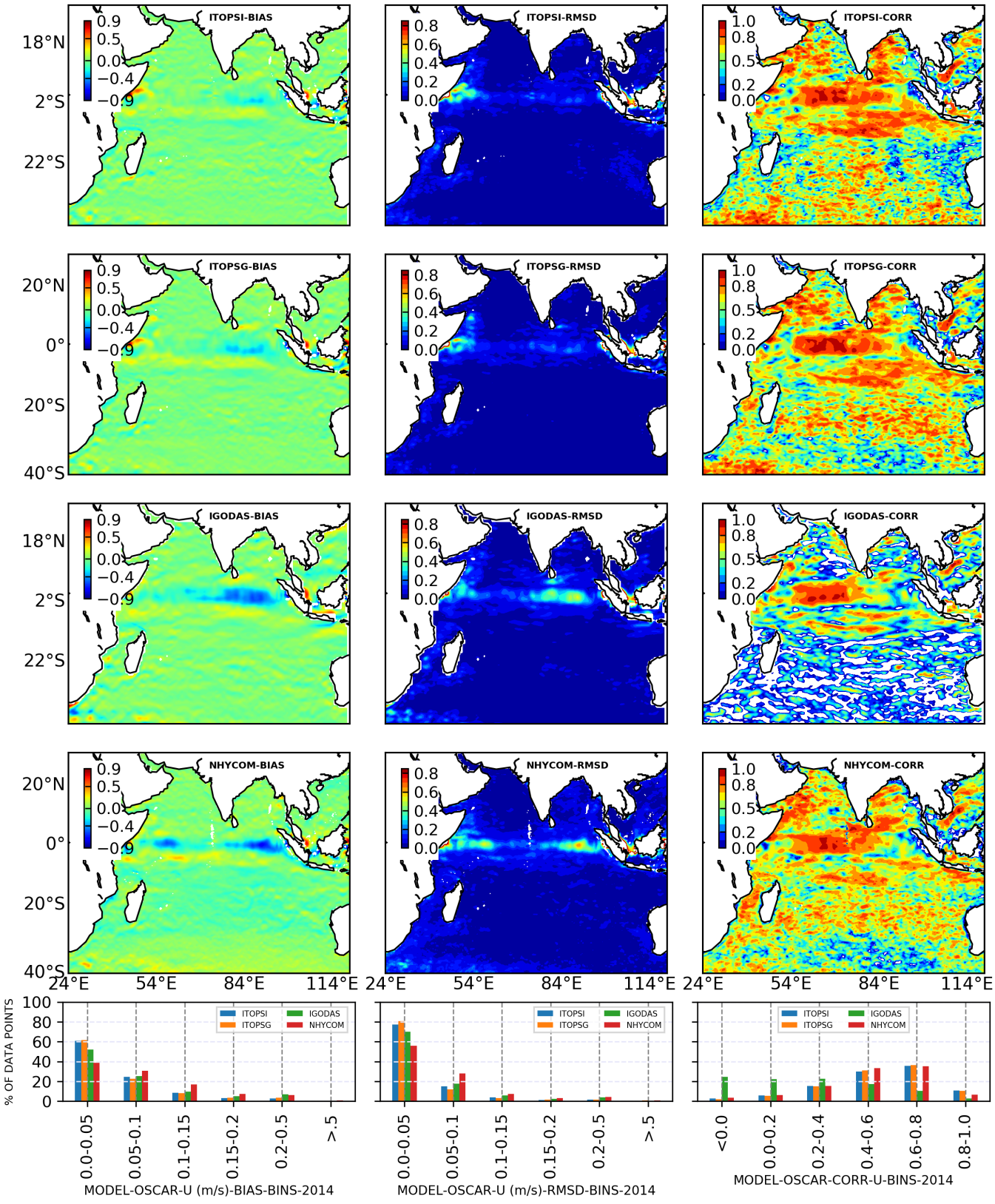

Figure 26: Comparison of 2014 Zonal current (u) simulations from ITOPSI, ITOPSG, IGODAS and NHYCOM with OSCAR Zonal Currents

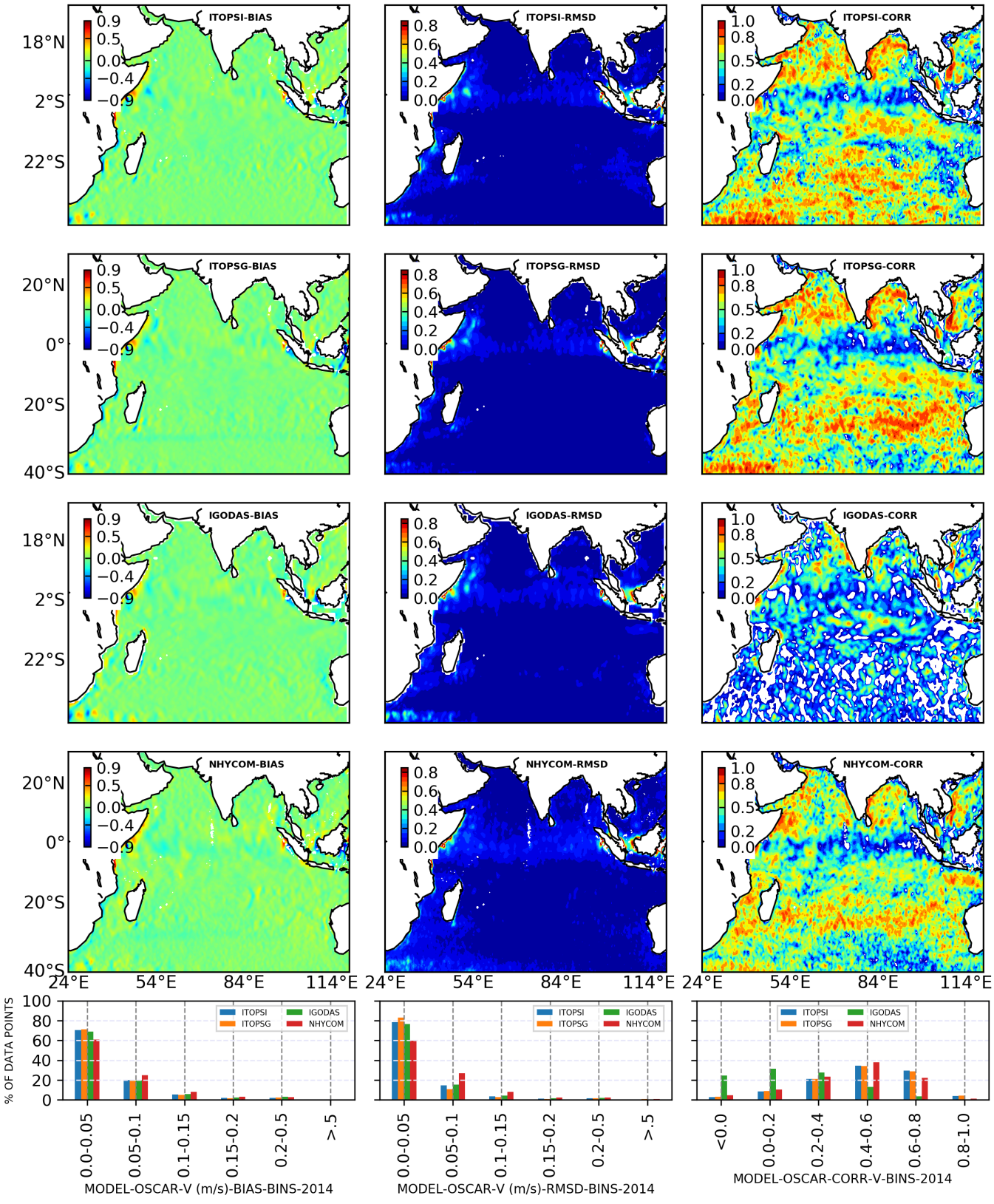

Figure 27: Comparison of 2014 meridional current (v) simulations from ITOPSI, ITPOSG, IGODAS and NHYCOM with OSCAR meridional Currents

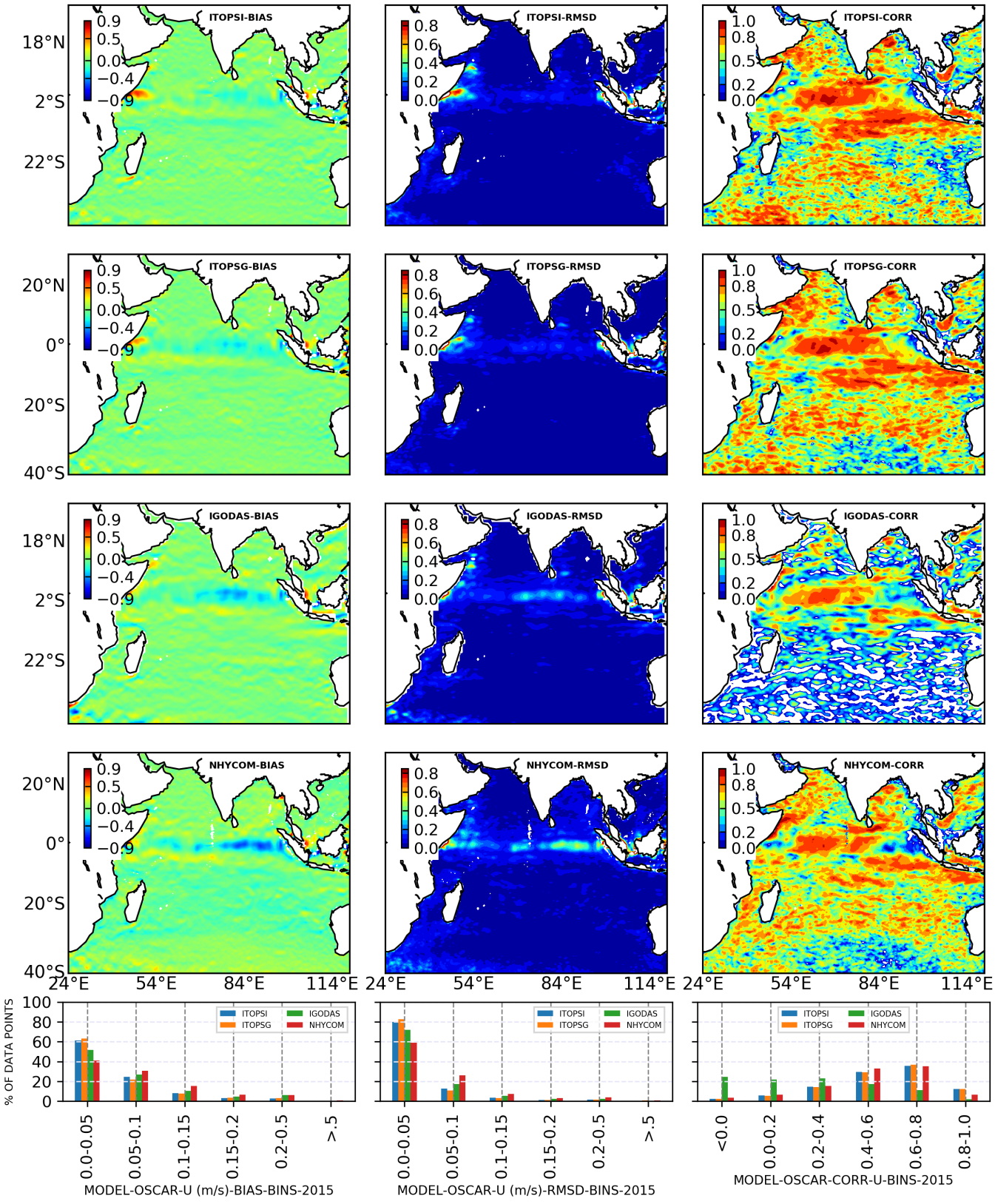

Figure 28: Comparison of 2015 Zonal current (u) simulations from ITOPSI, ITPOSG, IGODAS and NHYCOM with OSCAR Zonal Currents

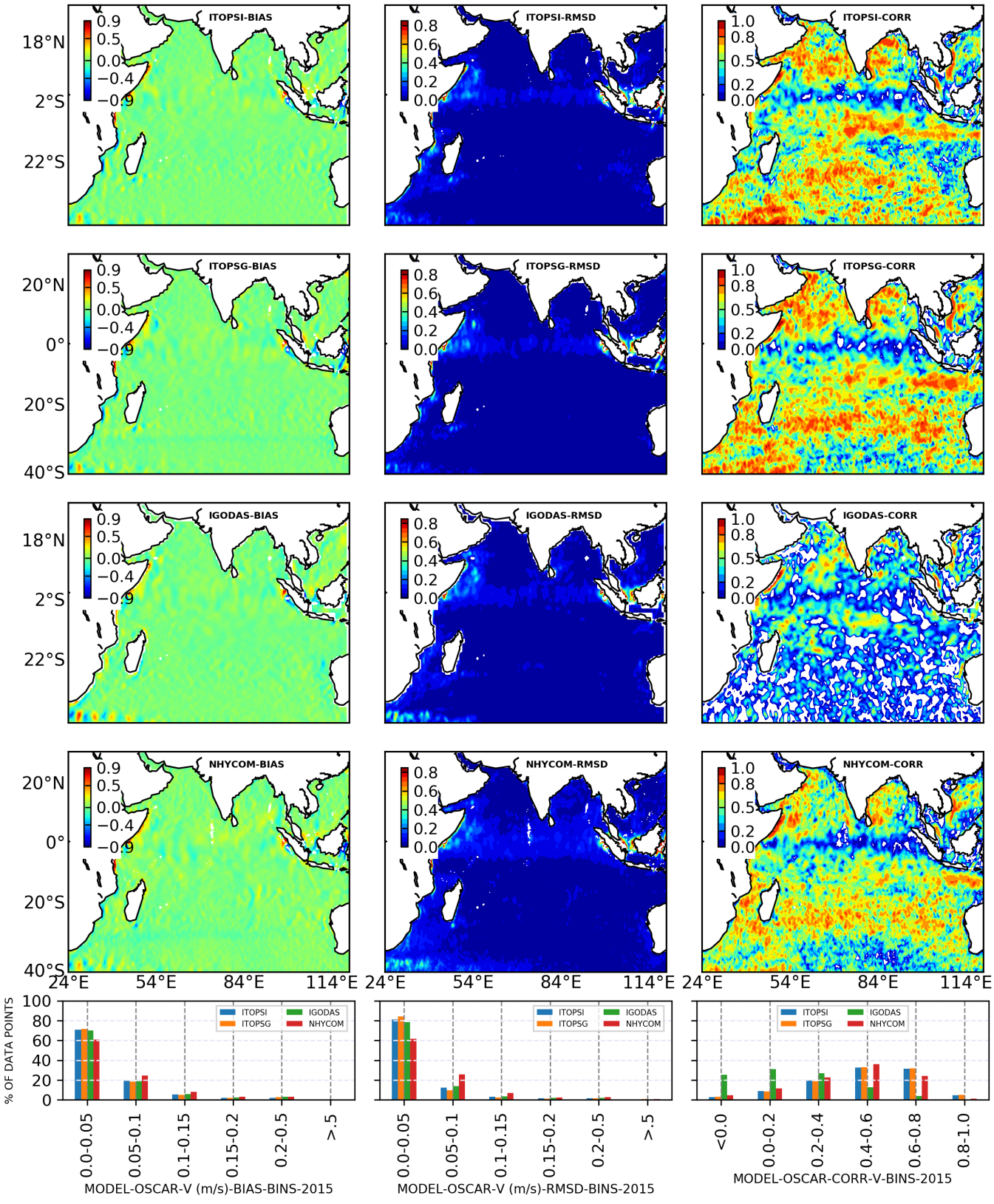

Figure 29: Comparison of 2015 meridional current (v) simulations from ITOPSI, ITPOSG, IGODAS and NHYCOM with OSCAR meridional Currents

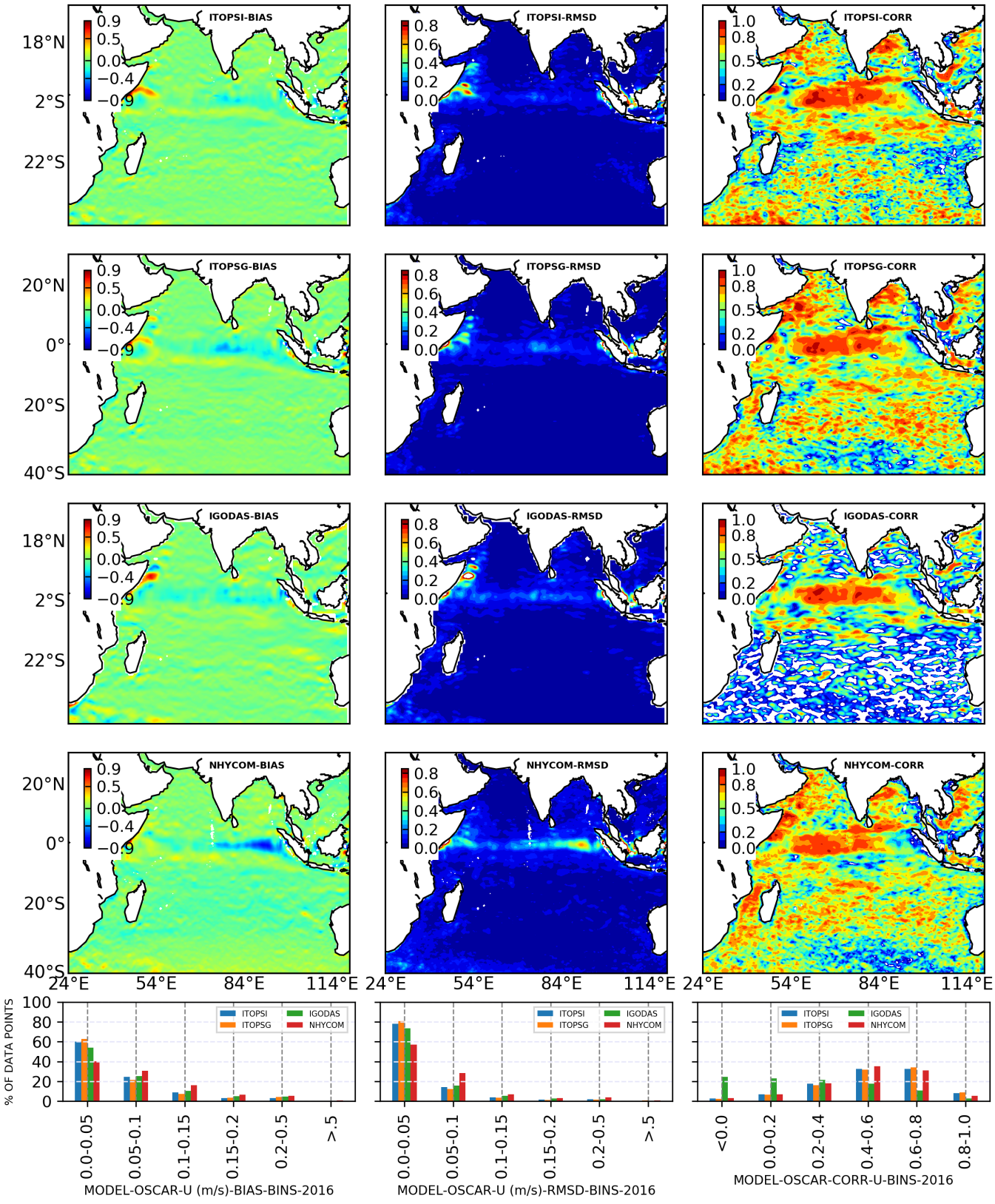

Figure 30: Comparison of 2016 Zonal current (u) simulations from ITOPSI, ITOPSG, IGODAS and NHYCOM with OSCAR Zonal Currents

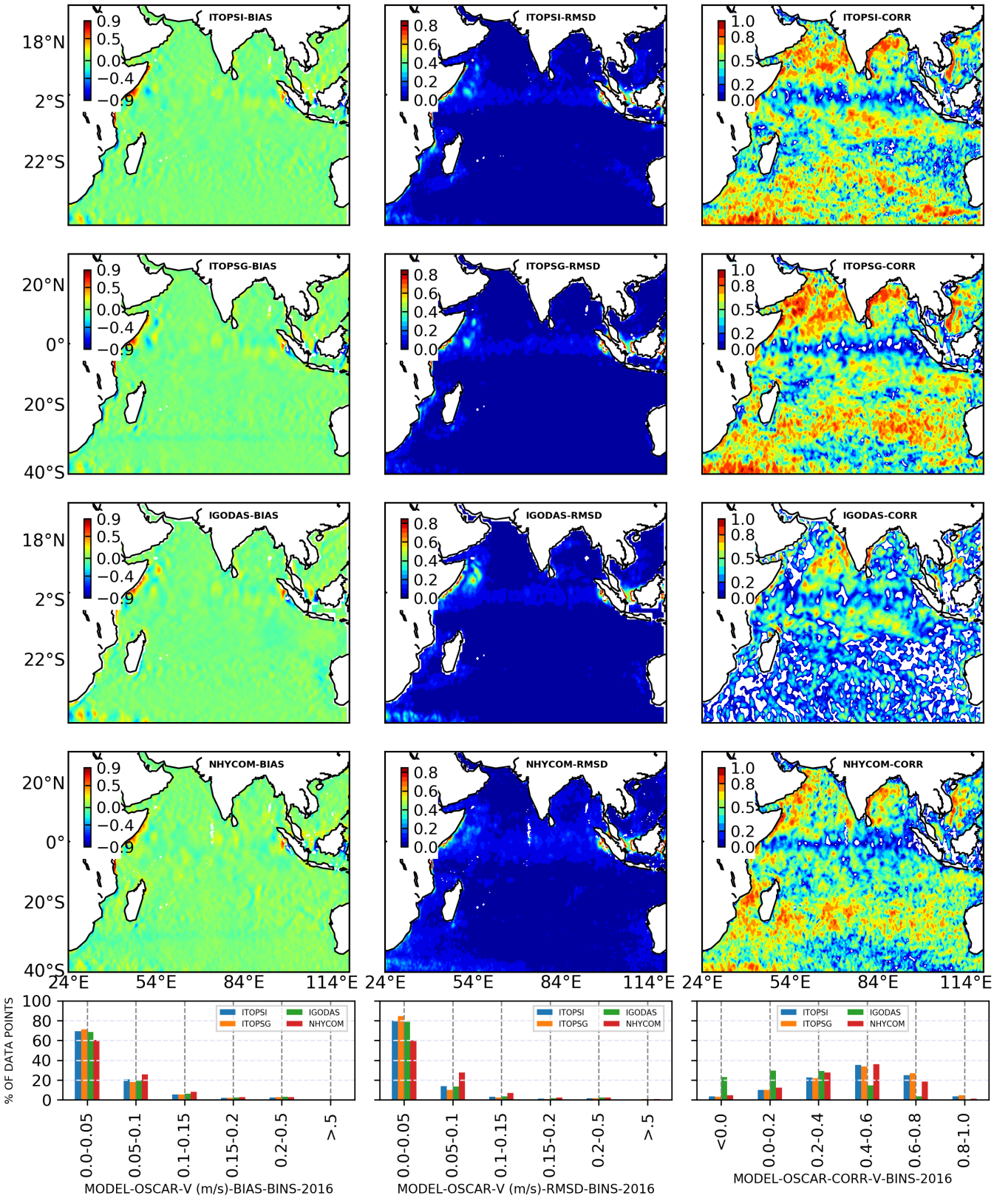

Figure 31: Comparison of 2016 meridional current (v) simulations from ITOPSI, ITPOSG, IGODAS and NHYCOM with OSCAR meridional Currents

5.1 Comparison of model currents using RAMA buoys

For the validation of currents simulated by the selected OGCM, we have chosen 21 RAMA buoys which had good quality current data for the period 2012–2016. Mean, standard deviation, bias, RMSD, correlation and Skill score for each model is calculated for both zonal and meridional components and presented as bar charts in Figure- 32 and 33 and in tabular form Tables - 10 to 15.

Figure- 32 and the tables with statistics show that the mean amplitudes of zonal currents captured by four models are not similar among them in most of the locations. The mean directions of zonal flows captured by all models were opposite to that of RAMA buoys in 9 out of 21 sites. Standard deviations of the zonal currents are represented well by all models with in a difference of ± 0.1 c except in case of 3 locations where NHYCOM overestimated the variability above 0.1 m and in one case where ITOPSI overestimated the variability of zonal currents beyond 0.1 m. Zonal velocities of all four models show positive biases ranging from 0.2 m to 0.4 m at the eastern side of the equator within 2 degrees on either side of the equator. Biases are minimum in ITOPSI followed by ITOPSG, IGODAS and NGHYCOM respectively in the increasing order. Spatially, biases are minimum for comparisons with RAMA buoys away from the equator (Figure- 32).

ITOPSG shows minimum RMSD at 14 locations followed by ITOPSI with seven sites of minimum RMSD followed by IGODAS with minimum RMSD in 4 places (Figure- 32). RMSD's in case of NHYCOM are in general highest compared to other models in all locations. Correlations of zonal velocity to RAMA buoys to the simulated values from all four models are positive for all positions except one location at 5S95E where all four models showed negative correlations. Comparison of four models show that ITOPSG is best among four, as it shows maximum correlation at 9 locations and second best correlations at 7 locations. ITOPSI stands second with six areas of highest correlation and nine places of second highest correlations. NHYCOM and IGODAS positions third and fourth regarding correlations among the four models at 21 locations of RAMA buoys. Skill scores are valid only if they are positive values, in case of zonal currents skill scores are positive at maximum sites (14) in case of ITOPSG followed by ITOPSI (13) locations. IGODAS and NHYCOM have positive skill scores in four and three positions respectively.

Figure - 33 (top panel) shows that the mean direction of meridional velocity is captured correctly in most of the locations by the selected models except for two places. However, there are differences in amplitude in comparison with RAMA among the four models. In many sites, NHYCOM over-estimated the meridional currents almost double the magnitude, and in some cases, it is more than double the amplitude of observed values. Nevertheless, the observed standard deviation is more closely simulated by NHYCOM indicated by its closest SDs to that found in RAMA buoys (Figure - 33 panel-2 from top). SD of ITOPSI stands closer to the observed SDs in 12 locations after NHYCOM, which is followed by IGODAS at 8 locations and ITOPSG at 6 locations ranking three and four respectively. Biases in meridional velocity are ≤ 0.06 m in case of both ITOPSG and ITOPSI. There are few locations where the biases of both IGODAS and NHYCOM are observed to be more than 0.15m.

Among the four models, RMSD ITOPSG shows minimum RMSD in 12 out of 21 locations followed by ITOPSI at six sites. IGODAS shows minimum RMSD in 4 places and in case of NHYCOM it has higher RMSD than other models in all areas. ITOPSG shows highest correlations at 12 locations followed by ITOPSI in 7 positions. Both IGODAS and NHYCOM shows highest correlations among the four models only in 2 places each. Among the four ITOPSG shows the best skill in simulating meridional currents with highest positive skill scores at 7 locations. ITOPSI has the second highest number of positive skill scores at 4 locations followed by IGODAS at just one site. NHYCOM do not have positive skill score at any of the RAMA buoy locations.

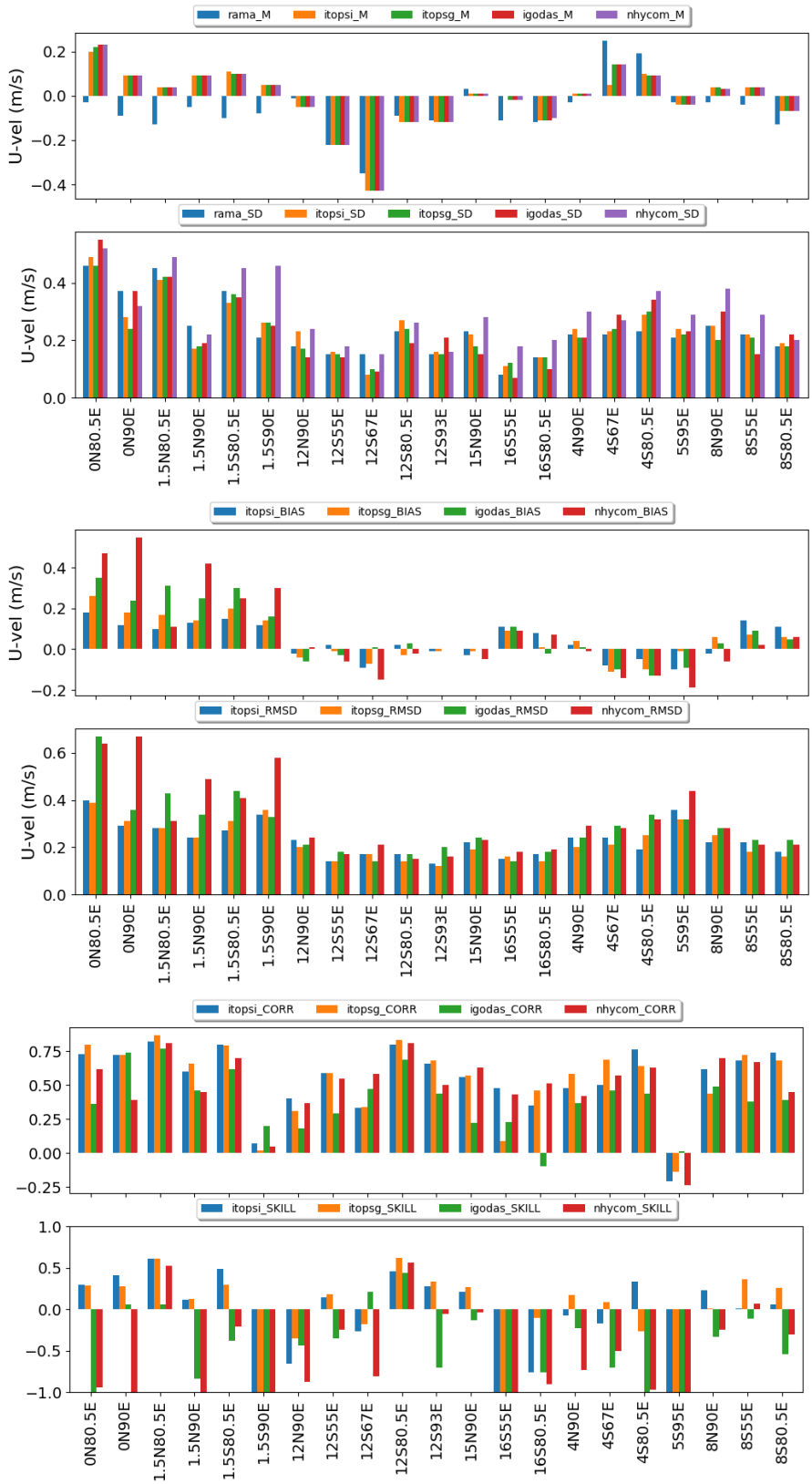

Figure 32: Comparison of zonal velocity (U) from 4 models in terms of mean,standard deviation, bias, rmsd, correlation and skill score with respect to RAMA buoys for the period 2012-2016.

Figure 33: Comparison of meridional velocity (V) from 4 models in terms of mean,standard deviation, bias, rmsd, correlation and skill score with respect to RAMA buoys for the period 2012-2016.

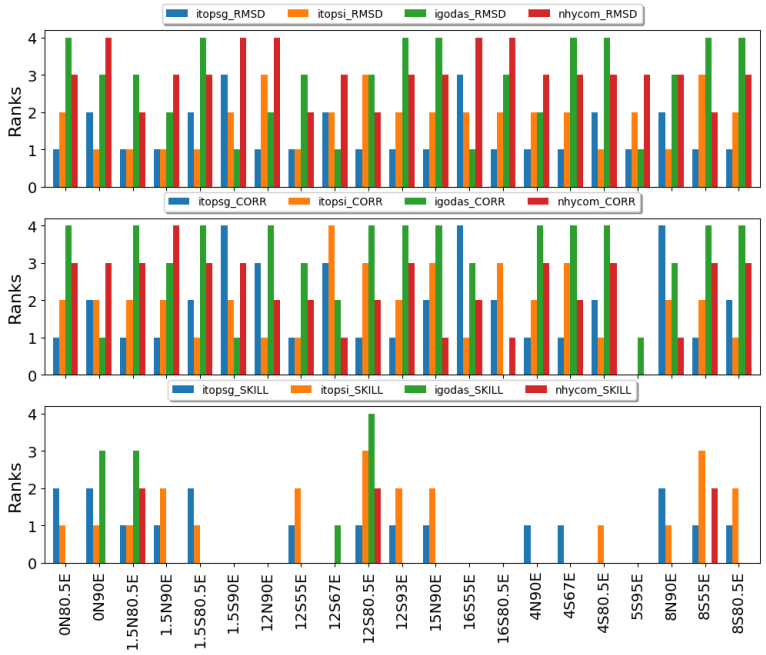

Figure 34: Ranks of four models for their zonal component of current in terms of RMSD, correlation and skill score from 21 RAMA buoy locations. Model with minimum rmsd maximum correlation & skill score are given a rank of 1 indicating best performance and the one with maximum RMSD, minimum correlation and minimum skill score is given a rank of 4. Intermediae ones are given ranks of 2 and 3.

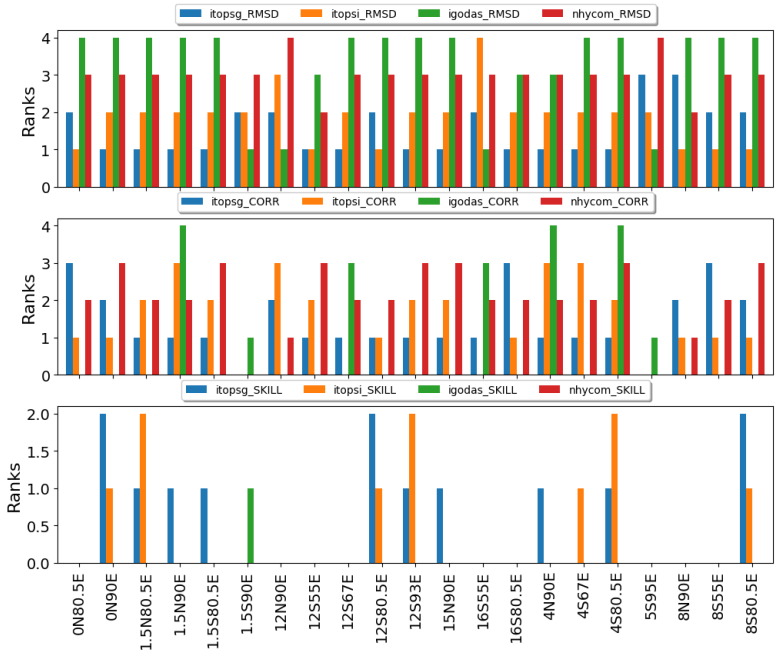

Figure 35: Ranks of four models for meridional component of current in terms of RMSD, correlation and skill score from 21 RAMA buoy locations. Model with minimum rmsd maximum correlation & skill score are given a rank of 1 indicating best performance and the one with maximum RMSD, minimum correlation and minimum skill score is given a rank of 4. Intermediae ones are given ranks of 2 and 3.

Table 17: Mean of zonal velocity from 21 RAMA buoys for the period 2012–2016 compared with same of selected four ocean models.

Location	Nobs	rama_M	itopsg_M	itopsi_M	igodas_M	nhycom_M
0N80.5E	670.0	-0.03	0.22	0.20	0.23	0.23
0N90E	624.0	-0.09	0.09	0.09	0.09	0.09
1.5N80.5E	382.0	-0.13	0.04	0.04	0.04	0.04
1.5N90E	376.0	-0.05	0.09	0.09	0.09	0.09
1.5S80.5E	908.0	-0.10	0.10	0.11	0.10	0.10
1.5S90E	365.0	-0.08	0.05	0.05	0.05	0.05
12N90E	851.0	-0.01	-0.05	-0.05	-0.05	-0.05
12S55E	912.0	-0.22	-0.22	-0.22	-0.22	-0.22
12S67E	25.0	-0.35	-0.43	-0.43	-0.43	-0.43
12S80.5E	714.0	-0.09	-0.12	-0.12	-0.12	-0.12
12S93E	792.0	-0.11	-0.12	-0.12	-0.12	-0.12
15N90E	1108.0	0.03	0.01	0.01	0.01	0.01
16S55E	132.0	-0.11	-0.02	-0.00	-0.02	-0.02
16S80.5E	554.0	-0.12	-0.11	-0.11	-0.11	-0.10
4N90E	1095.0	-0.03	0.01	0.01	0.01	0.01
4S67E	567.0	0.25	0.14	0.05	0.14	0.14
4S80.5E	843.0	0.19	0.09	0.10	0.09	0.09
5S95E	850.0	-0.03	-0.04	-0.04	-0.04	-0.04
8N90E	595.0	-0.03	0.04	0.04	0.03	0.03
8S55E	429.0	-0.04	0.04	0.04	0.04	0.04
8S80.5E	582.0	-0.13	-0.07	-0.07	-0.07	-0.07

Table 18: Mean of meridional velocity from 21 RAMA buoys for the period 2012–2016 compared with same of selected four ocean models.

Location	Nobs	rama_M	itopsg_M	itopsi_M	igodas_M	nhycom_M
0N80.5E	670.0	0.02	0.09	0.08	0.23	0.08
0N90E	624.0	-0.01	-0.02	-0.02	0.09	-0.02
1.5N80.5E	382.0	0.01	0.02	0.02	0.04	0.02
1.5N90E	376.0	0.00	0.04	0.04	0.09	0.04
1.5S80.5E	908.0	0.00	0.03	0.03	0.10	0.03
1.5S90E	365.0	0.01	0.01	0.01	0.05	0.01
12N90E	851.0	0.02	-0.01	-0.01	-0.05	-0.01
12S55E	912.0	-0.06	-0.05	-0.05	-0.22	-0.05
12S67E	25.0	-0.13	-0.11	-0.11	-0.43	-0.11
12S80.5E	714.0	-0.09	-0.05	-0.05	-0.12	-0.05
12S93E	792.0	-0.07	-0.10	-0.10	-0.12	-0.10
15N90E	1108.0	-0.01	0.04	0.05	0.01	0.04
16S55E	132.0	-0.00	-0.01	-0.01	-0.02	-0.01
16S80.5E	554.0	-0.07	-0.05	-0.05	-0.11	-0.05
4N90E	1095.0	-0.01	-0.01	0.01	0.01	-0.01
4S67E	567.0	-0.07	-0.00	-0.01	0.14	-0.00
4S80.5E	843.0	-0.02	-0.01	-0.02	0.09	-0.01
5S95E	850.0	-0.02	0.06	0.06	-0.04	0.06
8N90E	595.0	0.08	0.03	0.03	0.03	0.03
8S55E	429.0	-0.01	-0.02	-0.02	0.04	-0.02
8S80.5E	582.0	-0.05	-0.02	-0.02	-0.07	-0.02

Table 19: Standard deviation of zonal velocity from 21 RAMA buoys for the period 2012–2016 compared with same of selected four ocean models.

Location	Nobs	rama_SD	itopsg_SD	itopsi_SD	igodas_SD	nhycom_SD
0N80.5E	670.0	0.46	0.46	0.49	0.55	0.52
0N90E	624.0	0.37	0.24	0.28	0.37	0.32
1.5N80.5E	382.0	0.45	0.42	0.41	0.42	0.49
1.5N90E	376.0	0.25	0.18	0.17	0.19	0.22
1.5S80.5E	908.0	0.37	0.36	0.33	0.35	0.45
1.5S90E	365.0	0.21	0.26	0.26	0.25	0.46
12N90E	851.0	0.18	0.17	0.23	0.14	0.24
12S55E	912.0	0.15	0.15	0.16	0.14	0.18
12S67E	25.0	0.15	0.10	0.08	0.09	0.15
12S80.5E	714.0	0.23	0.24	0.27	0.19	0.26
12S93E	792.0	0.15	0.15	0.16	0.21	0.16
15N90E	1108.0	0.23	0.18	0.22	0.15	0.28
16S55E	132.0	0.08	0.12	0.11	0.07	0.18
16S80.5E	554.0	0.14	0.14	0.14	0.10	0.20
4N90E	1095.0	0.22	0.21	0.24	0.21	0.30
4S67E	567.0	0.22	0.24	0.23	0.29	0.27
4S80.5E	843.0	0.23	0.30	0.29	0.34	0.37
5S95E	850.0	0.21	0.22	0.24	0.23	0.29
8N90E	595.0	0.25	0.20	0.25	0.30	0.38
8S55E	429.0	0.22	0.21	0.22	0.15	0.29
8S80.5E	582.0	0.18	0.18	0.19	0.22	0.20

Table 20: Standard deviation of meridional velocity from 21 RAMA buoys for the period 2012–2016 compared with same of selected four ocean models.

Location	Nobs	rama_SD	itopsg_SD	itopsi_SD	igodas_SD	nhycom_SD
0N80.5E	670.0	0.20	0.16	0.17	0.18	0.19
0N90E	624.0	0.19	0.16	0.16	0.17	0.19
1.5N80.5E	382.0	0.21	0.16	0.18	0.16	0.21
1.5N90E	376.0	0.22	0.18	0.17	0.16	0.23
1.5S80.5E	908.0	0.18	0.16	0.19	0.19	0.23
1.5S90E	365.0	0.29	0.16	0.17	0.14	0.26
12N90E	851.0	0.19	0.16	0.19	0.10	0.22
12S55E	912.0	0.15	0.14	0.15	0.10	0.18
12S67E	25.0	0.12	0.06	0.03	0.06	0.10
12S80.5E	714.0	0.14	0.15	0.14	0.11	0.19
12S93E	792.0	0.15	0.13	0.13	0.15	0.15
15N90E	1108.0	0.19	0.16	0.20	0.09	0.24
16S55E	132.0	0.07	0.12	0.09	0.06	0.11
16S80.5E	554.0	0.10	0.11	0.14	0.08	0.15
4N90E	1095.0	0.21	0.18	0.17	0.18	0.25
4S67E	567.0	0.20	0.18	0.15	0.19	0.23
4S80.5E	843.0	0.17	0.17	0.17	0.22	0.25
5S95E	850.0	0.26	0.15	0.17	0.15	0.23
8N90E	595.0	0.21	0.18	0.20	0.18	0.27
8S55E	429.0	0.16	0.16	0.17	0.13	0.18
8S80.5E	582.0	0.17	0.17	0.17	0.17	0.22

Table 21: Bias of zonal velocity from 21 RAMA buoys for the period 2012–2016 compared with same of selected four ocean models.

Location	Nobs	itopsg_Bias	itopsi_Bias	igodas_Bias	nhycom_Bias
0N80.5E	670.0	0.26	0.18	0.35	0.47
0N90E	624.0	0.18	0.12	0.24	0.55
1.5N80.5E	382.0	0.17	0.10	0.31	0.11
1.5N90E	376.0	0.14	0.13	0.25	0.42
1.5S80.5E	908.0	0.20	0.15	0.30	0.25
1.5S90E	365.0	0.14	0.12	0.16	0.30
12N90E	851.0	-0.04	-0.02	-0.06	0.01
12S55E	912.0	-0.01	0.02	-0.03	-0.06
12S67E	25.0	-0.07	-0.09	0.01	-0.15
12S80.5E	714.0	-0.03	0.02	0.03	-0.02
12S93E	792.0	-0.01	-0.01	-0.00	0.00
15N90E	1108.0	-0.01	-0.03	0.00	-0.05
16S55E	132.0	0.09	0.11	0.11	0.09
16S80.5E	554.0	0.01	0.08	-0.02	0.07
4N90E	1095.0	0.04	0.02	0.01	-0.01
4S67E	567.0	-0.11	-0.08	-0.10	-0.14
4S80.5E	843.0	-0.10	-0.05	-0.13	-0.13
5S95E	850.0	-0.01	-0.10	-0.09	-0.19
8N90E	595.0	0.06	-0.02	0.03	-0.06
8S55E	429.0	0.07	0.14	0.09	0.02
8S80.5E	582.0	0.06	0.11	0.05	0.06

Table 22: Bias of meridional velocity from 21 RAMA buoys for the period 2012–2016 compared with same of selected four ocean models.

Location	Nobs	itopsg_Bias	itopsi_Bias	igodas_Bias	nhycom_Bias
0N80.5E	670.0	0.06	0.06	0.21	0.06
0N90E	624.0	-0.00	-0.00	0.10	0.00
1.5N80.5E	382.0	0.00	0.03	0.03	-0.02
1.5N90E	376.0	0.04	0.05	0.09	0.01
1.5S80.5E	908.0	0.02	0.06	0.11	0.07
1.5S90E	365.0	0.00	0.01	0.06	0.11
12N90E	851.0	-0.03	-0.05	-0.04	0.01
12S55E	912.0	0.01	0.01	-0.17	-0.01
12S67E	25.0	0.02	-0.07	-0.33	0.10
12S80.5E	714.0	0.03	0.02	-0.05	0.00
12S93E	792.0	-0.03	-0.03	-0.01	-0.06
15N90E	1108.0	0.05	0.06	0.02	0.11
16S55E	132.0	-0.00	0.03	0.03	0.03
16S80.5E	554.0	0.02	0.02	-0.04	0.01
4N90E	1095.0	0.00	0.01	0.03	-0.04
4S67E	567.0	0.06	0.05	0.19	0.17
4S80.5E	843.0	0.01	0.01	0.12	0.06
5S95E	850.0	0.07	0.06	-0.01	0.12
8N90E	595.0	-0.06	-0.04	-0.01	-0.05
8S55E	429.0	-0.00	0.04	0.07	0.03
8S80.5E	582.0	0.03	-0.00	-0.03	0.04

Table 23: Root Mean Square Difference (RMSD) of zonal velocity from 21 RAMA buoys for the period 2012–2016 compared with same of selected four ocean models.

Location	Nobs	itopsg_RMSD	itopsi_RMSD	igodas_RMSD	nhycom_RMSD
0N80.5E	670.0	0.39	0.40	0.67	0.64
0N90E	624.0	0.31	0.29	0.36	0.67
1.5N80.5E	382.0	0.28	0.28	0.43	0.31
1.5N90E	376.0	0.24	0.24	0.34	0.49
1.5S80.5E	908.0	0.31	0.27	0.44	0.41
1.5S90E	365.0	0.36	0.34	0.33	0.58
12N90E	851.0	0.20	0.23	0.21	0.24
12S55E	912.0	0.14	0.14	0.18	0.17
12S67E	25.0	0.17	0.17	0.14	0.21
12S80.5E	714.0	0.14	0.17	0.17	0.15
12S93E	792.0	0.12	0.13	0.20	0.16
15N90E	1108.0	0.19	0.22	0.24	0.23
16S55E	132.0	0.16	0.15	0.14	0.18
16S80.5E	554.0	0.14	0.17	0.18	0.19
4N90E	1095.0	0.20	0.24	0.24	0.29
4S67E	567.0	0.21	0.24	0.29	0.28
4S80.5E	843.0	0.25	0.19	0.34	0.32
5S95E	850.0	0.32	0.36	0.32	0.44
8N90E	595.0	0.25	0.22	0.28	0.28
8S55E	429.0	0.18	0.22	0.23	0.21
8S80.5E	582.0	0.16	0.18	0.23	0.21

Table 24: Root Mean Square Difference (RMSD) of meridional velocity from 21 RAMA buoys for the period 2012–2016 compared with same of selected four ocean models.

Location	Nobs	itopsg_RMSD	itopsi_RMSD	igodas_RMSD	nhycom_RMSD
0N80.5E	670.0	0.21	0.20	0.54	0.22
0N90E	624.0	0.18	0.19	0.42	0.22
1.5N80.5E	382.0	0.17	0.20	0.49	0.22
1.5N90E	376.0	0.19	0.24	0.30	0.25
1.5S80.5E	908.0	0.17	0.21	0.44	0.25
1.5S90E	365.0	0.36	0.36	0.18	0.41
12N90E	851.0	0.23	0.25	0.21	0.26
12S55E	912.0	0.16	0.16	0.25	0.19
12S67E	25.0	0.12	0.14	0.37	0.17
12S80.5E	714.0	0.14	0.13	0.26	0.17
12S93E	792.0	0.13	0.14	0.22	0.18
15N90E	1108.0	0.18	0.20	0.25	0.24
16S55E	132.0	0.11	0.13	0.09	0.12
16S80.5E	554.0	0.14	0.15	0.16	0.16
4N90E	1095.0	0.21	0.24	0.26	0.26
4S67E	567.0	0.20	0.23	0.37	0.28
4S80.5E	843.0	0.15	0.16	0.32	0.24
5S95E	850.0	0.34	0.33	0.23	0.38
8N90E	595.0	0.27	0.22	0.31	0.26
8S55E	429.0	0.18	0.17	0.27	0.19
8S80.5E	582.0	0.15	0.12	0.26	0.19

Table 25: Correlation of zonal velocity from 21 RAMA buoys for the period 2012–2016 compared with same of selected four ocean models.

Location	Nobs	itopsg_CORR	itopsi_CORR	igodas_CORR	nhycom_CORR
0N80.5E	670.0	0.80	0.73	0.36	0.62
0N90E	624.0	0.72	0.72	0.74	0.39
1.5N80.5E	382.0	0.87	0.82	0.77	0.81
1.5N90E	376.0	0.66	0.60	0.46	0.45
1.5S80.5E	908.0	0.79	0.80	0.62	0.70
1.5S90E	365.0	0.02	0.07	0.20	0.05
12N90E	851.0	0.31	0.40	0.18	0.37
12S55E	912.0	0.59	0.59	0.29	0.55
12S67E	25.0	0.34	0.33	0.47	0.58
12S80.5E	714.0	0.83	0.80	0.69	0.81
12S93E	792.0	0.68	0.66	0.44	0.50
15N90E	1108.0	0.57	0.56	0.22	0.63
16S55E	132.0	0.09	0.48	0.23	0.43
16S80.5E	554.0	0.46	0.35	-0.10	0.51
4N90E	1095.0	0.58	0.48	0.37	0.42
4S67E	567.0	0.69	0.50	0.46	0.57
4S80.5E	843.0	0.64	0.76	0.44	0.63
5S95E	850.0	-0.14	-0.21	0.01	-0.24
8N90E	595.0	0.44	0.62	0.49	0.70
8S55E	429.0	0.72	0.68	0.38	0.67
8S80.5E	582.0	0.68	0.74	0.39	0.45

Table 26: Correlation of meridional velocity from 21 RAMA buoys for the period 2012–2016 compared with same of selected four ocean models.

Location	Nobs	itopsg_CORR	itopsi_CORR	igodas_CORR	nhycom_CORR
0N80.5E	670.0	0.39	0.46	0.00	0.42
0N90E	624.0	0.43	0.45	-0.03	0.33
1.5N80.5E	382.0	0.59	0.47	-0.11	0.47
1.5N90E	376.0	0.60	0.33	0.12	0.39
1.5S80.5E	908.0	0.53	0.42	-0.02	0.37
1.5S90E	365.0	-0.23	-0.18	0.56	-0.05
12N90E	851.0	0.20	0.18	-0.00	0.21
12S55E	912.0	0.46	0.40	-0.09	0.39
12S67E	25.0	0.28	-0.19	0.10	0.24
12S80.5E	714.0	0.59	0.59	-0.05	0.54
12S93E	792.0	0.57	0.54	-0.12	0.33
15N90E	1108.0	0.56	0.52	-0.01	0.51
16S55E	132.0	0.44	-0.14	0.26	0.33
16S80.5E	554.0	0.22	0.28	-0.03	0.23
4N90E	1095.0	0.45	0.23	0.14	0.39
4S67E	567.0	0.48	0.39	-0.12	0.46
4S80.5E	843.0	0.60	0.59	0.10	0.42
5S95E	850.0	-0.21	-0.09	0.21	-0.09
8N90E	595.0	0.08	0.43	-0.04	0.43
8S55E	429.0	0.39	0.48	-0.04	0.40
8S80.5E	582.0	0.60	0.74	-0.07	0.58

Table 27: Skill score of zonal velocity from 21 RAMA buoys for the period 2012–2016 compared with same of selected four ocean models.

Location	Nobs	itopsg_SKILL	itopsi_SKILL	igodas_SKILL	nhycom_SKILL
0N80.5E	670.0	0.29	0.30	-1.14	-0.94
0N90E	624.0	0.28	0.41	0.06	-2.27
1.5N80.5E	382.0	0.61	0.61	0.06	0.52
1.5N90E	376.0	0.12	0.11	-0.84	-2.69
1.5S80.5E	908.0	0.30	0.49	-0.38	-0.21
1.5S90E	365.0	-2.01	-1.80	-1.63	-6.97
12N90E	851.0	-0.35	-0.66	-0.44	-0.88
12S55E	912.0	0.18	0.14	-0.35	-0.25
12S67E	25.0	-0.18	-0.27	0.21	-0.81
12S80.5E	714.0	0.62	0.46	0.44	0.56
12S93E	792.0	0.33	0.28	-0.70	-0.06
15N90E	1108.0	0.27	0.21	-0.13	-0.04
16S55E	132.0	-3.21	-2.35	-2.13	-4.51
16S80.5E	554.0	-0.10	-0.76	-0.76	-0.90
4N90E	1095.0	0.17	-0.08	-0.23	-0.73
4S67E	567.0	0.09	-0.17	-0.70	-0.50
4S80.5E	843.0	-0.27	0.33	-1.30	-0.97
5S95E	850.0	-1.44	-2.02	-1.43	-3.52
8N90E	595.0	0.01	0.23	-0.33	-0.25
8S55E	429.0	0.36	0.01	-0.11	0.07
8S80.5E	582.0	0.26	0.06	-0.54	-0.30

Table 28: Skill score of meridional velocity from 21 RAMA buoys for the period 2012–2016 compared with same of selected four ocean models.

Location	Nobs	itopsg_SKILL	itopsi_SKILL	igodas_SKILL	nhycom_SKILL
0N80.5E	670.0	-0.13	-0.01	-0.37	-0.19
0N90E	624.0	0.02	0.06	-0.30	-0.36
1.5N80.5E	382.0	0.32	0.04	-0.20	-0.10
1.5N90E	376.0	0.28	-0.16	-0.38	-0.31
1.5S80.5E	908.0	0.16	-0.26	-0.39	-0.83
1.5S90E	365.0	-0.54	-0.54	0.22	-1.03
12N90E	851.0	-0.42	-0.67	-0.39	-0.82
12S55E	912.0	-0.04	-0.17	-1.76	-0.53
12S67E	25.0	-0.00	-0.53	-4.58	-1.09
12S80.5E	714.0	0.11	0.16	-0.32	-0.34
12S93E	792.0	0.16	0.11	-1.17	-0.53
15N90E	1108.0	0.16	-0.06	-0.18	-0.59
16S55E	132.0	-1.05	-2.07	-0.36	-1.47
16S80.5E	554.0	-0.73	-1.16	-0.47	-1.59
4N90E	1095.0	0.06	-0.32	-0.45	-0.49
4S67E	567.0	-0.03	0.05	-1.68	-0.94
4S80.5E	843.0	0.22	0.19	-1.00	-1.00
5S95E	850.0	-0.64	-0.59	-0.25	-1.13
8N90E	595.0	-0.68	-0.12	-0.61	-0.61
8S55E	429.0	-0.28	-0.18	-0.51	-0.47
8S80.5E	582.0	0.18	0.48	-0.96	-0.19

Taylor Diagram comparison of Zonal & Meridional Currents

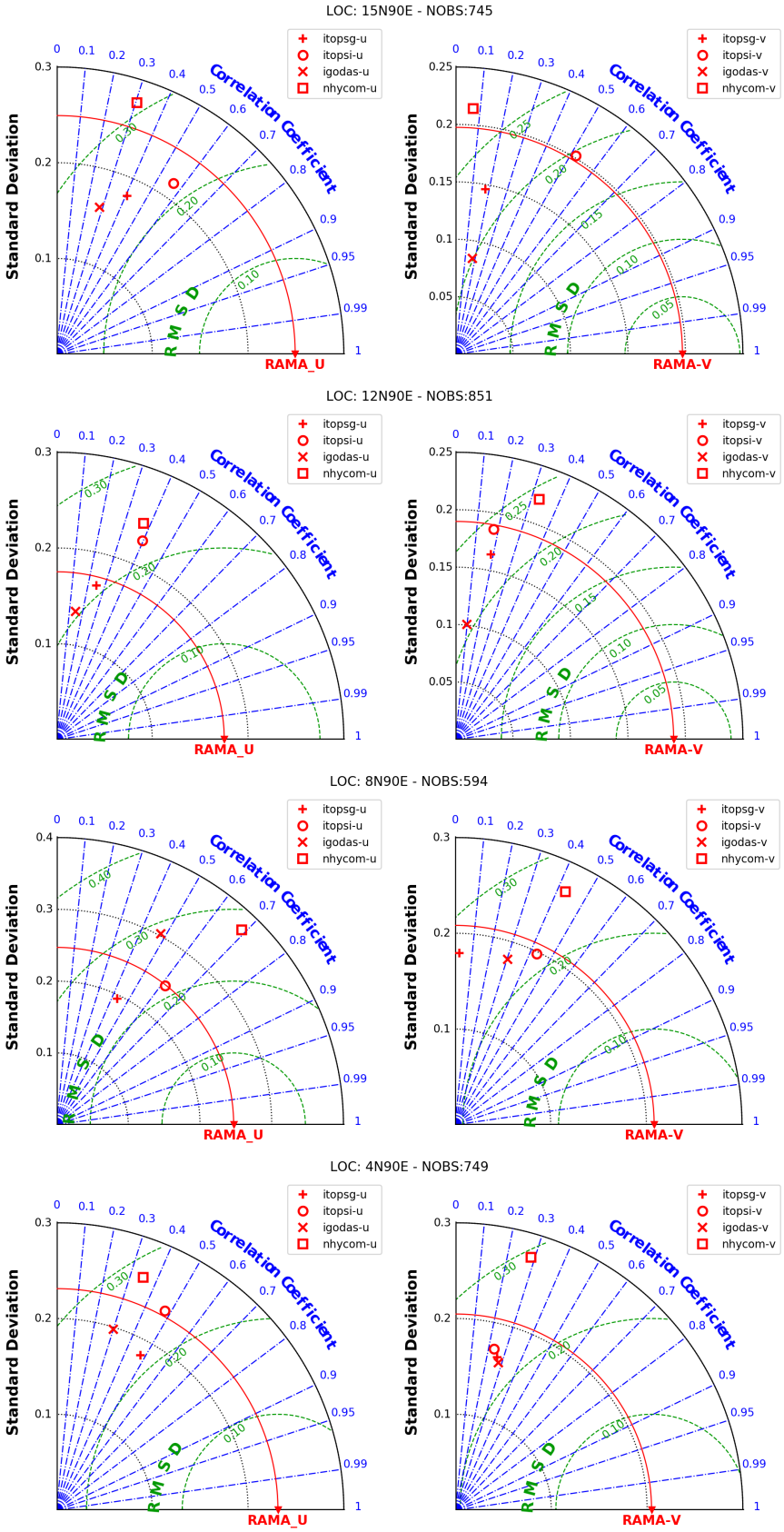

Figure 36: Comparison of 2012-16 UV components of currents from ITOPSI, ITPOSG, IGODAS and NHYCOM with RAMA from BoB.

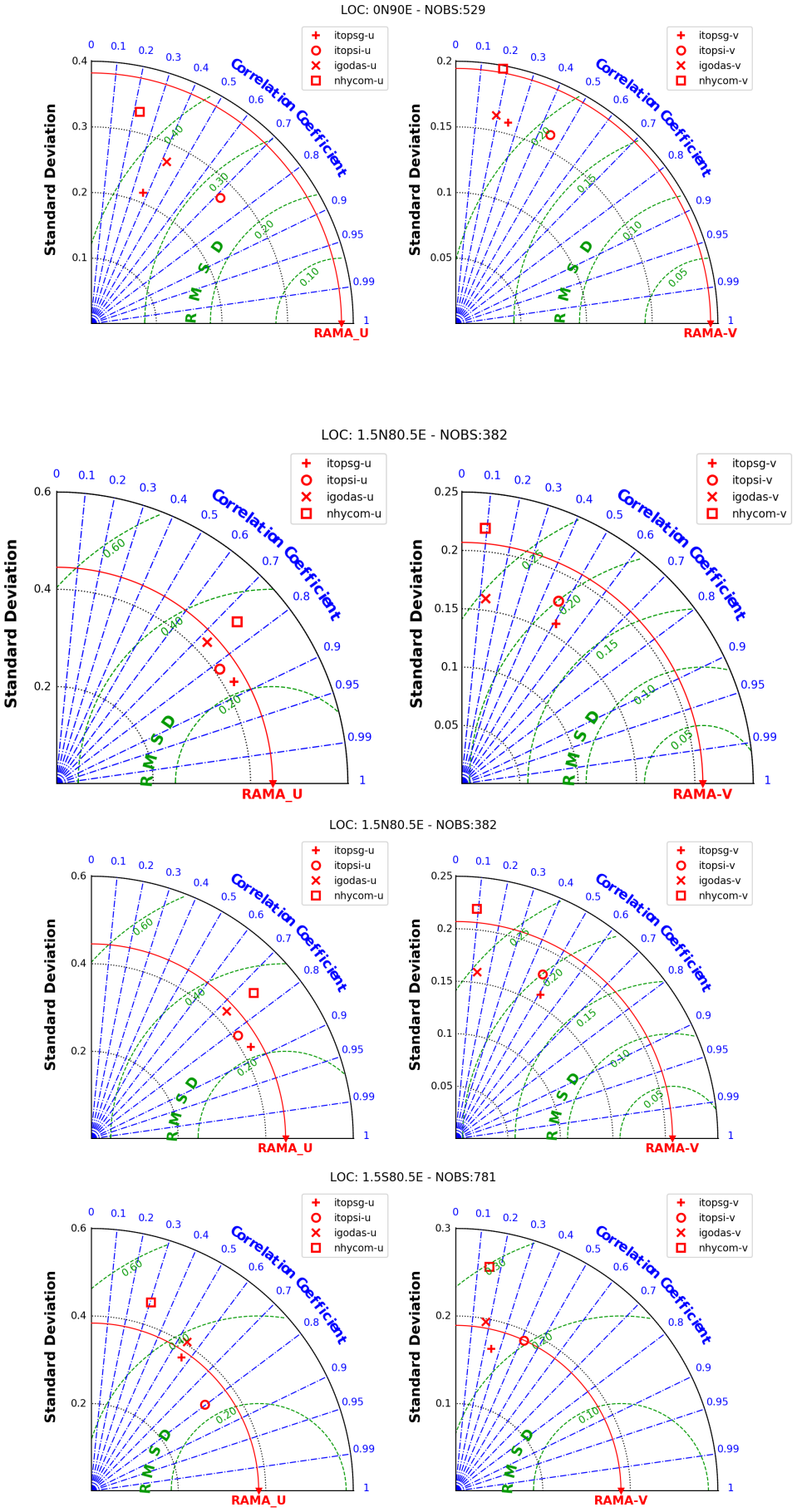

Figure 37: Comparison of 2012-16 UV components of currents from ITOPSI, ITPOSG, IGODAS and NHYCOM with RAMA from EEIO.

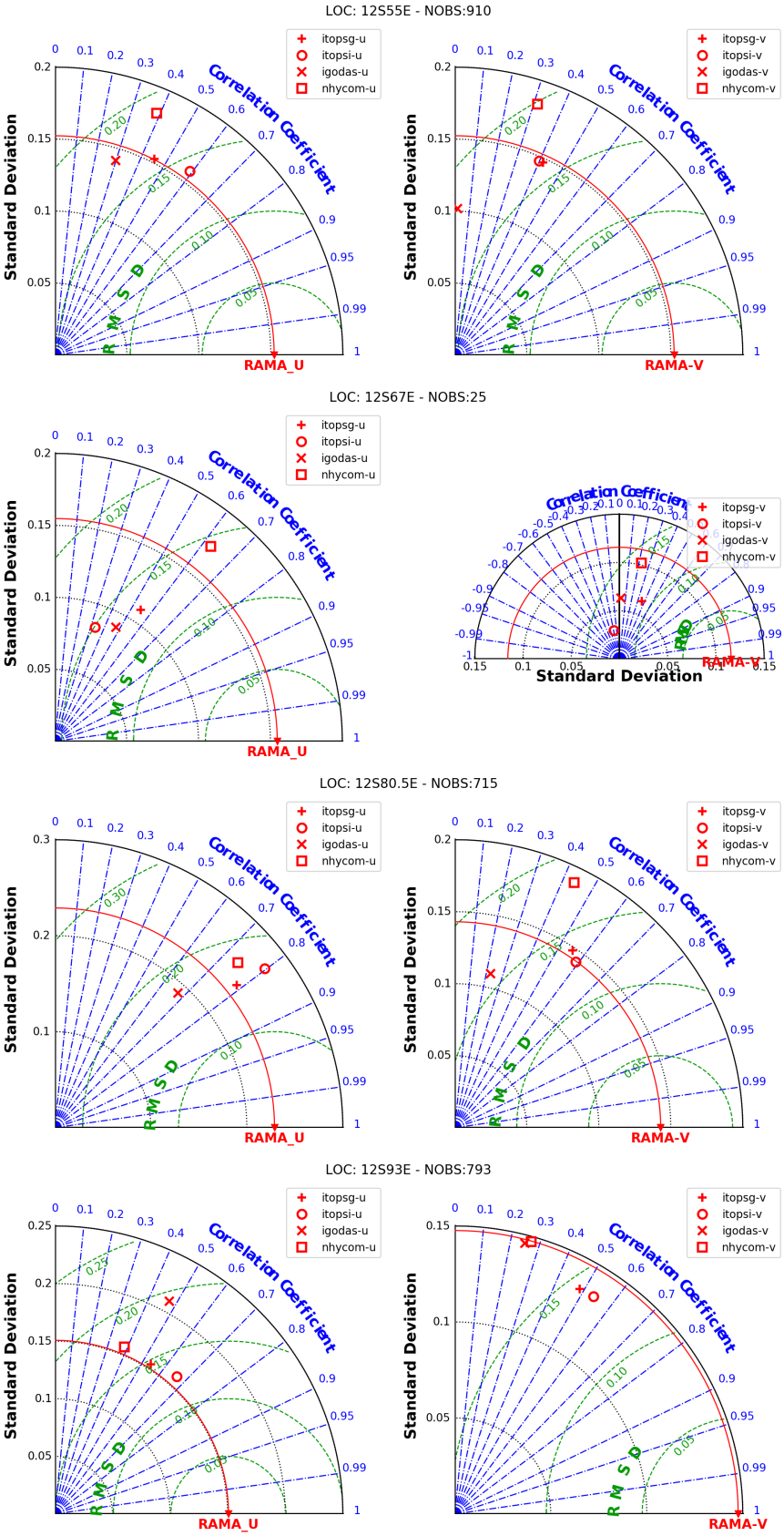

Figure 38: Comparison of 2012-16 UV components of currents from ITOPSI, ITPOSG, IGODAS and NHYCOM with RAMA along 12S.

6 Evaluation of Vertical profiles of T&S using RAMA buoys

Vertical temperature and salinity profiles from each model are evaluated using both independent observations of RAMA buoys [which are not used for assimilation in ITOPS(I&G)] and using ARGO profiles which are assimilated by all models. Each model is sampled at time and space positions of above observations. Statistics regarding mean, standard deviation, RMSD and correlation are calculated up to 500 m from each model at standard depth levels sampled by the observational platform. Total 12 RAMA buoys, where T&S profiles were available are used for validation.

Comparison of RAMA buoys along 90E longitude in BoB is presented in Figure-39 & 40. At 15N-90E, up to 150 m depth, ITOPSG and NHYCOM show lower RMSD compared to STD of RAMA with higher correlations compared to IGODAS & ITOPSI. Below 150 meter the variability is much lower, and all models show similar performance with ITPOS models having a higher edge compared to other two. Salinity data is limited to upper 150-200 m depth. At this location salinity from ITOPS models are relatively better compared to other models regarding their RMSD and correlation.

The temperature of site 12N-90E for the upper 100 m depth, from IGODAS is slightly better compared to other models, but below 100m depth, ITOPG and NHYCOM are better. Salinity from RAMA is available only up to top 100 m at this location. All four models show relatively poor simulations compared to RAMA indicated by higher RMSD comparison with STD. However, IGODAS has a slight performance edge over other models at this location.

At 8N-90E both ITOPSI and IGODAS show better simulations of temperature indicated by their minimum RMSD and higher correlation compared to ITOSG and NHYCOM. ITOPSG shows large RMSD above 2.5°C at 100 m depth. At this site too salinity measurements are limited to upper 100m and all models, ITOPSG followed by NHYCOM and ITOPSI, and IGODAS shows minimum RMSD.

At 4N-90E both ITOPS(G&I) are having lower RMSD followed by IGODAS and NHYCOM. In case of salinity, NHYCOM is better in upper 80 m, below which ITOPSG, IGODAS and IOTPI showed relatively better performance. At this location, ITOSP(G&I) have minimum RMSD of $\tilde{1}$°C for the temperature at thermocline compared to other two models, where the RMSD goes up to 2°C. However, all four models have RMSD less than STD at thermocline region.

At 0N-90E ITOPS(G&I) and IGODAS shows similar performance but NHYCOM has poor performance with higher RMSD and lower correlation in case of both T&S. AT 0N-80.5E also models exhibit identical behaviour. However, at 80.5E at thermocline ITOPS(I&G) has slightly inferior performance compared to IGODAS and NHYCOM.

Figure-41 shows comparison of selected models with a set of RAMA buoys deployed in south-west IO. At 4S-67E all models show similar performance above the thermocline. But at thermocline IGODAS has relatively lower correlation compared to other models. Below thermocline, ITOPSI leads with higher correlation followed by ITOPSG, NHYCOM&IGODAS. Salinity measurement is limited to upper 100 m, and all models show relatively lower correlation with RAMA salinity at this location.

At 08S-55E near surface all models show an excellent simulation of Temperature with minimum RMSD and higher correlation, but with depth, there is a considerable reduction in correlation and correlation reduces to 0.5 for ITOPSG and further down for other models. Salinity also shows a similar pattern of association, which decreases with depth up to 100 m. At 12S-67E, RAMA buoy apparently has a negative spike in temperature which is marked with a near zero correlation for all models. As the depth increases, the model performance slightly reduces regarding correlation in all cases, and there is a higher rate of reduction in case of IGODAS.

Figure-42 present statistics of four models with RAMA buoys deployed in south-east

IO. At 08S-80.5E standard deviation of subsurface temperature is much lower compared to the south-west region. Here, all models show relatively lower RMSD and higher correlation compared to other locations. There is a spike in Temperature at 20 m depth, which is marked by near-zero correlations in all models. Salinity has above 0.5 correlation only near the surface in case of all models, and all models show a decrease in performance with increasing depth.

At 8S-95E all models show relatively lower correlations up to 100 m depth. Further, down all models show a decrease in correlation with depth which is more intense in case of ITOPSI. Salinity here has only limited measurements above 100 m here and may not be worth considering for statistics.

At 12S-93E, RAMA buoy shows a temperature spike around 140 m depth, marked by poor correlation in all models. All models show broadly similar values for RMSD and correlations with IGODAS and ITOPSI having a slightly higher RMSD and lower correlations for complete profile.

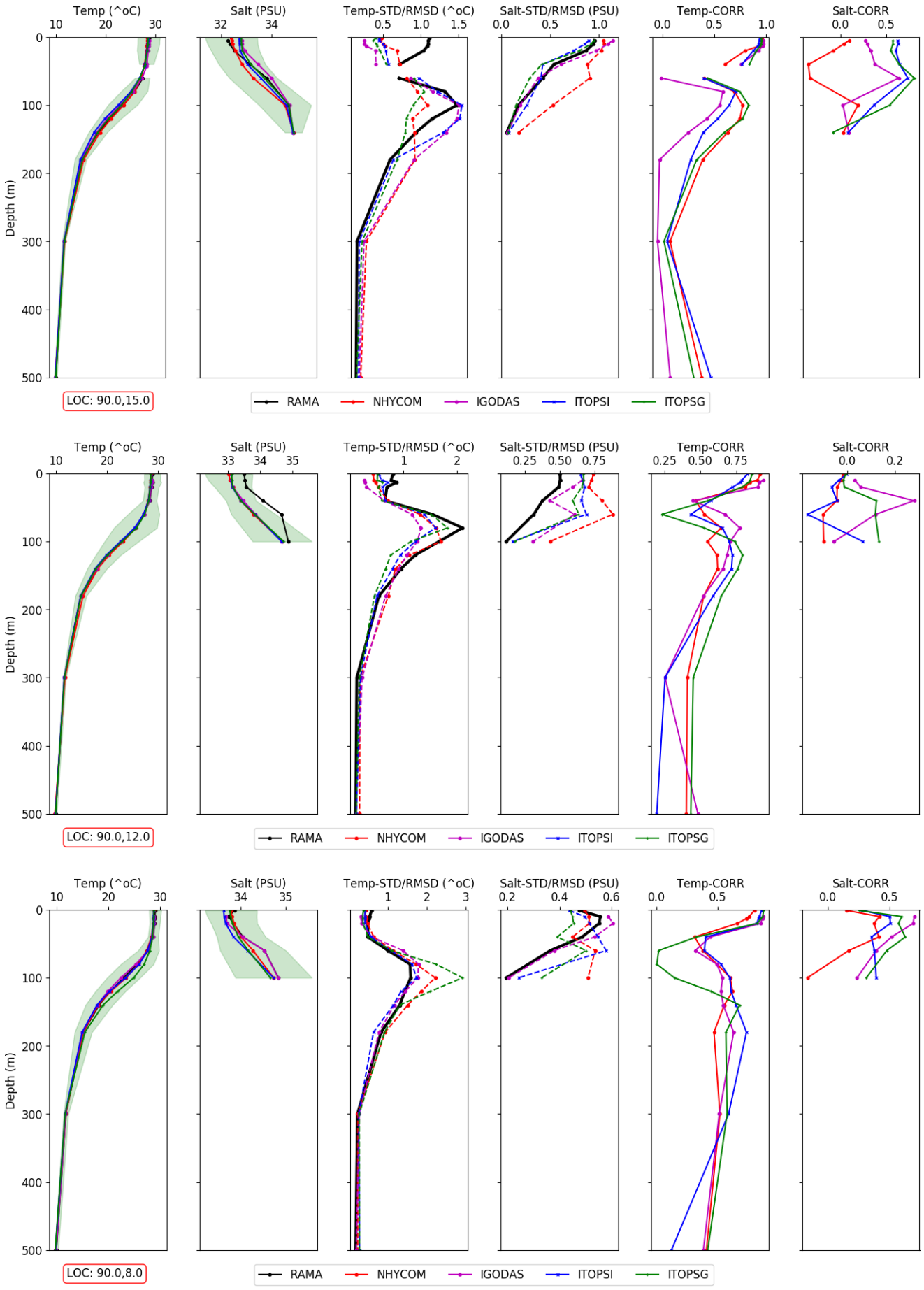

Figure 39: Comparison of TS profiles of 4 models with RAMA TS profiles from BoB. Dashed lines indicate RMSD between RAMA and corresponding model.

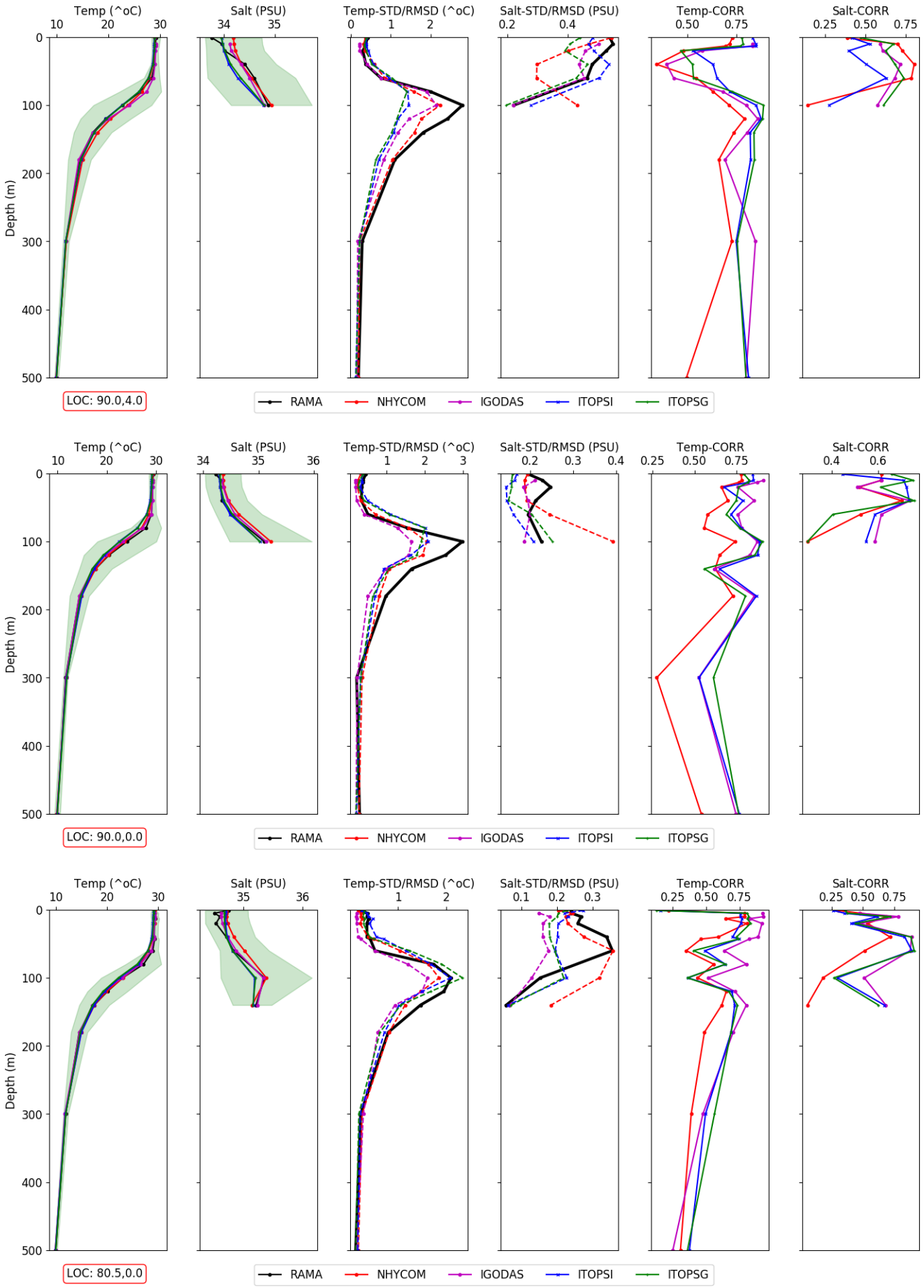

Figure 40: Comparison of TS profiles of 4 models with RAMA TS profiles from EEIO. Dashed lines indicate RMSD between RAMA and corresponding model

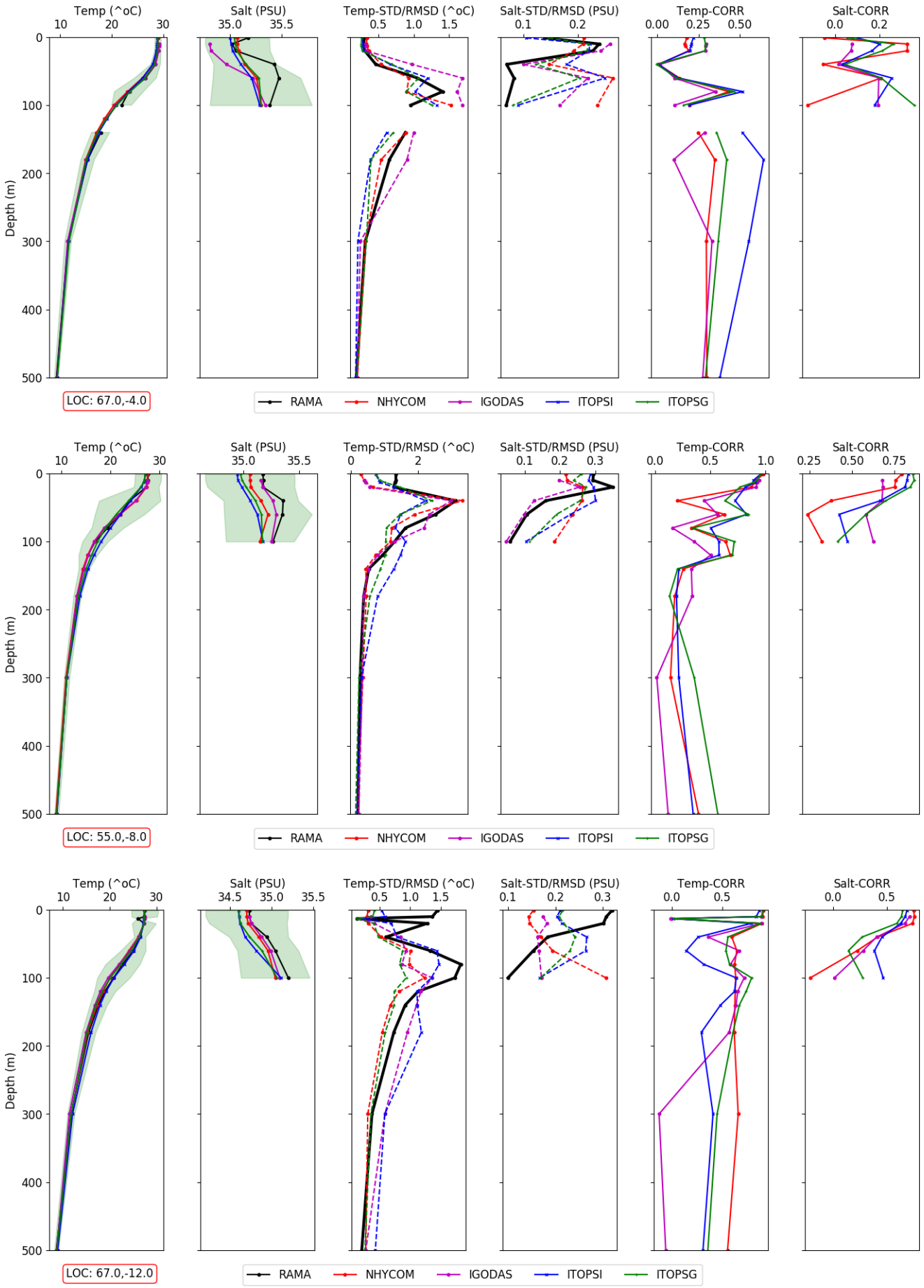

Figure 41: Comparison of TS profiles of 4 models with RAMA TS profiles from 67/55°E longitude. Dashed lines indicate RMSD between RAMA and corresponding model.

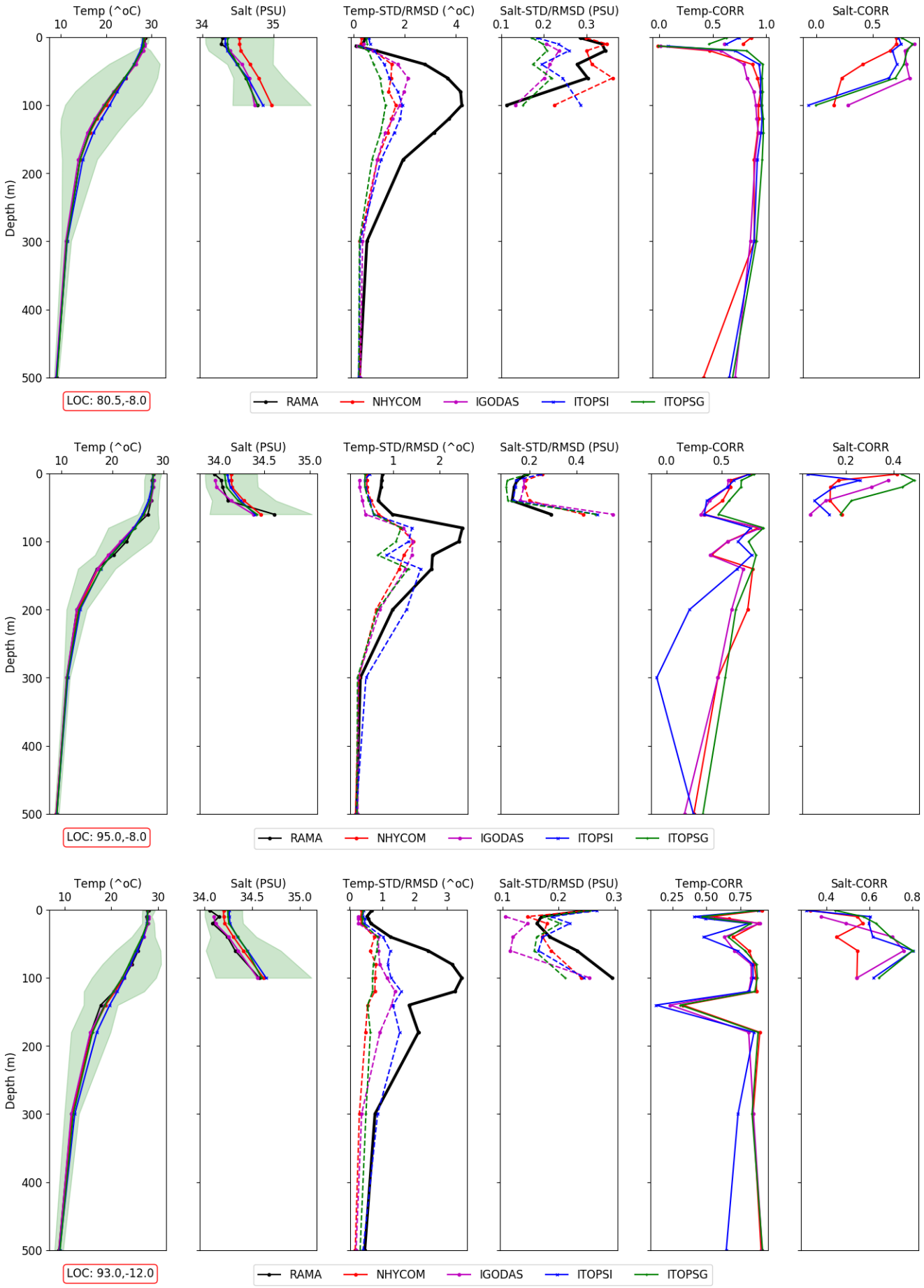

Figure 42: Comparison of TS profiles of 4 models with RAMA TS profiles from 80.5/93 /95°E longitude. Dashed lines indicate RMSD between RAMA and corresponding model.

6.1 Evaluation of Vertical T&S profiles using ARGO floats

6.1.1 Pathological floats which degraded all model simulations

We have compared many of the available ARGO floats for the period 2012 to 2016 within the Indian Ocean with the ITOPSI, ITOPSG, IGODAS and NHYCOM. During this analysis, we came across pathological cases of ARGO floats which escaped the preliminary quality checks and made severe damage to simulations of all models compared here. This issue needs urgent attention and needs to be fixed as it can severely damage analysis, and the impact can be spread to other regions too. Hence we present here the selected floats of such category before we show other floats with a better comparison.

Float-2901471: Float-2901471 is positioned at the boundary of Red-Sea to the Arabian Sea. The float did not undergo much positional shifts compared to other floats. However, due to the dynamic nature of the region and Red-Sea outflow to Arabian-Sea, it stays in a region with larger TS variability. As evident from the Figure-43 top right panel, there is the presence of anomalously lower salinity around 400 m depth during February of 2016, which resulted large standard deviation in salinity. This single event resulted in replicating the error in all models which assimilated the float as evident from highest RMSD in all models at 400 m depth level. However, as seen in the figure, the impact is not limited to 400 m depth level but spreading on either side of 400 m level. Such floats can do collateral damage to the analysis unless filtered out through proper quality control procedures.

Float-2901899: This float has a fresh-water spike at 100 m depth during mid-November which was not removed by QC and affected the analysis of all models with an anomalous spike at about 100 m depth level (Figure-44). This spike resulted in RMSD of about 5 PSU and negative correlation, which is one of the worst impacts of observation on analysis among all models.

Float-2901459: Float 2901459 is located near the confluence of Red-Sea and the Arabian Sea. The float showed relatively small spatial movements. The float showed an anomalously fresh patch of water between 300 to 400 m depth which escaped standard quality checks, resulting in extremely high standard deviation. This anomaly resulted in STD as high as 1.5 PSU in all models at 300 m depth and correlation dropping close to zero at that depth.

Float-2902649: This float sampled ocean between 60-65E above the equator. It has anomalous spikes in both temperature and salinity which escaped quality control. The salinity from this float is characterized by strong seasonality and hence resulted in an STD as high as 2.5 PSU. All models are strongly constrained by this observation and follow observation very closely as evident from the figure. Apart from this, there are anomalous high-temperature spikes below 300 m during September of 2016 along with fresh water anomalies at same depth levels. Such spikes create inflated STD in both temperature and salinity resulting in poor correlations below 300 m depth.

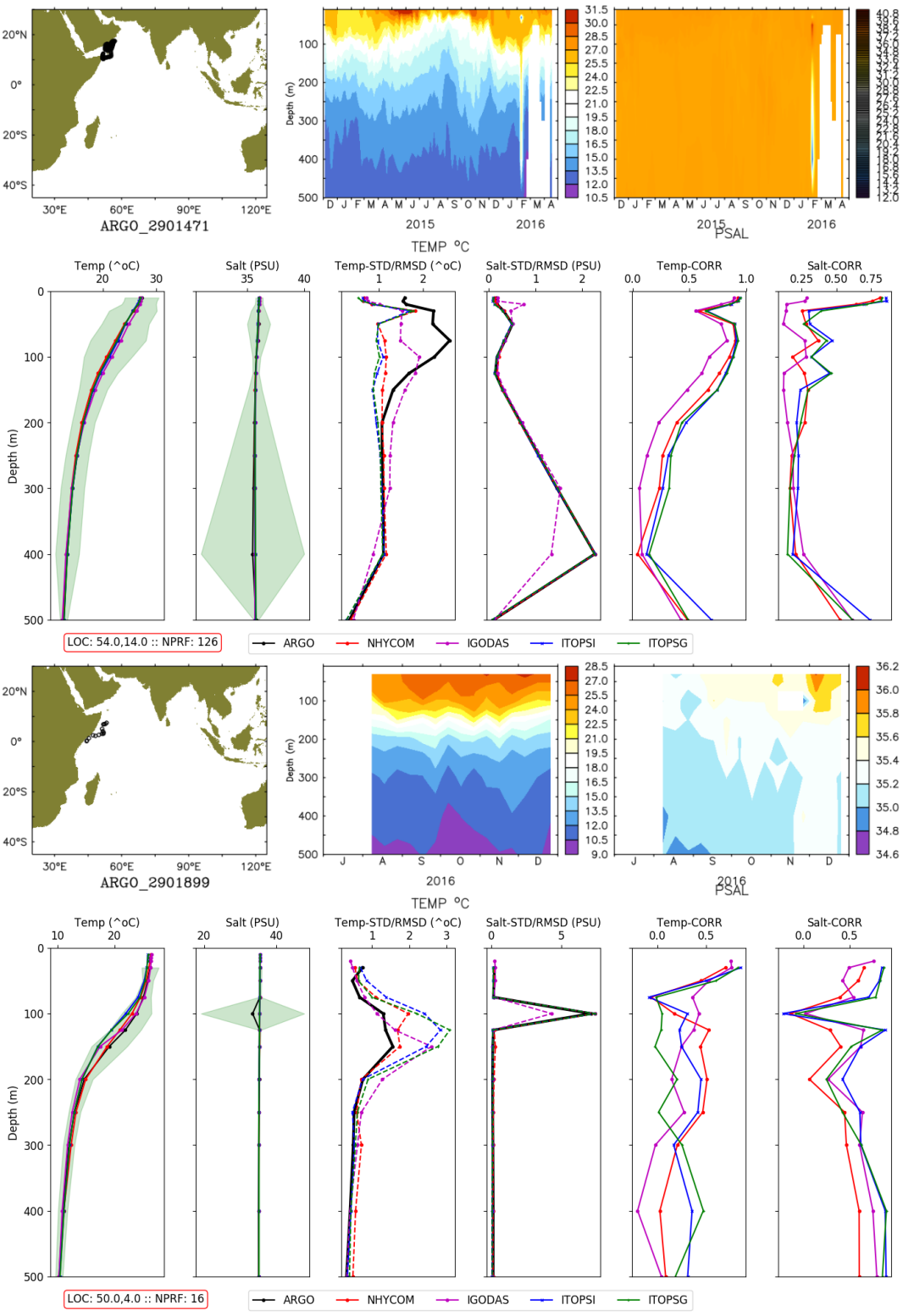

Figure 43: ARGO floats from western Arabian sea western equatorial Indian Ocean with strong anomalies in salinity.

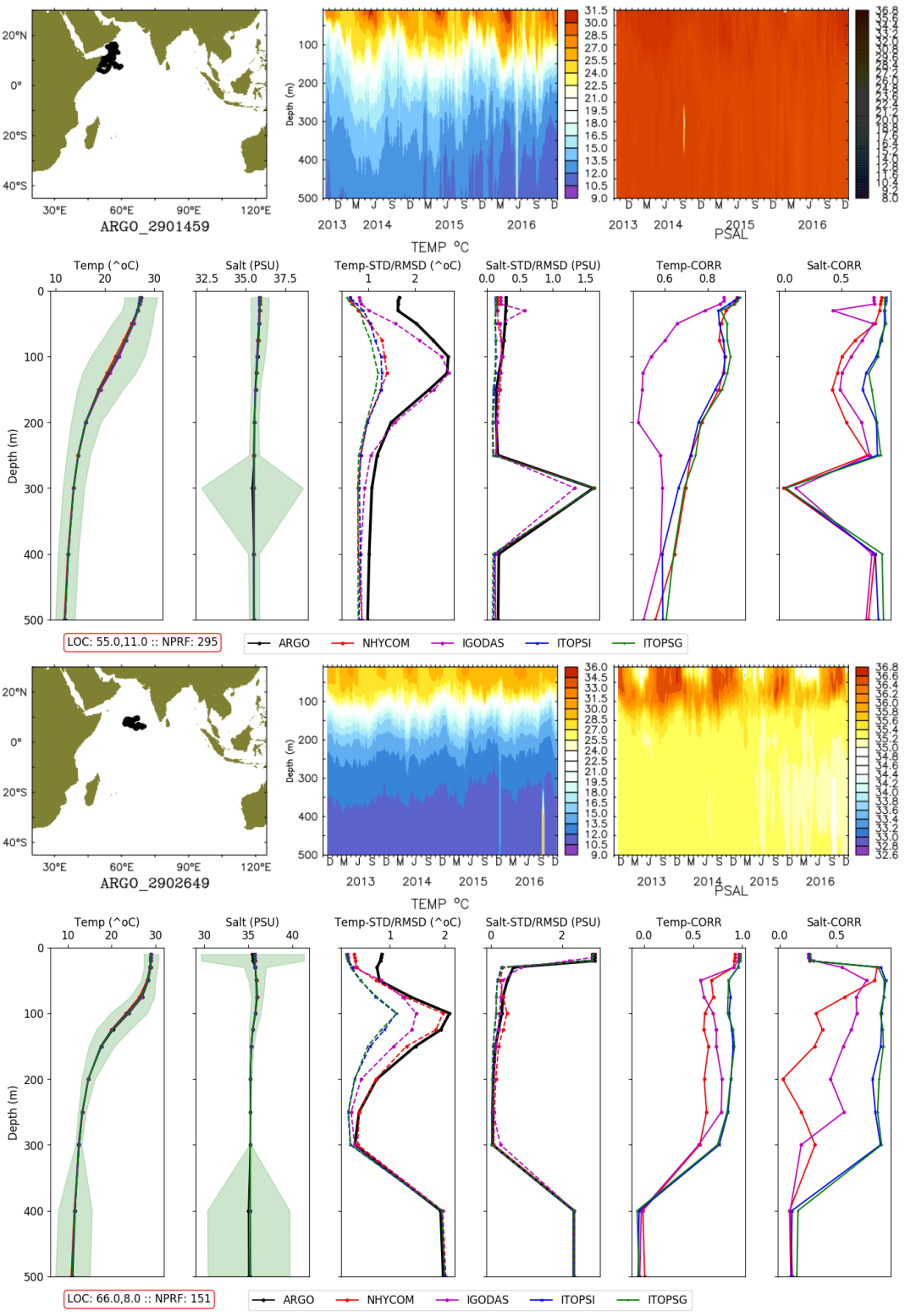

Figure 44: ARGO floats from western and southern Arabian sea Indian Ocean with strong anomalies in temperature/salinity.

6.1.2 Arabian Sea

In this section, we present statistics of four models in comparison with ARGO floats from the Arabian Sea. We have chosen floats with relatively long time-series of data. Vertical mean profiles of all models are within 2 STD of the ARGO T&S (columns one & two from left among vertical profiles). However, there are marked differences when we compare RMSD of each model with the standard deviation of ARGO T&S at different depth

levels. In general RMSD from ITOPSI & ITOPSG are minimal compared to NHYCOM and GODAS. Similarly, there is consistently better correlation particularly for salinity profiles of ITPOSI & ITOPSG with ARGO when compared with other two models.

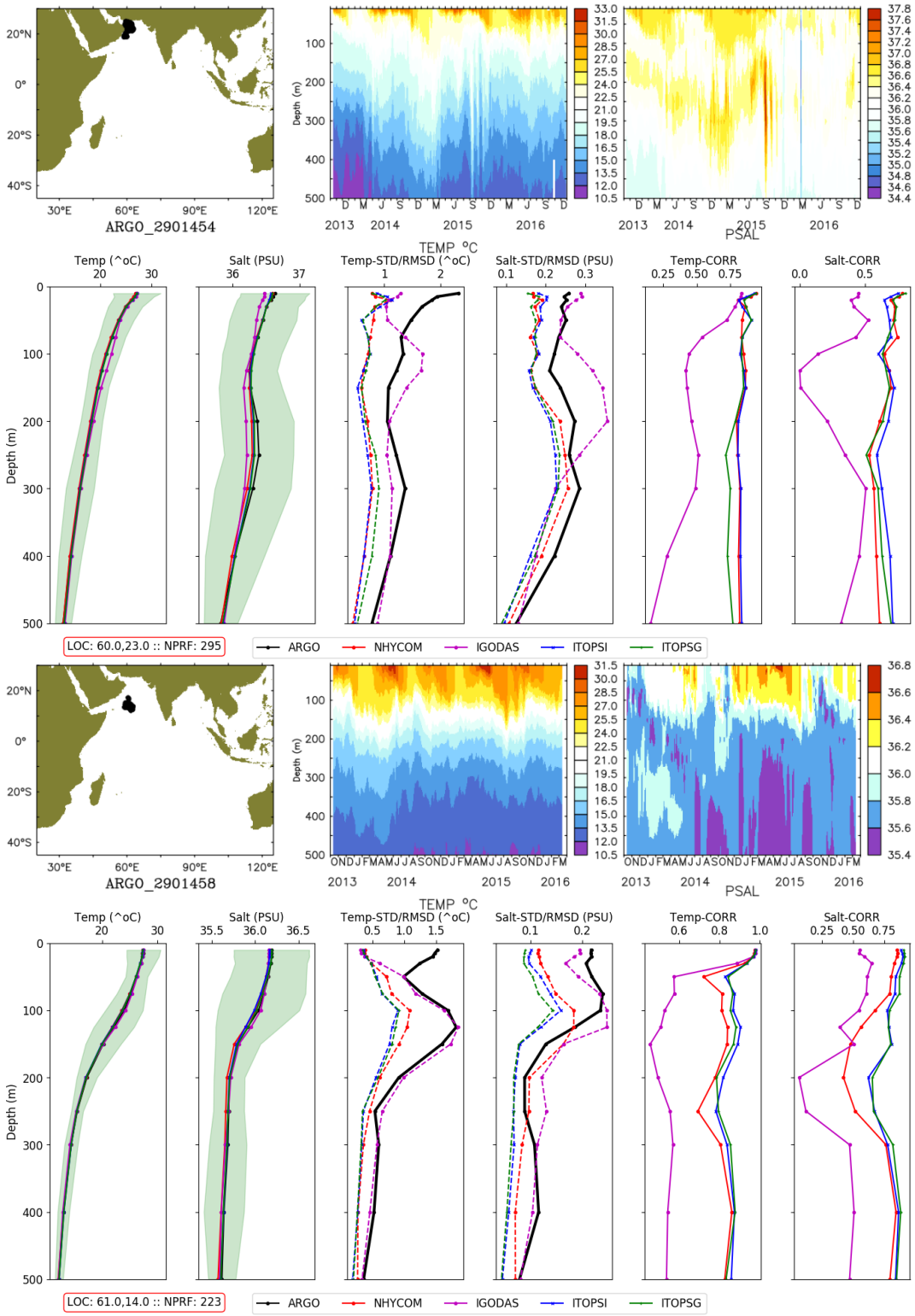

Figure 45: ARGO floats from north western & western Arabian sea with four models

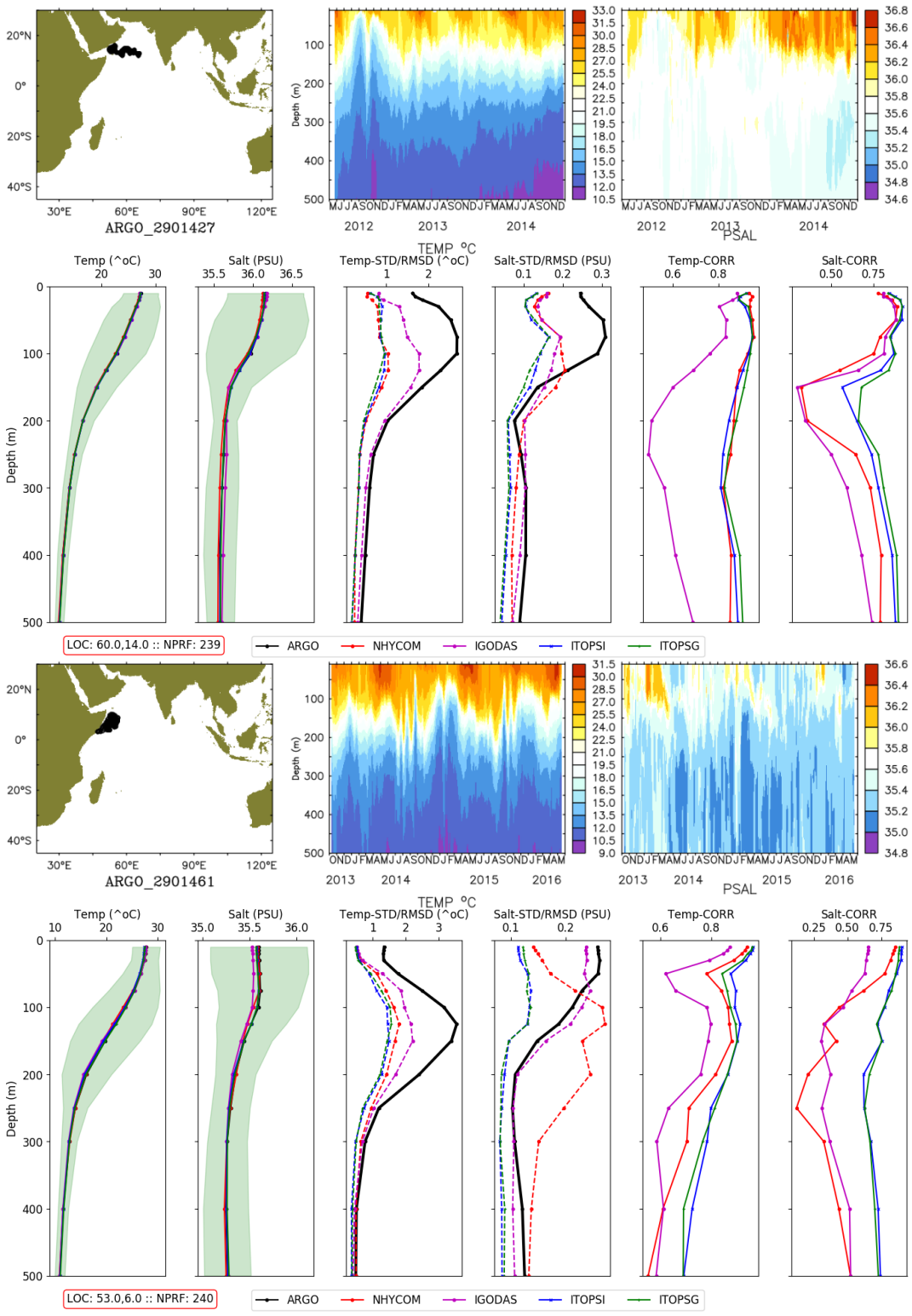

Figure 46: ARGO floats from western Arabian sea and western equatorial Indian ocean with four models

6.1.3 Bay of Bengal (BoB)

In case of BoB, the spread of T&S around their mean is lesser compared to their spread in AS. As in case of AS all model means are within 2 STD envelope. However, there is considerable variability along depth levels when the performance regarding correlation and RMSD is assessed among four different models. For example in case of Float: 6901562, NHYCOM and IGODAS T&S show minimum RMSD and maximum correlation

in the upper 100 m depth. Nevertheless, below 100 m up to 300 m, ITOPI & ITOPSG show better correlation for salinity. Further down NHYCOM and IGODAS shows better correlation and lower RMSD in comparison with ITOPSI & ITOPSG.

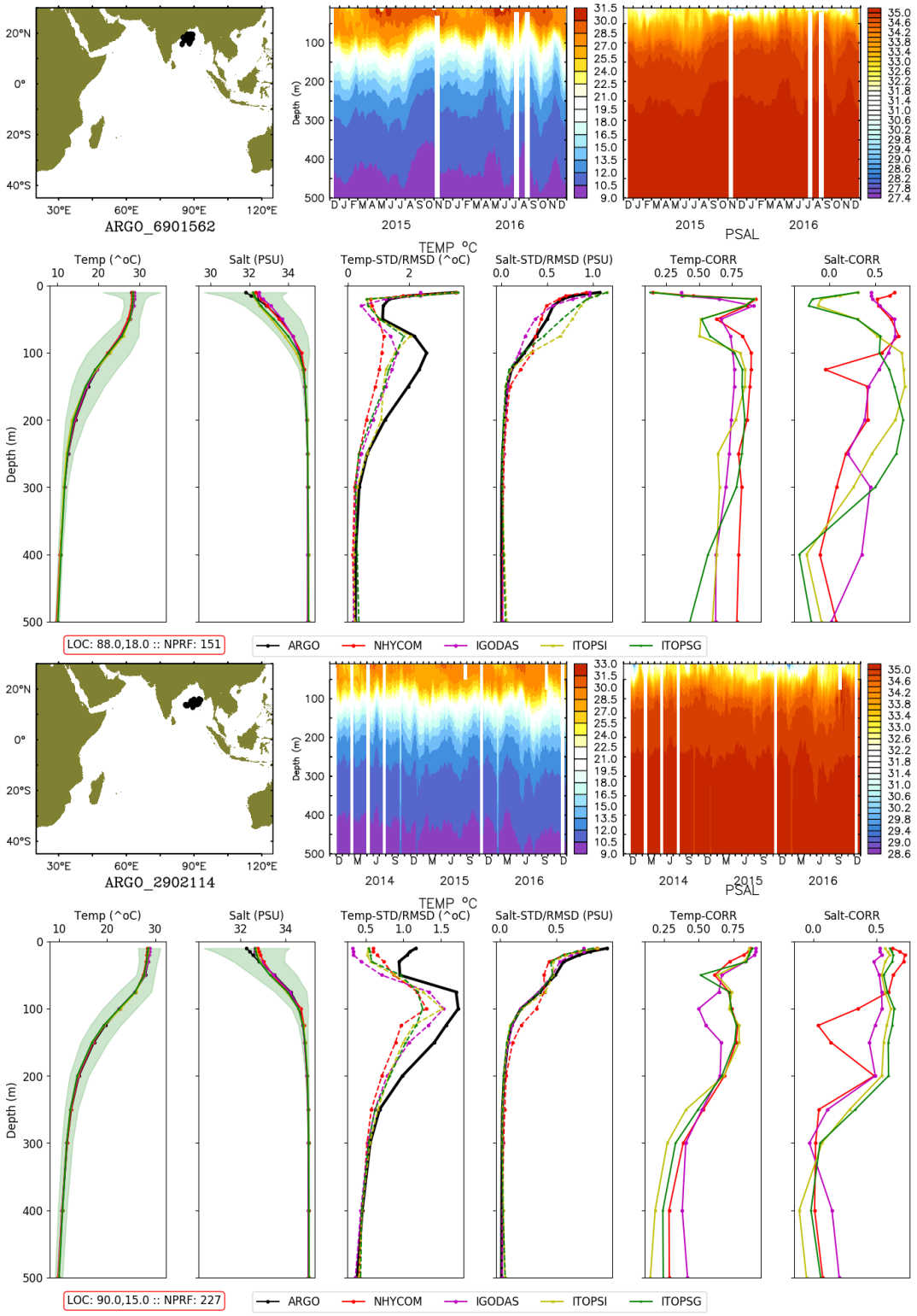

Figure 47: ARGO floats from north and central Bay of Bengal with four models

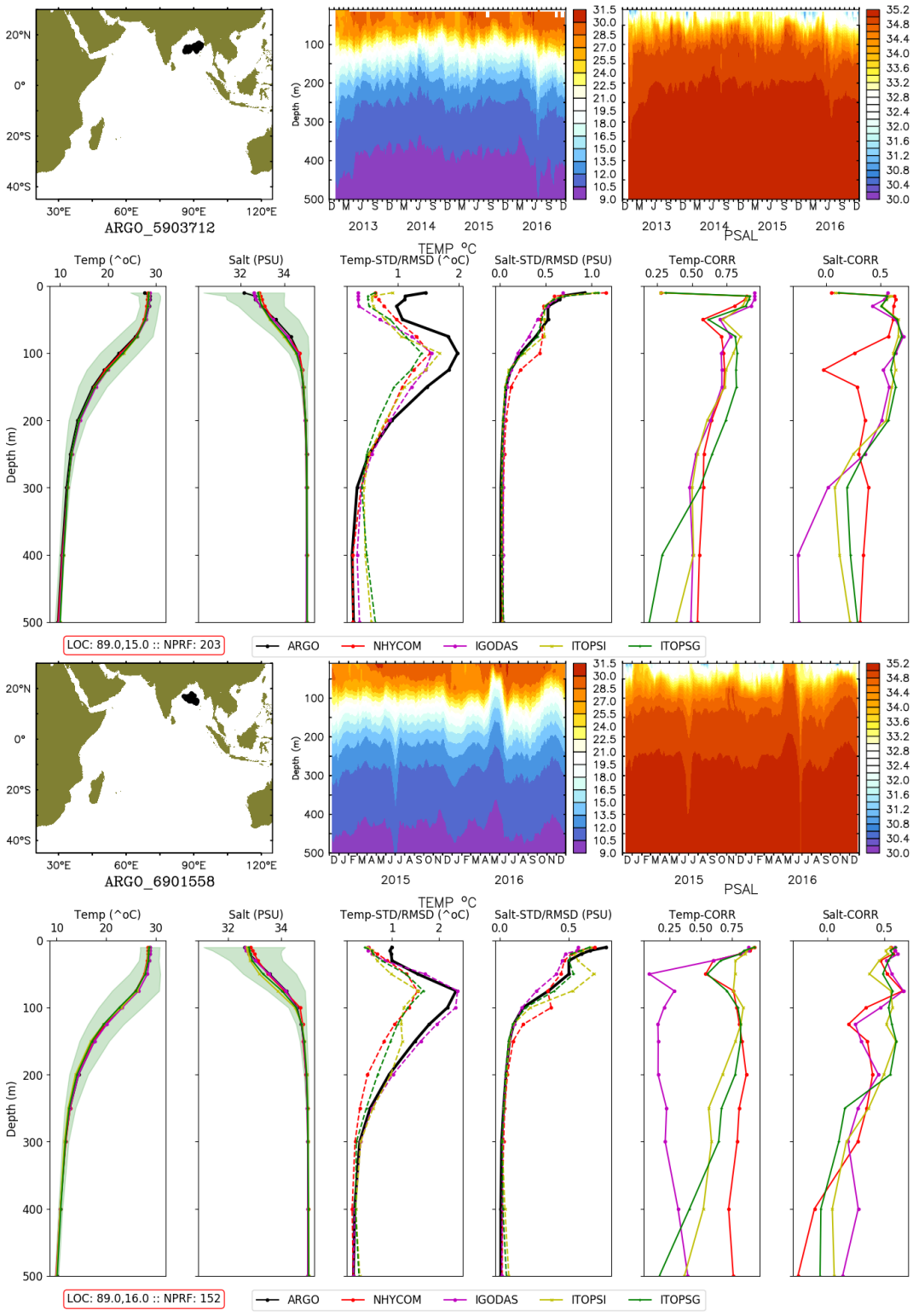

Figure 48: Comparison of ARGO floats from Bay of Bengal with four models

In case of Float: 2902114, NHCOM shows better performance up to top 100 depth, followed by GODAS in case of Temperature and ITPOS(G&I) in case of salinity. Below 100 m up to 400 m the ITOPS in better compared to other two models. Similarly, in other two floats compared here too, there is no consistent better performance in case of any models in BoB.

6.1.4 Equatorial Indian Ocean(EIO)

Unlike floats in AS & BoB, EIO floats have moved along the equator to a larger extent under the influence of equatorial currents. Here the STD spread of salinity is much higher in the upper 100 m in comparison with Temperature.

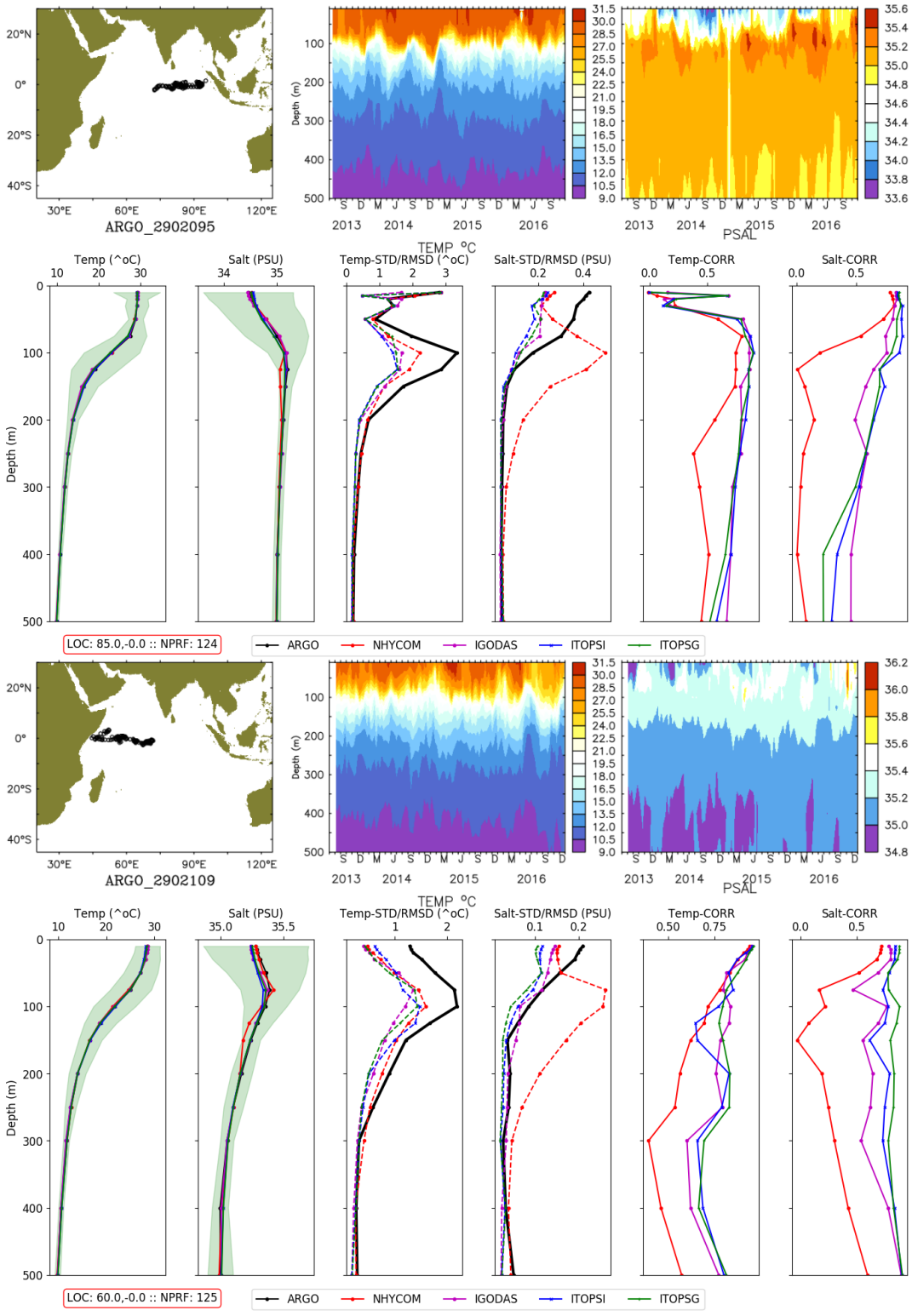

Figure 49: Comparison of ARGO floats from EIO with four models

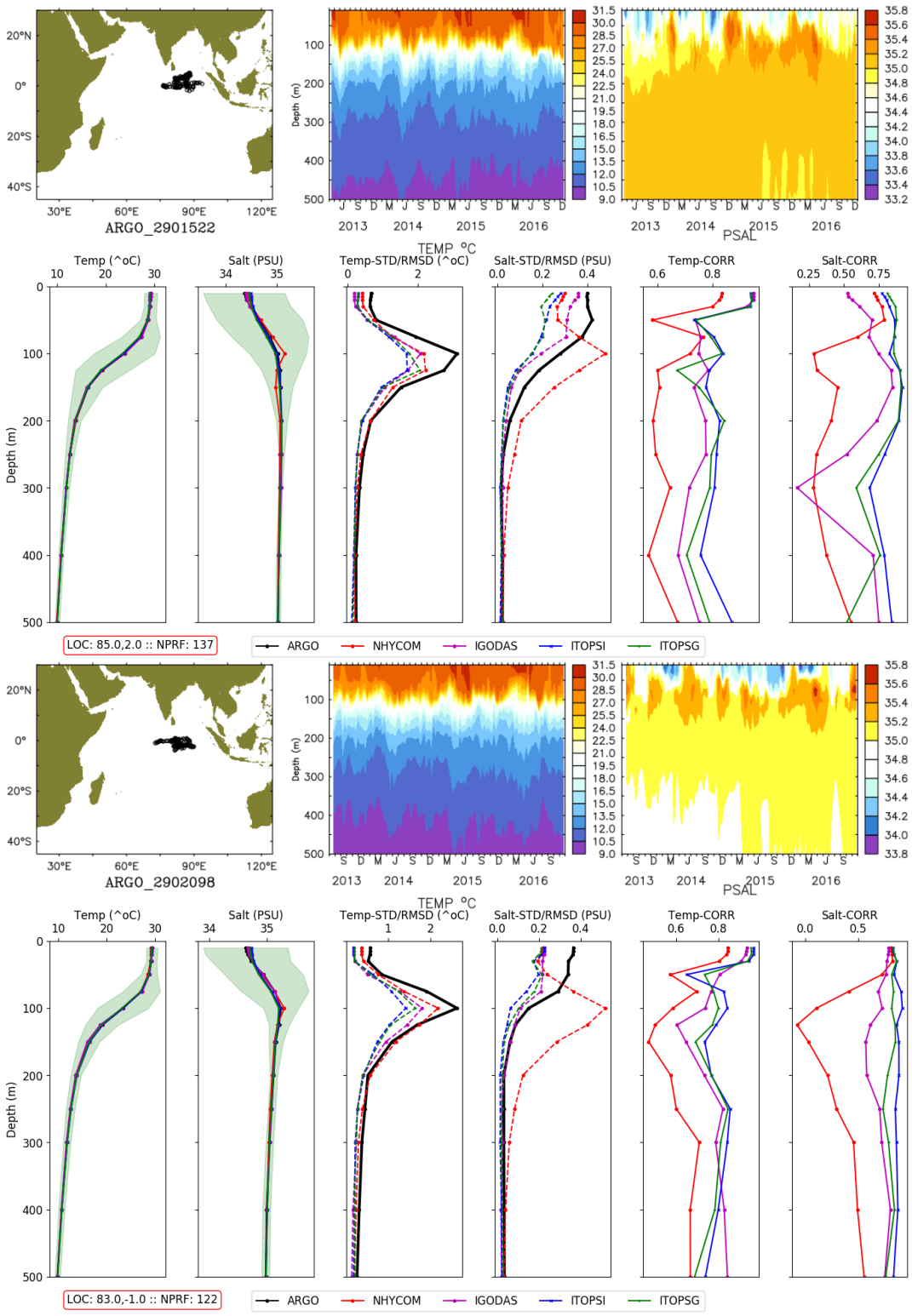

Figure 50: Comparison of ARGO floats from EIO with four models.

In the EIO, both ITOPS(G&I) shows consistently improved performance at all depth levels compared to NHYCOM and IGODAS except in case of Float-2902095, where IGODAS shows higher correlation below 250 m in case of salinity. It needs to be noted that unlike in other cases NHYCOM shows consistent poor performance in EIO.

6.1.5 Southern Indian Ocean(SIO)

SIO floats maximum spatial drift, and therefore samples are obtained from a broader space of ocean. As a result, in this sub-region, both T&S shows higher standard deviations

compared to other sub-regions. Except in case of Float-5903862, ITOPS(G&I) shows consistently improved performance over IGODAS and NHYCOM in SIO.

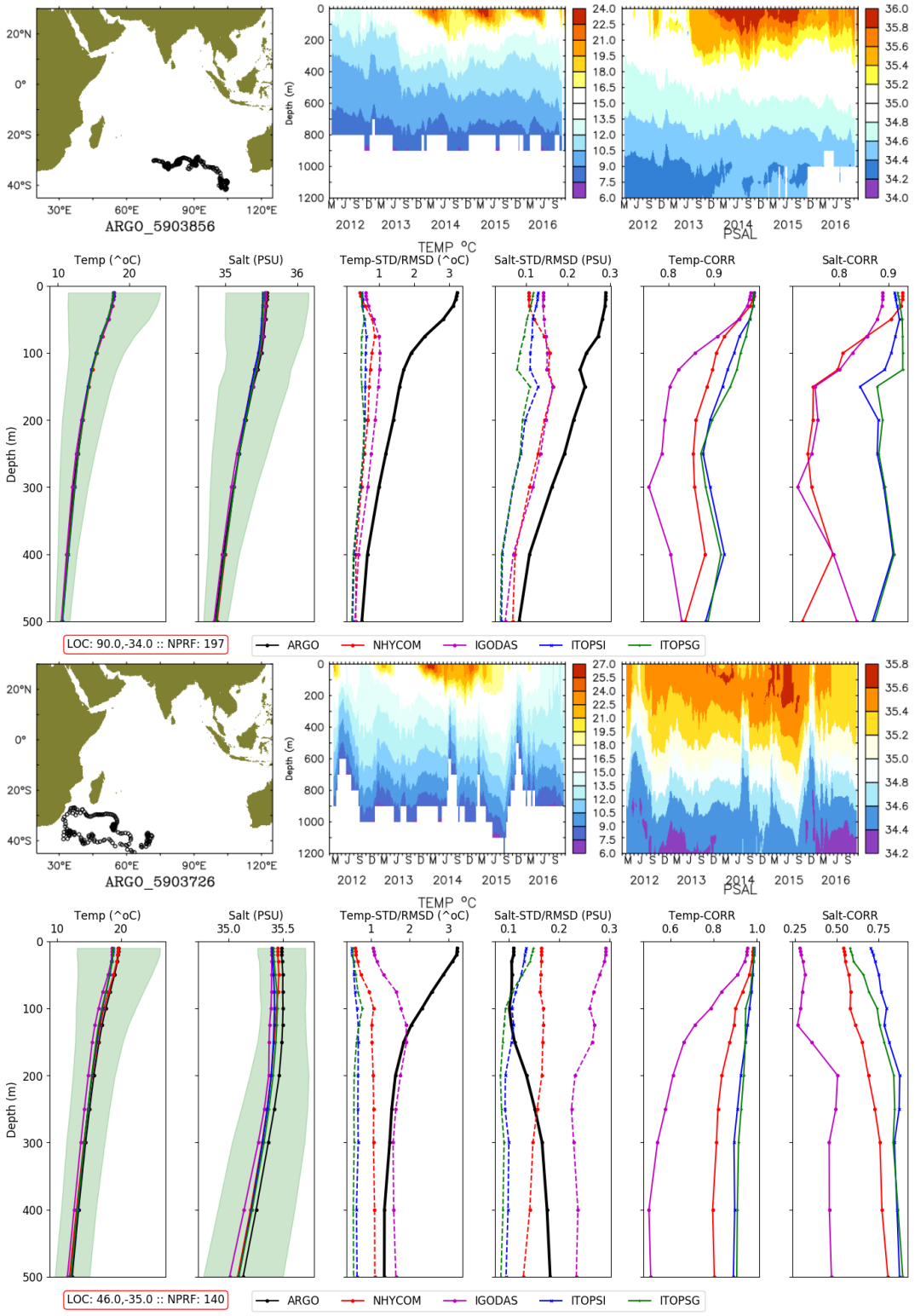

Figure 51: Comparison of four models with ARGO floats from eastern and western part of SIO

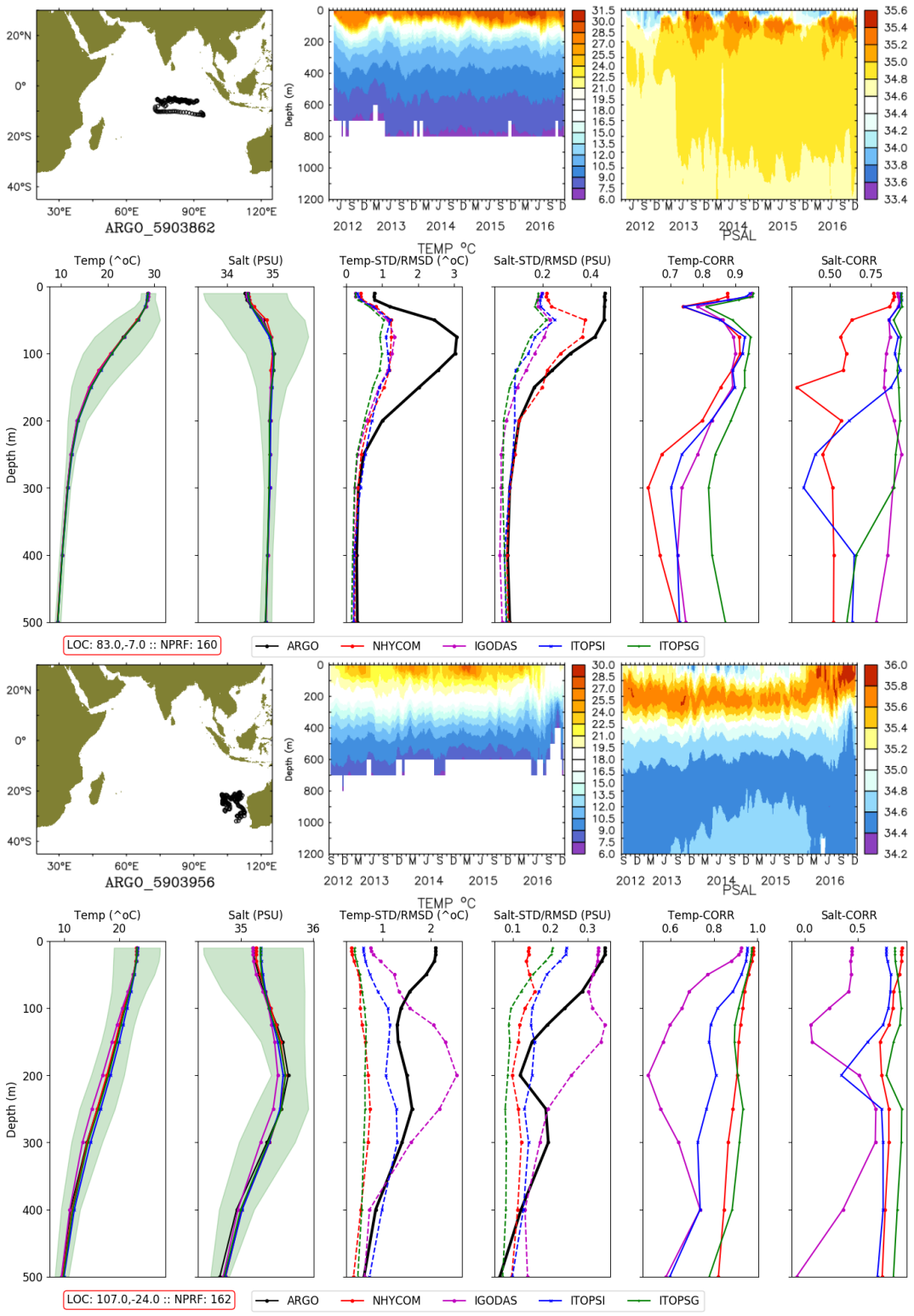

Figure 52: Comparison of four models with ARGO floats close to Australian coast and from central part of SIO

7 Summary and Conclusions

In this report, we present a detailed evaluation of two newly implemented configurations of data assimilating HYCOM models for the Indian Ocean ($\frac{1}{16}^\circ$) and Global domain ($\frac{1}{4}^\circ$) compared to observations and two other established systems, NRL HYCOM and INCOIS GODAS. The model performance is assessed using hindcast simulations during the period 2012–2016 for simulated SST, SSS, SLA, currents along with vertical profiles of temperature and salinity.

Comparison of basin scale SST with gridded GHRSST showed that all models simulate SST well and there are minimal differences regarding performance. However, count of grid points for absolute bias and RMSD show that for these two parameters NHYCOM is slightly better compared to other models followed by IGODAS, ITOPSG and ITOPSI. For correlation, ITOPSI has slightly higher edge over other models if all five years are considered followed by ITOPSG, IGODAS and NHYCOM respectively.

Comparison of model-simulated SST with SST of 24 RAMA buoys showed that IGODAS has the highest skill for simulating SST in a maximum number of locations followed by NHYCOM, IOTOPG and ITOPSI. However, all models show higher correlations in the range 0.8 to 0.9 except for one or two sites.

Among the four models, NHYCOM and IGODAS captured the surface salinity variability closest to the observations in most of the cases when compared with observed SSS from 24 RAMA locations. IGODAS shows minimum bias followed by ITOPSG, ITOPSI and NHYCOM respectively. Maximum SSS biases demonstrated by all four models are within +/-0.2 PSU except three places among which, highest bias is around 0.7 PSU for location 8S100E. Comparison of skill scores among the four shows that ITOPSG and NHYCOM have best skills at 9 locations compared to other two models which showed best skills at three positions each.

Simulated SLA assessed using gridded AVISO SLA shows that RMSD is less than 2 cm for 80% of data coverage for all the models for the years compared. RMSD is more than 7 cm for many places in eddy rich south-western Indian Ocean for all four models with varying intensity. IGODAS has high RMSD in general for the southern Indian Ocean compared to other models, as its resolution is only about half a degree there. Spatial maps of correlation show a similar spatial distribution in case of ITOPSI, ITOPSG and NHYCOM. In case of IGODAS, the highest correlation is limited to the equatorial Indian Ocean and the southeastern Arabian Sea. Among the four models ITOPSG followed by ITOPSI, NHYCOM and IGODAS shows highest correlaton in maximum number of gridpoints in decreasing order.

Correlation of gridded fields of currents with same from OSCAR shows that among the four models, ITOPSG consistently showed the best correlation with 34 to 38% grid points having values between 0.6 to 0.8 followed by ITOPSI with 31 to 35% grid points falling same range of correlation. NHYCOM has 30 to 35% grid points falling in above range of correlation. IGODAS shows lower correlations among the four.

Simulated currents when compared with 21 RAMA buoys showed that ITOPSG followed by ITOPSI has the highest skill among the four models for both zonal and meridional velocities. IGODAS stands third followed by NHYCOM.

Comparison of vertical profiles of temperature and salinity with those of RAMA buoys shows that all four models simulated vertical profiles reasonably well and closer to each other and RAMA profiles. Statistical parameters show variations at different depth levels indicating their varying performances and is difficult to quantify. However, no model can be said to be consistently outstanding or performing poorly from the comparison with RAMA buoys.

Vertical profiles are also compared with selected ARGO floats which had a maximum number of profiles during the hindcast period. In general ITOPSI and ITOPSG shows slightly higher performance regarding correlation and RMSD compared to other models in case of Argo floats.

In short, the performance of different model simulated parameters are quantified in this report, and it demonstrates that the new system is capable of simulating the evaluated variables well in comparison with observations and other models for the Indian Ocean.

8 Acknowledgements

Director INCOIS and Secretary, MoES are acknowledged for infrastructural support. Authors thank the TFE committee chairman, Dr. Ravichandran, and members Dr.Rashmi Sharma, Dr. Gnana Seelan, Dr. Vinaychandran, Dr. A. D. Rao for their scientific inputs and encouragement. We also acknowledge Sri. K.K.V. Chary and Sri. Ramalingeswara Rao for their guidance regarding administrative and financial matters related to this project. The first author thanks Dr. Shailesh Nayak, former secretary, MoES for his inspiration in initiating HYCOM model at INCOIS. RAMA data used in this study is from $http://www.pmel.noaa.gov/tao/drupal/disdel$. We thank the developers of the HYCOM model. The altimeter products are taken from Copernicus Marine and Environment Monitoring Service (CMEMS,$http://www.marine.copernicus.eu$). Argo profile data is obtained from $https://www.nodc.noaa.gov/argo/floats\_data.htm.$. Hycom consortium is thanked for making the NRL HYCOM simulations available online $https://hycom.org/data/glba0pt08/expt-90pt9-expt\_91.2$.

References

R. Bleck. An oceanic general circulation model framed in hybrid isopycnic-cartesian coordinates. *Ocean Modelling*, 4(1):55–88, 2002.

Rainer Bleck and Douglas Boudra. Wind-driven spin-up in eddy-resolving ocean models formulated in isopycnic and isobaric coordinates. *Journal of Geophysical Research: Oceans*, 91(C6):7611–7621, 1986.

Rainer Bleck and Linda T Smith. A wind-driven isopycnic coordinate model of the north and equatorial atlantic ocean: 1. model development and supporting experiments. *Journal of Geophysical Research: Oceans*, 95(C3):3273–3285, 1990.

Fabrice Bonjean and Gary SE Lagerloef. Diagnostic model and analysis of the surface currents in the tropical pacific ocean. *Journal of Physical Oceanography*, 32(10):2938–2954, 2002.

EP Chassignet, HE Hurlburt, OM Smedstad, GR Halliwell, and PJ Hogan. *Ocean Prediction with the Hybrid Coordinate Ocean Model (HYCOM)ˆ Book chapter*. 2006a.

E.P. Chassignet, H.E. Hurlburt, O.M. Smedstad, G.R. Halliwell, P.J. Hogan, A.J. Wallcraft, R. Baraille, and R. Bleck. The hycom (hybrid coordinate ocean model) data assimilative system. *Journal of Marine Systems*, 65(1-4 SPEC. ISS.):60–83, 2007a.

E.P. Chassignet, H.E. Hurlburt, O.M. Smedstad, G.R. Halliwell, P.J. Hogan, A.J. Wallcraft, R. Baraille, and R. Bleck. The hycom (hybrid coordinate ocean model) data assimilative system. *Journal of Marine Systems*, 65(1-4):60–83, 2007b.

E.P. Chassignet, and E. J. Metzger H. E. Hurlburt, and G. R. Halliwell and R. Bleck and R. Baraille and A.. J. Wallcraft O. M. Smedstad, and J. A. Cummings, and H. L. Tolman C. Lozano, and P. Cornillon and R. Weisberg A. Srinivasan, and S. Hankin, and R. He A. Barth, F. Werner, and J. Wilkin. Us godae: Global ocean prediction with the hybrid coordinate ocean model (hycom). *Oceanogarphy*, 22:64–75, 2009.

Eric P. Chassignet, Linda T. Smith, George R. Halliwell, and Rainer Bleck. North atlantic simulations with the hybrid coordinate ocean model (hycom): Impact of the vertical coordinate choice, reference pressure, and thermobaricity. *Journal of Physical Oceanography*, 33(12):2504–2526, 2003.

P. Chassignet, Eric., H.E. Hurlburt, O.M. Smedstad, G.R. Halliwell, A.J. Wallcraft, E.J. Metzger, B.O. Blanton, C. Lozano, D.B Rao, P.J. Hogan, and A. Srinivasan. Generalized vertical coordinates for eddy-resolving global and coastal ocean forecasts. *Oceanograohy*, 19(1):20–31, March 2006b.

Mike Cooper and Keith Haines. Altimetric assimilation with water property conservation. *Journal of Geophysical Research: Oceans*, 101(C1):1059–1077, 1996.

Gregory Gaspari and Stephen E Cohn. Construction of correlation functions in two and three dimensions. *Quarterly Journal of the Royal Meteorological Society*, 125(554): 723–757, 1999.

M Iskandarani, JC Levin, B-J Choi, and DB Haidvogel. Comparison of advection schemes for high-order h–p finite element and finite volume methods. *Ocean Modelling*, 10(1-2): 233–252, 2005.

A. B. Kara, C. N. Barron, A. J. Wallcraft, T. Oguz, and K. S. Casey. Advantages of fine resolution ssts for small ocean basins: Evaluation in the black sea. *J. Geophys. Res.*, 113:–, August 2008. doi: http://www.agu.org/journals/jc/jc0808/2007JC004569/2007JC004569.pdf.

A. Birol Kara, Peter A. Rochford, and Harley E. Hurlburt. Efficient and accurate bulk parameterizations of air - sea fluxes for use in general circulation models. *Journal of Atmospheric and Oceanic Technology*, 17(10):1421–1438, 2000.

A. Birol Kara, Harley E. Hurlburt, and Alan J. Wallcraft. Stability-dependent exchange coefficients for air-sea fluxes. *Journal of Atmospheric and Oceanic Technology*, 22(7): 1080–1094, 2005. doi: 10.1175/JTECH1747.1.

W. G. Large, J. C. McWilliams, and S. C. Doney. Oceanic vertical mixing: A review and a model with a nonlocal boundary layer parameterization. *Rev. Geophys.*, 32(4): 363–403, 1994. ISSN 8755-1209.

M Ravichandran, D Behringer, S Sivareddy, MS Girishkumar, Neethu Chacko, and R Harikumar. Evaluation of the global ocean data assimilation system at incois: The tropical indian ocean. *Ocean Modelling*, 69:123–135, 2013.

R Sadourny. Compressible model flows on the sphere. *Journal of the Atmospheric Sciences*, 32(11):2103–2110, 1975.

Sanikommu Sivareddy, Muthalagu Ravichandran, Madathil Sivasankaran Girishkumar, and Koneru Venkata Siva Rama Prasad. Assessing the impact of various wind forcing on incois-godas simulated ocean currents in the equatorial indian ocean. *Ocean Dynamics*, 65(9-10):1235–1247, 2015.

W.C. Thacker, S.-K. Lee, and G.R. Halliwell Jr. Assimilating 20 years of atlantic xbt data into hycom: A first look. *Ocean Modelling*, 7(1-2):183–210, 2004.

Steven T Zalesak. Fully multidimensional flux-corrected transport algorithms for fluids. *Journal of computational physics*, 31(3):335–362, 1979.